

NEURAL RESPONSES TO INJURY: PREVENTION, PROTECTION, AND REPAIR

Annual Technical Report 1996

Submitted by

**Nicolas G. Bazan, M.D., Ph.D.
Project Director**

Period Covered: 20 September, 1995, through 19 September, 1996

Cooperative Agreement DAMD17-93-V-3013

between

**United States Army Medical Research and Development Command
(Walter Reed Army Institute of Research)**

and

**Louisiana State University Medical
Center
Neuroscience Center of Excellence**

Volume 2 of 9

Repair and Regeneration of Peripheral Nerve Damage

Project Directors:
Roger Beuerman, Ph.D.
David Kline, M.D.
Austin Sumner, M.D.

DTIC QUANTITY REQUESTED 4

19980323 148

ANIMAL USE
SEPTEMBER 20, 1995 THROUGH JULY, 1996

DAMD17-93-V-3013

The experimental animals used during this period for the project, Neural Responses to Injury: Prevention, Protection, and Repair, Subproject: Repair and Regeneration of Peripheral Nerve Damage, are as follows:

Species	Number Allowed	Number Used	LSU IACUC#
Rhesus	15	8 (4 ordered)	1059
Rabbit	20	20	1060

LW Bennerum

Investigator Signature

Volume 2 Repair and Regeneration of Peripheral Nerve Damage

Project Directors

Roger Beuerman, Ph.D.
David Kline, M.D.
Austin Sumner, M.D.

Participating Scientists:

John England, M.D.
Leo Happel, Ph.D.
Daniel Kim, M.D.,
Cheryl Weill, Ph.D.

Animal Use	i
Table of Contents	ii
Goals	1
Introduction	1
Immunolocalization of Basic and Acidic Fibroblast Growth Factor (FGF) and FGFR-1 in Cells of Human Peripheral Nerve	6
Introduction	6
Materials and Methods	7
Tissue Preparation and Primary Cell Culture	7
Antibodies	9
Immunofluorescence Microscopy	9
Immunoelectron-microscopy	10
Western Blot	10
Flow Cytometry	11
Results	12
Light Microscopic Localization	12
Immunoelectron Microscope Localization	13
Western Blot Analysis	14
Flow Cytometry	14
Figure Legends	17
References	19
Growth Factors Regulation of Injury Nerve Fibroblast Proliferation Requires Activation of MAPK Signal Tranduction Pathway	35
Introduction	35
Growth Factors Induce Activation of MAPK and DNA Synthesis in Human Neuroma Fibroblasts	36
Prevention of Growth Factor Involved Mitogenic Effects by Inhibition of MAPK Pathway	37
Wounding a Fibroblast Monolayer Induces a Rapid Activation of MAP Kinase	38
Minoxidil Suppresses Human Neuroma Fibroblast Proliferation	39

Increase of GAP-43 Protein in Sciatic Nerve Injury and Neuroma Formation	45
Changes of Energy Related Metabolites in Cerebro-Spinal Fluid After Brachial Plexus Injury	47
References	49
Goals for Fourth Year	51
Central Nervous System Changes Associated with Chronic Pain in Peripheral Nerve Injury	54
Abstract	54
Hypothesis	54
Year III Goals	54
First Specific Aim	55
Second Specific Aim	55
Third Specific Aim	55
Results of Year III Goals	55
Behavioral Results	55
Preliminary Anatomical Results	57
Present Goals	59
Current Results	62
Goals for Year 4	63
Ion Channels in Injured Peripheral Nerves	64
Specific Aims	64
Studies and Results	64
Significance	67
Plans	68
Human Subjects	69
Vertebrate Animals	69
Publications	70

England JD, Happel LT, Kline DG, Gamboni F, Thouron C, Liu ZP, Levinson SR (1996) Sodium channel accumulation in human painful neuromas. *Neurology* 47:272-276.

England JD, Levinson SR, Shranger P (1996) Immunocytochemical investigations of sodium channels along nodal and internodal portions of demyelinated axons. *Microscopy Research Technique* 33:445-451.

Lu G, Beuerman RW, Zhao S, Sun G, Nguyen DH, Ma S, Kline DG. Tumor Necrosis Factor Alpha and Interleukin-1 Induce Activation of MAP Kinase and SAP Kinnase in Human Neuroma Fibroblasts. *Neurochemistry International: Cytokine*, in press.

Varnell RJ, Freeman JY, Maitchouk D, Beuerman RW, Gebhardt BM. Detection of Substance P in Human Tears By Laser Desorption Mass Spectrometry and Immunoassay. *Neuroscience Letters*, in press.

Zhao S, Beuerman RW, Kline DG. Neurotization of motor nerves innervating lower extremity by utilizing lower intercostal nerves. *Reconstructive Microsurgery*, in press.

IMMUNOLocalization OF BASIC AND ACIDIC FIBROBLAST GROWTH FACTOR (FGF) AND FGFR-1 IN CELLS OF HUMAN PERIPHERAL NERVE NEUROMA

INTRODUCTION:

The fibroblast growth factors (FGFs) are a family of nine structurally related polypeptides. The best characterized members are acidic FGF (FGF-1) and basic FGF (FGF-2). Other members of the FGF family include FGF-3 (int-2), FGF-4 (hst/Kfgf), FGF-5, FGF-6, FGF-7 (keratinocyte growth factor, KGF), FGF-8 (AIGF) and FGF-9 (glial-activating factor, GAF) (1-3). FGF types 1 and 2 share 53% amino acid sequence homology (4), suggesting that they are derived from a common ancestral gene. They also have a strong affinity for heparin (5,6) and bind to the same cell surface receptor (7). FGFs are involved in various biological activities, including angiogenesis, mitogenesis, cellular differentiation, tumorigenesis, and repair of tissue injury (5, 8, 9). These actions are mediated through specific, high affinity, transmembrane receptors. Four structurally related genes encoding high affinity receptors have been identified (10-13). The FGF receptor has diverse forms, FGFR-1, FGFR-2, FGFR-3 and FGFR-4. FGF-1 binds to all four members of the FGF receptor family and FGF-2 binds to all but FGFR (14-15).

FGF is found in many tissues including peripheral nerve, and it is suggested that due to its action on fibroblasts may participate in neuroma formation, a complication of peripheral nerve injury and characterized by accumulation of collagen and extracellular matrix which form a barrier that regenerating axons cannot penetrate, resulting in bulb-

like enlargement or neuroma (16). The mechanism of neuroma formation is not understood. FGF may mediate interactions between regenerating neuritic and cell adhesion molecules (CAM) (17). Fibroblast growth factor has been found to be in the internal environment of peripheral nerve and in an earlier study in this DOD funded project, it was most commonly found in human nerve. In this initial study, tissue samples of human peripheral nerve neuroma were analyzed by the western blot procedure for a number of growth factors. Basic fibroblast growth factor was found in large amounts in all twenty-one tissue samples and was the only growth factor analyzed that was found in all of the tissue samples. Recently, it has been found that activation of the FGF receptor in the pathway underlies neurite outgrowth stimulated by CAMs (L1, N-CAM, and N-cadherin).

Fibroblast growth factor and its receptor have been detected in both normal (18, 19) and pathological tissues (20). BFGF has also been detected in fibroblasts of mouse gastric ulcer bed (21) and fibroblasts are a normal source of bFGF. In a previous study using an animal model of neuroma, an increased expression of bFGF and FGFR-1 in neuromas from sciatic nerve when compared normal sciatic nerve (22). However, there is little data regarding the cellular localization of FGFs and their receptors in human peripheral nerve neuromas. Since fibroblasts are a primary cellular element in neuroma formation, the present study not only examined localization of bFGF, aFGF in human neuroma tissue, but also examined their subcellular localization in cultured fibroblasts from neuromas using light and electron microscopy as well as Western blot analysis. In a previous study, we measured membrane growth factor

receptors using a flow cytometry technique (23). In the present study, quantitation of membrane FGFR1 on cultured fibroblasts from human neuroma was determined using flow cytometry as well as immunolocalization of the protein and receptor at the light and electron microscopic levels.

MATERIALS AND METHODS

Tissue preparation and primary cell culture

Peripheral nerve neuroma samples were obtained at the time of surgical correction. All patients were male and the average age was 25.2 years (14-38 years). These patients all had previous trauma to their brachial plexus, and surgery to correct the neuroma was carried out 8 to 10 months after the accident. The tissue samples were immediately sectioned longitudinally and one-half were frozen in liquid nitrogen for western blot analysis while the other half was used for cell culture.

Tissue samples were cut into 1 mm³ blocks and put into T25 flasks. Cultures were maintained in Dulbecco's Modified Eagle Medium (D-MEM) plus 20% fetal bovine serum (FBS) and 1% antibiotic-antimycotic with 5% CO₂, 95% air at 37°C. (Gibco BRL, life Technologies Inc.). Confluent cells were transferred after 14 days into T75 flasks containing 10% FBS and 1% antibiotic-antimycotic in D-MEM. Cells were used for immunocytochemical and immunoblotting studies. To avoid potential interference from FBS, culture medium was replaced with serum free D-Mem, 12-24 hr before experimental studies.

Antibodies

Regents used in this study were the following: Antibodies to fibroblast growth factor-basic and acidic from rabbit polyclonal IgG fraction (Sigma); anti-FGFR-1 (VBS6) monoclonal IgG fraction (Santa Cruz Biotechnology); for western blot analysis, basic FGF from mouse monoclonal IgGL; and FGF receptor-1, mouse monoclonal IgG2b (Transduction Laboratories) anti-mouse 1GFG1 conjugate and anti-rabbit IgG TRITC conjugates (Sigma) colloidal gold (15 nm diameter) goat-anti-rabbit and goat antimouse IgG (BBI international); antimouse and anti-rabbit Ig horseradish per oxidase (Amersham Life Science); anti-mouse IgG-phycoerythrin (PE) conjugate (Sigma).

Immunofluorescence microscopy

Cells were grown in multi-well glass chamber slides (Nunc). Confluent monolayers were washed with 0.1M PBS pH 7.4 and fixed with 4% paraformaldehyde/0.1M PBS pH 7.4 for 30 min at room temperature (RT). Tissue specimens were embedded in OCT compound. Sections (12 μ m) were cut on a cryostat, washed and fixed in 4% paraformaldehyde in 0.1M PBS pH 7.4 for 10 min. Cells grown on glass chamber slides and tissue sections were washed in 0.1M PBS and incubated with a 5% solution of normal goat serum in 0.1M PBS for 30 min at RT. They were incubated overnight with primary antibody diluted with 0.1M PBS/1% BSA, 0.3% triton x-100, bFGF and aFGF 1:200, FGFR-1:60) at 4°C. Antibody binding was detected by incubating the slides and sections with fluorescein (FITC or TRITC)

conjugated secondary antibody diluted with 0.1M PBS, 1% BSA and 0.3% triton X-100 for 1 hr at RT. After final washing with 0.1M PBS, the slides and sections were examined using a fluorescence microscope (Nikon). Controls used 0.1M PBS instead of the primary antibody.

Immunoelectron-microscopy

Cells were grown on multi-well plastic chamber slide, washed with 0.1M PBS pH 7.4 and 4% paraformaldehyde in 0.1M PBS for 30 min at 37°C. This was followed by washing and treating again with 0.1M PBS plus 0.1% saponin and 5% normal goat serum for 30 min at RT. After incubation with primary antibody diluted with 0.1M PBS containing 1% BSA overnight at 4°C, after washing with 0.1M PBS, the slide was treated with colloidal gold (15 nm diameter) conjugated anti-mouse IgG or anti-rabbit IgG for 1 hr at RT. After washing with 0.1M PBS and distilled water, the slide was silver enhanced (BBI Inc.) for 15 min. After washing, the slide was fixed with 2% glutaraldehyde for 10 min, then treated with 0.2% osmium tetroxide, en bloc mordanted with 1% urinal acetate buffer at pH 5.0, finally dehydrated through a graded series of ethyl alcohol and embedded in Epon. Ultrathin sections were cut on a Reichart ultra microtome observed with a Zeiss TEM 10 C/R. In controls, primary antibody was replaced by 0.1 M PBS.

Western blot

The cultured cells grown in sixteen well plates were rinsed with 0.1M PBS and

lysed with 1.0 ml per 10 mm diameter dish of a boiling lysis solution (1% SDS, 10 mM Tris pH 7.4). The cells were then scraped from the dish and transferred to a micro centrifuge tube, and boiled for an additional 5 minutes. The viscosity of the samples was reduced by several passages through a 26 gauge needle. The samples were centrifuged for 5 min to remove insoluble material. Tissue samples were prepared by rapidly homogenizing in 5 volumes of boiling lysis buffer and boiling 5 minutes. Fifteen minutes of low speed centrifugation was used to remove insoluble material. Water content was determined using the BCA method. Blots were prepared using 15 μ g total protein on a 7.5-15% SDS-PAGE gel, and transferred to a nitrocellulose membrane (Hybond-Amersham). The membrane was blocked with 5% dried milk, 1% BSA in Tris buffer saline with 10 Mm Tris pH 7.5, 100 mM NaCl, 0.1% Tween 20 (TBS-T buffer) and incubated at 37°C for 30 min. After blocking and decanting the blocking buffer, the membrane was treated with primary antibody (1:500-1000 dilution with TBS-T buffer and 1% BSA) directed specifically against the particular antigen of interest at 37°C for 30 min. After washing, the blots were incubated with anit-mouse horseradish peroxidase conjugated affinity purified secondary antibody (1:1000-2000 diluted with TBS-T buffer and 5% dried milk) for 30 min at 37°C. After washing again with TBS-T buffer and adding ECL (Amersham Life Science Inc.) for 1 min, reacted blots were exposed to x-ray film for detection of antigen-antibody complexes.

Flow cytometry

Quantification of cellular FGF receptors on fibroblasts was determined using a

new immunocytochemical flow cytometry technique according to Zagursky's method (24). It provides a rapid qualitative method for determining the number of binding sites (receptors) on the surface of cells using immunofluorescence. Cultured fibroblasts were grown in plastic tissue culture T 125 flask (Corning Scientific Products, Corning, NY). Confluent monolayers were harvested using trypsinization. Pellets were washed with ice cold indicator free Hank's balanced salt solution, two times and suspended in D-PBS (pH 7.4) containing 0.1% sodium azide (to prevent receptor internationalization) at a concentration of 5×10^5 cells per 100 μl sample. Immunofluorescence staining of cell surface receptors was performed using a primary antibody (2 μl antiFGFR-1 was added to 100 μl of cells) for 30 min at 4° C. After incubation, the cells were washed three times with D-PBS containing 0.1% sodium azide and 2% (w/v) BSA and incubated with the secondary antibody (anti-mouse IgG R-phycoerythrin conjugate, dilution 1:40 with PBS) for 30 min at 4° C. After final washing with D-PBS contained 2% BSA and 0.1% sodium azide three times, the cells were maintained in light-proof containers containing 500 μl D-PBS at 4°C until analysis by flow cytometry. Fluorescence quantitation was performed using a Quantum Simply Cellular PE Micro beads kit (Sigma Chemical Com. Stock No. QSC-20W).

RESULTS

Cellular Localization

bFGF, aFGF and FGFR-1 were found to be expressed in tissue sections from neuroma specimens using indirect immunofluorescence (Fig. 1 A, B, C). Fibroblasts

within the neuroma were strongly positive for the protein as well as the receptor.

Schwann cells were also positive for bFGF, aFGF and FGFR-1. Positive identification of Schwann cells was carried out by using a receptor antibody which was found to be specific for Schwann cells in double-labeled immunofluorescence examination (anti-NGF receptor and anti-aFGF, anti-NGF receptor and anti-bFGF). Schwann cells with neural tissue still expressed immunoreactivity for FGFR-1.

Cells cultured to passage 4-5 were used for the cellular localization of bFGF, aFGF and FGFR-1. Both bFGF and a aFGF were localized throughout the cytoplasm of fibroblasts. In addition, the nucleus of fibroblasts were strongly stained for bFGF (Fig. 2 A) as compared to the staining pattern for a aFGF (Fig. 2B). Fibroblasts were also positively stained with FGFR-1. However, nuclear staining was not found for FGFR-1. Double-labeled immunofluorescence was used to examine if fibroblasts express both bFGF and FGFR1. Fibroblast samples were treated with two antibodies respectively (mouse monoclonal antibody to FGFR-1 and polyclonal rabbit antiserum to bFGF), followed by incubation with FITC labeled anti-mouse and TRICT-labeled anti-rabbit second antibodies. Results showed that the nuclei of fibroblasts were positively stained with bFGF (Fig. 2C), but not with FGFR-1 (Fig. 2D).

Immunoelectron microscopic localization

Subcellular localization of the growth factor and FGFR-1 were examined in cultured fibroblasts from neuroma samples using pre-embedding, immunogold labeling technique. Gold particles (15 nm diater) binding to bFGF sites were present in the

nucleus as well as cytoplasm (Fig. 3A). Gold particles binding to aFGF were found throughout the cytoplasm of fibroblasts. In comparison, gold particles were rare in nucleus (Fig. 3B). It was interesting to find gold particles binding to FGFR-1 focally present at regular intervals along the inner plasma membrane (Fig. 3C). However, bFGF, aFGF, and FGFR-1 were absent in all cytoplasmic organelles. These results further confirmed the above observations with immunofluorescence microscopy. All of the control studies using PBS instead of primary antibody gave negative results.

Western blot analysis

Extracts from human peripheral nerve neuroma tissue and cultured fibroblasts samples were examined with specific anti-bFGF and anti-FGFR-1 antibody respectively. Western blot analysis showed that immunoreactivity for bFGF expressed three different isoforms of molecular weight (18, 22 and 24 kDa)(Fig. 4). An increased expression for bFGF was observed in cultured fibroblasts than tissue samples. Immunoblot for FGFR-1 showed one band at 95 KDa in tissue samples and cultured fibroblasts (Fig. 5).

Flow cytometry

Cell membrane receptor quantitation by flow cytometry relies upon fluorescence and light scatter measurement of individual cells. Mean FGF receptor densities on the surface of live fibroblast were derived by comparison with standard R-phycoerythrin (PE)-labeled micro beads on which the number of equivalent soluble PE molecules per bead (range from 10^4 to 5×10^5) was plotted against the log of fluorescence intensity. It

permits the direct conversion of fluorescence intensity of the labeled cells into the number of molecules of equivalent soluble fluorochrome. The QuickCal software in the kit is designed to automatically construct a calibration curve and process data. The results showed that number of FGF receptor-1 on surface of per fibroblast was on the average 5600.

DISCUSSION

Recently, the biologic role of fibroblast growth factors and their receptors in normal and pathologic conditions has generated much interest. The best characterized are bFGF, aFGF and FGF receptor-1. Although they have been identified in a variety of cell type and tissues, available information about their localization in tissue and cell from human peripheral nerve neuroma is very limited. Our immunolocalization study revealed that fibroblasts in connective tissues and Schwann cells from human peripheral nerve neuroma expressed immunoreactivity for bFGF, aFGF and FGFR-1 in vivo. Since fibroblasts are a major component in the formation of a neuroma, further, cellular localization of bFGF, aFGF and FGFR-1 was examined using cultured fibroblasts from neuroma samples. We found that bFGF was mainly localized in the nucleus and less intensely to the cytoplasm of fibroblasts while aFGF was mainly distributed throughout the cytoplasm. FGFR-1 localized mainly along fibroblast plasma membrane and in a regular fashion. Moreover, membrane surface FGF receptor-1 on living fibroblasts was detected to be about 5600 per cell. However, FGFR-1 was not detected in the nucleus of fibroblasts. The detailed characterization of these FGF

factors and FGFR-1 provide a necessary prerequisite for understanding their function in formation of human neuroma.

The biological response of FGFs is mediated by their binding to specific cell surface receptors. High affinity receptors for bFGF and aFGF have been found on the surface of many cell types including endothelial cells, smooth muscle cells, fibroblasts, gliomas, chondrocyte, hepatocyte and epithelia cells (25- 26). Our study found that FGFR-1 was located at regular intervals along cell membrane surface of fibroblasts. The same distribution pattern of FGFR-1 was observed in the endothelial plasma membrane (27). A significant correlation is found between the expression level of FGFR-1 and that of bFGF in tissues of human glioma (28). Moreover, FGFR-1 shows higher binding affinity for bFGF than for aFGF (29). Thus, the results suggest that bFGF may play a more important role than aFGF in neuroma growth. Particularly, cytoplasm distribution of aFGF and bFGF as well as membrane localization of FGF receptor-1 were simultaneously found in fibroblasts in our study. To our knowledge, no one has reported the same observation in human peripheral nerve neuroma. It suggests that after injury of peripheral nerve, fibroblasts not only can initiate a series of cellular reactions that include invasion of the injury site by inflammatory cells and activation of the Schwann cells by producing and releasing the growth factors, but also may participate in repair of injury through an autocrine mechanism. Recently, activation of the FGF receptor has been found to underlie neurite outgrowth stimulated by CAMs (such as L1, N-CAM, and N-cadherin) (17), with the initiation of tyrosine phosphorylation and the formation of arachidonic acid as a second messenger.

Moreover, they have identified a CAM homology domain in the FGF family of receptors and show that antibodies which bind to this domain specifically inhibit neurite outgrowth stimulated by the above CAMs. It is more interesting that a synthetic peptide derived from this domain can differentially and specifically direct neurite outgrowth stimulated by these CAMs.

In the normal nerve, an important function of Schwann cells and endoneurium is to insulate axons from the surrounding tissues. When a nerve trunk is damaged, regrowing axons leave the nerve trunk through the defect. The perineurial cells such as fibroblasts enclose small numbers of myelinated or unmyelinated axons, leading to the formation of nodule, bulb or neuroma that consists mainly of fibroblasts and Schwann cells (16).

In conclusion, the present immunolocalization study in tissue section found that both fibroblasts and Schwann cells express bFGF, aFGF and FGFR-1. Further study in cultured fibroblasts from neuroma samples found different localization feature of three peptides. Characterization of localization of bFGF, aFGF and FGFR-1 in various cells type as well as different localization feature in same cells will be useful for understanding of different important role of the growth factors in formation of peripheral nerve neuromas.

FIGURE LEGENDS

Fig. 1. Immunofluorescent staining of human peripheral nerve neuroma tissue frozen sections with specific antibody against bFGF (Fig. 1A), aFGF (Fig. 1B), FGFR-1 (Fig. 1C). These sections (12 μm) were fixed with 4% paraformaldehyde. Abundant fibroblasts in connective tissue and Schwann cells were positively stained for aFGF bFGF and FGF receptor-1, this included abundant fibroblasts and a few Schwann cells and remnants of axons. bFGF expressed stronger positivity as compared with aFGF and FGFR-1. Original magnification, Fig. 1A and 1B X 125; Fig. 1C X 62.5.

Fig. 2. Immunofluorescent staining of cultured fibroblasts from human peripheral nerve neuroma with specific antibody against bFGF and aFGF. Although fibroblasts were positively stained with both bFGF and aFGF, there is strong positivity in the nucleus of fibroblasts with bFGF (Fig. 2A). aFGF expressed immunoreactivity mainly in cytoplasm of fibroblasts (Fig. 2B). Double-labeling Immunofluorescent staining in cultured fibroblast with specific antibody against bFGF and FGFR-1. The results showed that fibroblasts were positively stained with both bFGF and FGFR-1. Strong immunoreactivity for bFGF was observed in the nucleus of fibroblasts. (Fig. 2C) but less staining for FGFR-1 was observed in the nucleus of fibroblasts. (Fig. 2D). Original magnification X 125.

Fig. 3. Immunoelectron microscopic localization of bFGF, aFGF and FGFR-1 in

cultured fibroblasts from human peripheral nerve neuroma using pre-embedding immunogold labeling. Gold particles (15 nm diameter) binding to bFGF sites mainly expressed at the nucleus and a few at cytoplasm of fibroblasts (Fig. 3A). Immunogold particles binding to aFGF sites were present largely in cytoplasm of fibroblasts (Fig. 3B). It is interesting that gold particles binding to FGFR-1 were focally present at regular interval along the fibroblast plasma membrane (Fig. 3C). However, the gold particles binding to these peptide were absent in all cytoplasmic organelles. Bar: A and B = $60\mu\text{m}$; C and D= $1\mu\text{m}$.

Fig. 4. Western blot analysis of tissue samples and cultured fibroblasts of human peripheral nerve neuroma. The samples were electrophoresed on 15% SDS gels, and transferred to a nitrocellulose membrane. Immunoreactivity for bFGF was expressed using $1\mu\text{g/ml}$ mouse monoclonal antibody against human bFGF, bFGF showed to have three different molecular weight (18, 22 and 24 Kda). Lane 1 is a positive control from human fibroblasts. Lane 2, 3 and 4 are tissues from human neuroma; lanes 5 and 6 are cultured fibroblasts from human neuromas. Increased expression of bFGF was observed in cultured fibroblasts as compared to tissue samples.

Fig. 5. Western blot analysis of tissue samples and cultured fibroblasts of human peripheral nerve neuroma. The samples were electrophoresed on 7.5% SDS gels, and transferred to a nitrocellulose membrane. Immunoreactivity for FGFR-1 was expressed using $1\mu\text{g/ml}$ mouse monoclonal antibody against human FGFR-1. The results

showed that FGFR-1 was seen at 95 kDa. Lanes 1 and 4 are cultured fibroblasts from human neuromas, lanes 2 and 3 are tissues samples from human neuroma, lane 5 is a positive control from human fibroblasts.

REFERENCES

1. Thomas KA, Gimenez-Gallego G: Fibroblasts growth factors: broad spectrum mitogen with potent angiogenic activity. *Trends Biochem Sci* 1986;11:81-84.
2. Tanaka AK, Miyamoto N, Minamino M, Takeda M, Sato M, Matsuo H and Matsumoto K: Cloning and characterization of an androgen-induced growth factor essential for the androgen-dependent growth of mouse mammary

carcinoma cells. *Proc Natl Acad Sci USA* 1992;89:8928-8932.

3. Abraham JA, Mergia A, Whang JL, Tumolo J, Friedman D, Gospodarowicz D and Fiddes JC: Nucleotide sequence of a bovine clone encoding the angiogenic protein, basic fibroblast growth factor. *Sciences* 1986;233:543-546.
4. Esch F, Ueno N, Baird A et al.: Primary structure of bovine brain acidic fibroblast growth fact (FGF). *Biochem Biophys. Res. Commun* 1985;133:554-562.
5. Burgess WH and Maciag T: The heparin-binding (fibroblast) growth factor family of proteins. *Ann Rev Biochem* 1989;58:575-606.
6. Rifkin DB and Moscatelli D: Recent developments in the cell biology of basic fibroblast growth factor. *J Cell Biol* 1989;109:1-6.
7. Neufeld G, Gospodarowicz D: Basic and acidic fibroblast growth factor interact with the same cell surface receptor. *J. Biol Chem* 1986;261:5631-5637.
8. Folkman J, Klagsbrun M: Angiogenic factors. *Science* 1987;235:442-447.
9. Gospodarowicz D: Fibroblast growth factor and its involvement in developmental processes. *Curr Top Dev Biol* 1990;24:57-93.

10. Houssaint E, Blanquet PR, Champion-Arnaud P, Gesnel MC, Torriglia A, Courtois Y, Breathnach R: Related fibroblast growth factor receptor genes exist in the human genome. *Proc Natl Acad Sci USA* 1990;87:8180-8184.
11. Keegan K, Johnson DE, Williams LT, Hayman MJ: Isolation of additional member of the fibroblast growth factor receptor family. FGFR-3. *Proc Natl Acad Sci USA* 1991;88:1095-1099.
12. Partanen J, Makela TP, Erola E, Kohonen J, Hirovenen H, Claesson-Welsh L, Alitalo L: FGFR-4, a novel acidic fibroblast growth factor with a distinct expression pattern *EMBO J* 1991;10:1347-1354.
13. Ruta M, Burgess W, Givol D, Epstein J, Neiger N, Kaplow J, Crumley G, Dionne C, Jaye M, Schlessinger J: Receptor for acidic fibroblast growth factor is related to the tyrosine kinase encoded by the fms-like gene (FLG). *Proc Natl Acad Sci USA* 1989;86:8722-8726.
14. Johnson DE, Lee PL, Lu J, Williams LT: Diverse forms of a receptor for acidic and basic fibroblast growth factor. *Mol Cel Biol* 1990;10:4728-4736.
15. Yazaki N, Hosoi Y, Kawabata K et al.: Differential expression patterns of mRNAs for members of the fibroblast growth factor receptor family, FGFR-1, FGFR-4, in

rat brain. *J Neuro Res* 1994;37:445-452.

16. Sunderland S: *Nerve and Nerve Injury*, 2nd ed, Churchill Livingstone, New York, pp. 180-193.

17. Williams EJ, Furness J, Walsh FS, Doherty P: Activation of the FGF receptor underlies neurite outgrowth stimulated by L1, N-CAM, and N-cadherin. *Neuro* 1994;13:583-594.

18. Root L, Shipley GD: Human dermal fibroblasts multiple bFGF and aFGF proteins. *Vitro Cell Dev Biol* 1991;27A:815-822.

19. Hughes SE and Hall PA: Immunolocalization of fibroblast growth factor receptor 1 and its ligand in human tissues. *Lab Invest* 1993;69:173-182.

20. Suzui H, Takahashi JA, Fukumoto M et al: Immunohistochemical study for basic fibroblast growth factor and fibroblast growth factor receptor I in pituitary adenomas. *Neuroscience letters* 1994;171: 192-196.

21. Yabu M, Shinomura Y, Minami T, Matsuzawa Y: Immunohistochemical localization of basic fibroblast growth factor in the healing stage of mouse gastric ulcer. *Histochemistry* 1993;100:409-413.

22. Zhao S, Zhang D, Kline DG, Beuerman RW et al: Increase in basic fibroblast growth factor and fibroblast growth factor receptor-1 following sciatic nerve injury and neuroma formation. *Abstracts of Society for Neuroscience* 1995;21: 497.

23. Lopez JG, Chew SJ, Thompson HW, Malter JS, Insler MS, Beuerman RW: EGF cell surface receptor quantitation on ocular cells by an immunocytochemical flow cytometry technique. *Invest Ophthalmol Vis Sci* 1992;33:2053-2062.

24. Zagursky RJ, Sharp D, Solomon KA, Schwartz A: Quantitation of cellular receptors by a new immunocytochemical flow cytometry technique. *BioTechniques* 1995;18:504-509.

25. Eckenstein FP, Kuzis K, Nisei et al: Cellular distribution, subcellular localization and possible functions of basic and acidic fibroblast growth factors. *Biochemical Pharmacology* 1994; 47:103-110.

26. Klagsbrun M: The fibroblast growth factor family: structural and biological properties: Progress in growth factor research. *Great Britain Pergamon Press* 1989: 207-235.

27. Amin R, Puklin JE, Frank RN: Growth factor localization in choroidal neovascular membranes of age-related macular degeneration. *Invest Ophthalmol Vis Sci*

1994;35:3178-3188.

28. Ueba T, Takahashi JA, Fukumoto M et al: Expression of fibroblast growth factor receptor-1 human glioma and meningioma tissues. *Neurosurgery* 1994;34:221-226.
29. Duan DR, Werner S, Williams LT: A naturally occurring secreted form of fibroblast growth factor (FGF) receptor 1 binds basic FGF in preference over acidic FGF. *J Biol Chem* 1992;267:16076-16080.

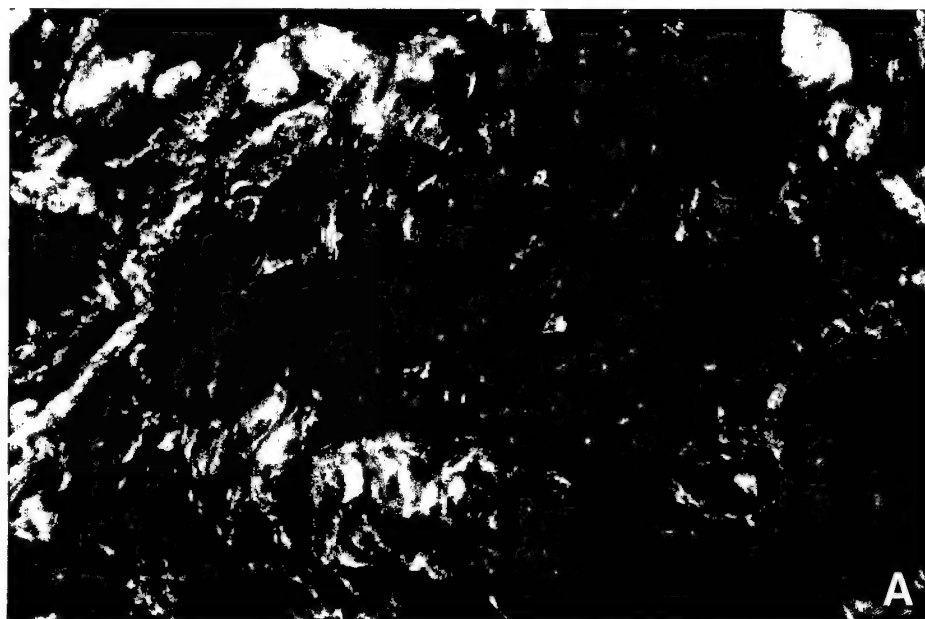


Figure 1A.

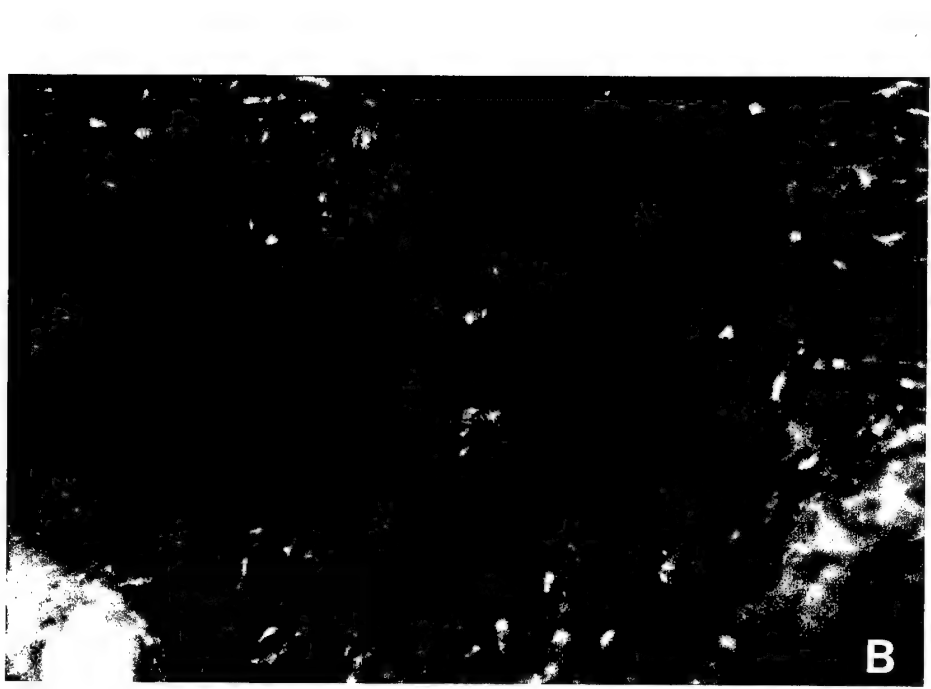


Figure 1B.



Figure 1C.

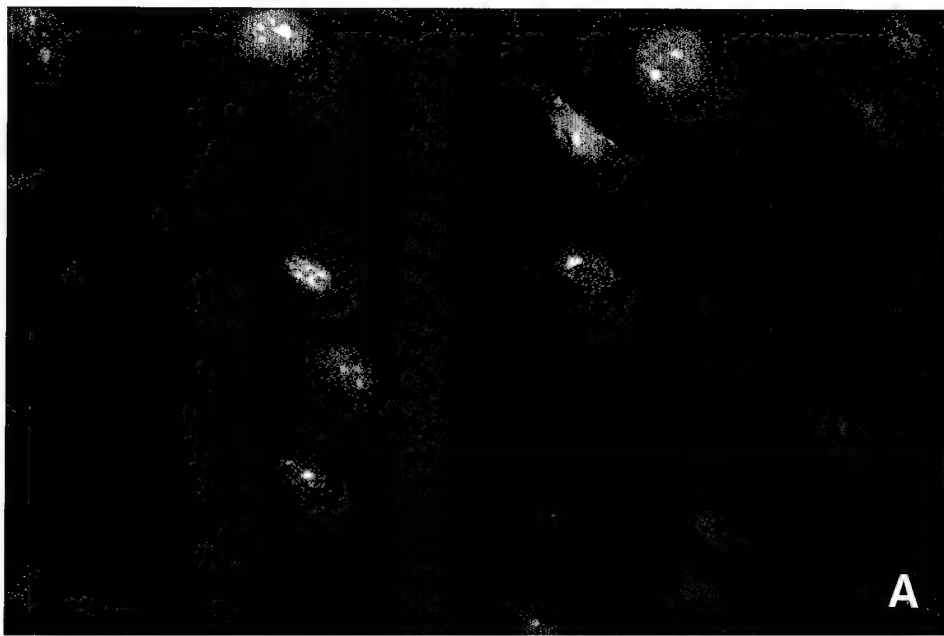


Figure 2A.

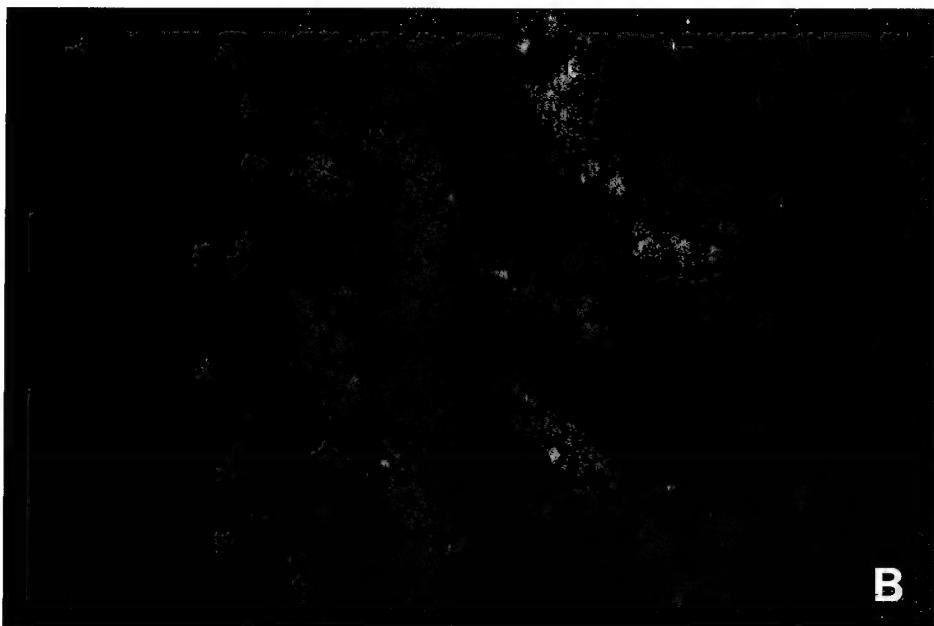


Figure 2B.



Figure 2C.



Figure 2D.

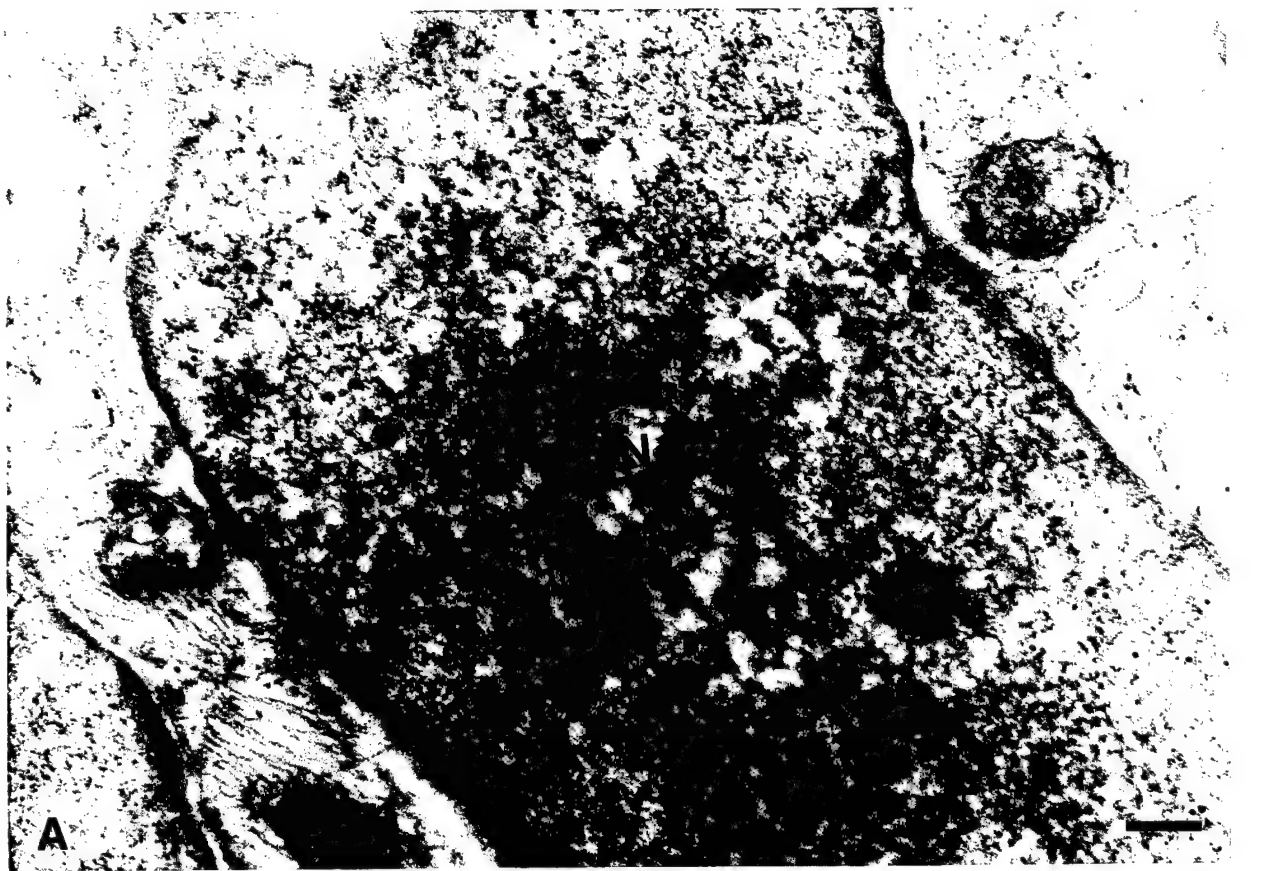


Figure 3A.

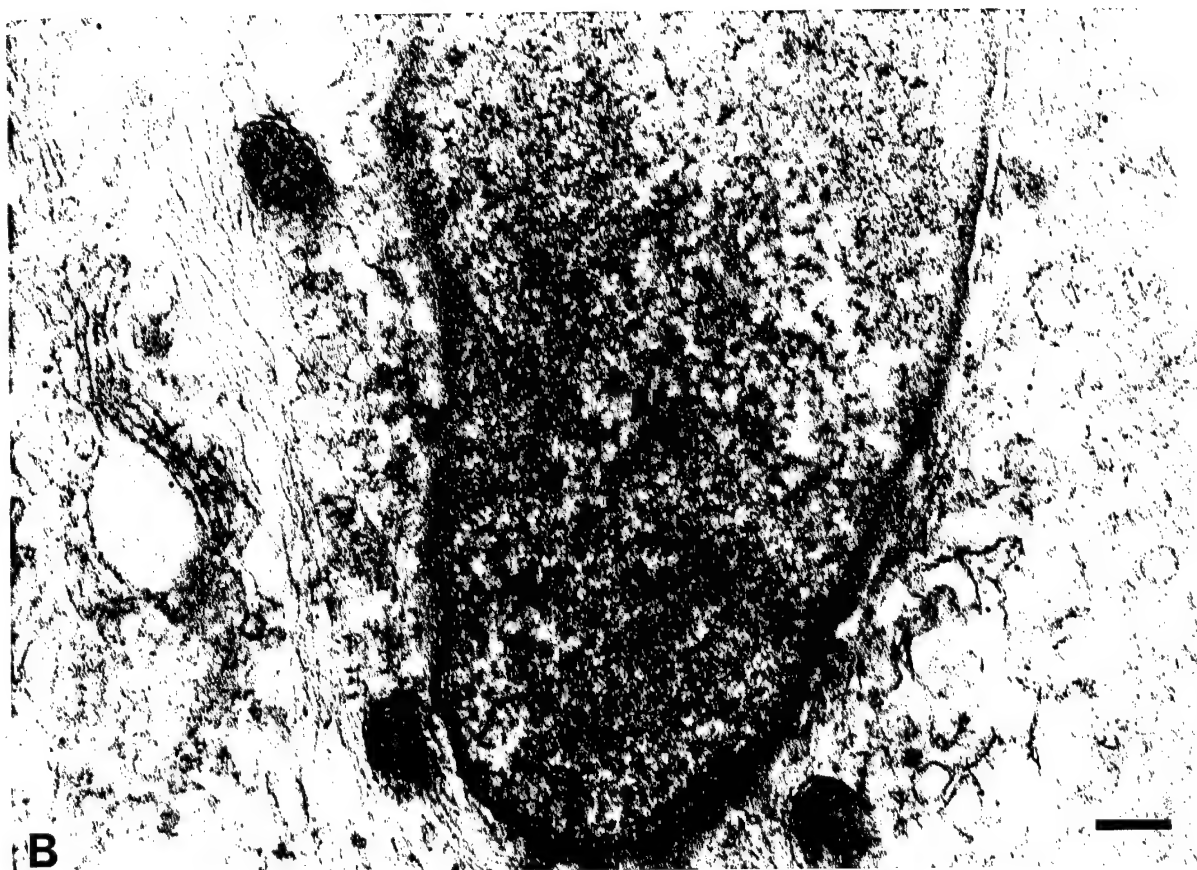


Figure 3B.

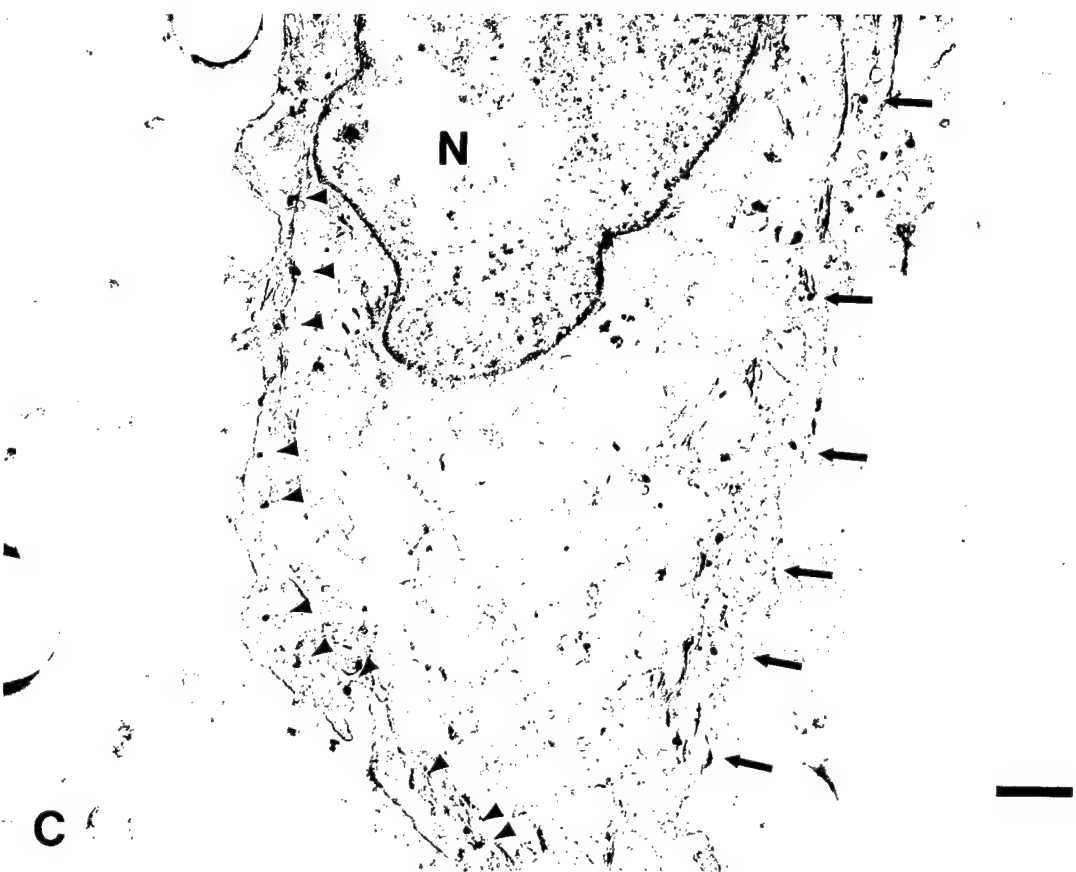


Figure 3C.

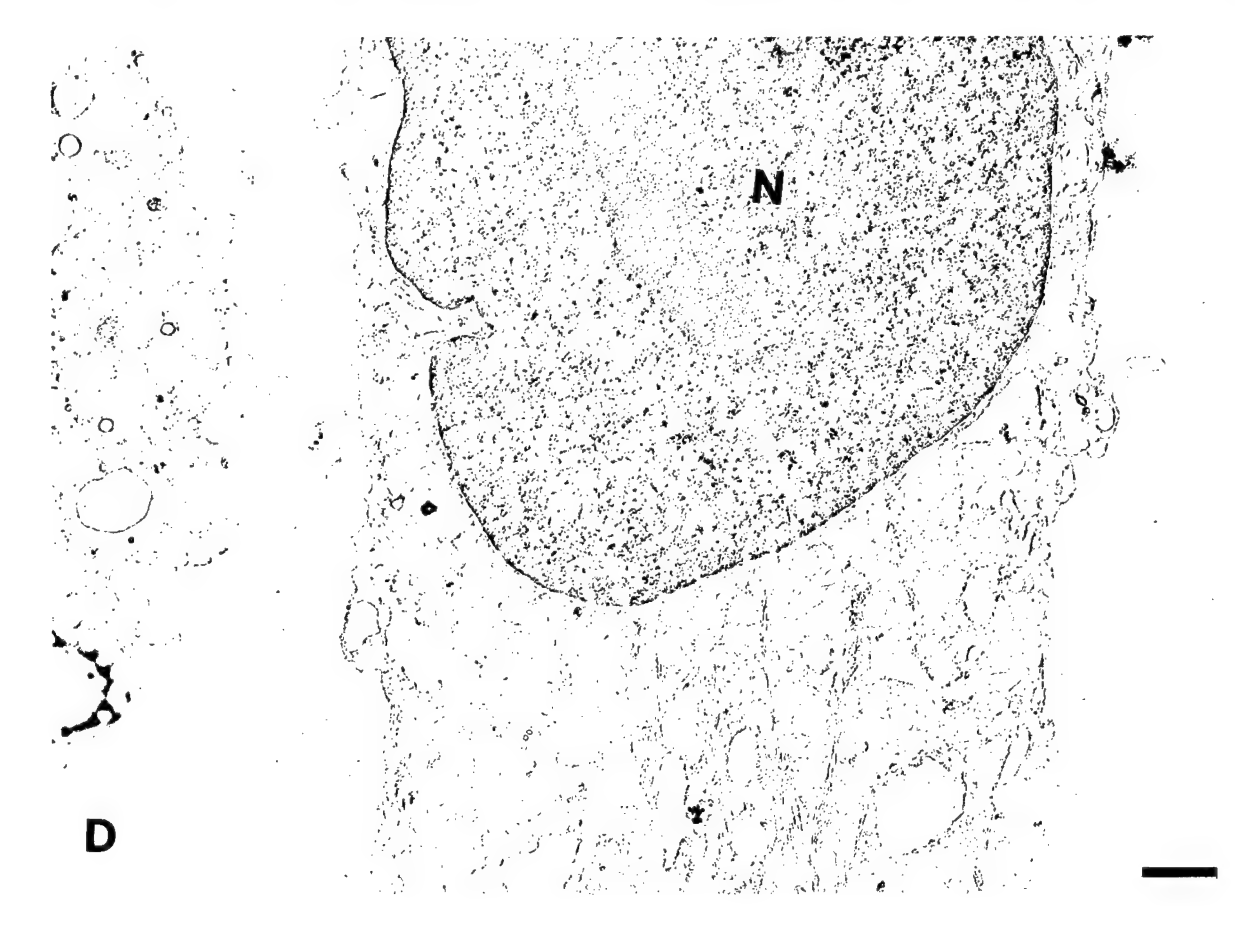


Figure 3D.

Fig. 4

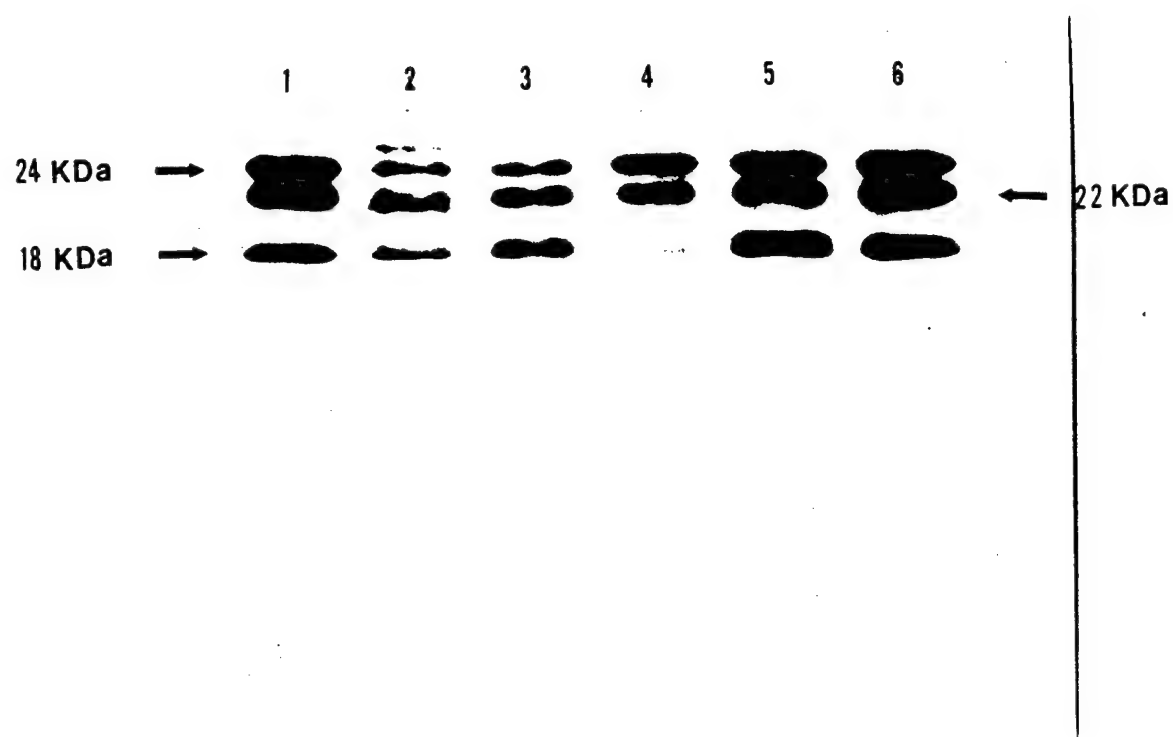
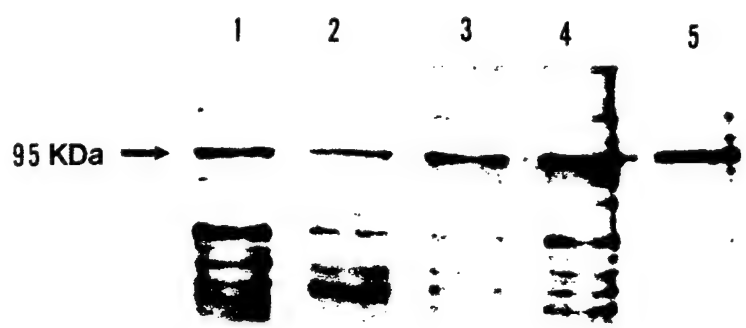


Fig. 5



IV. GROWTH FACTORS REGULATION OF INJURY NERVE FIBROBLAST PROLIFERATION REQUIRES ACTIVATION OF MAPK SIGNAL TRANSDUCTION PATHWAY

INTRODUCTION

Peripheral nerve injuries are often the result of accidents. The successful restoration of damaged nerve function depends on correct repairing and properly directed axonal regeneration. Unfortunately, a lesion or neuroma in continuity, is often formed in the damaged nerves, even at the site of surgical repair, which blocks axons from reaching the distal stump. A neuroma is mainly composed of excessively proliferating fibroblasts along with collagen and extra cellular matrix. Nerves are found to be of small caliber, and disorganized Schwann cells fail to form myelin of proper thickness. In the injured site, the endoneurial and perineurial elements rapidly proliferate and lay down poorly structured collagen, which interferes with axonal regeneration. At the same time, regeneration of axons must first make up the retrograde damage proximal to the injury site. Moreover, in suturing or grafting sites, the epineurial and interfascicular epineurial connective tissue proliferation is mainly involved in the neuroma. On the other hand, if connective tissue involvement is mild with relative preservation of perineurial and endoneurial tissue moderate proliferation of intraneurial cells, axons regenerate well, the regenerative units reach distal structures after minimal branching, and individual axons come close to prior innervational inputs and eventually regain an adequate degree of caliber and myelination which leads to a good outcome, restoration of useful function. The biological behavior and activity of the fibroblasts in the injury sites play a vital role in the process of nerve regeneration and restoration of its function, yet when uncontrolled the fibrosis may lead to loss of regeneration.

It is clear that multiple growth factors and preinflammatory factors are involved in nerve peripheral regeneration and fibroblast proliferation. Our previous studies also demonstrated that bFGF and its receptor (bFGFR) are active within in neuroma tissues (1-2). Moreover, growth factors promote fibroblast proliferation in human diploid FS-4 skin fibroblasts, NIH 3T3 cells, and other cells by activation of Raf-1, MEKK, MAPKK (MEK), and MAPK signal transduction pathway. The mitogen activated protein kinase (MAPK), or extracellular regulated kinase (ERKs), is in the center of this pathway, between membrane events and gene activation. Mutations in the regulatory domain of MAPKK and MAPK have been used to show a direct linkage of these enzymes to proliferation. Overexpression of nonactivateable forms of MEK-1 in NIH-3T3 cells significantly reduced their rate of proliferation, which was correlated to a similar reduction in MAPK activity. Constitutively activated MEK-1 raised the basal MAPK activity and caused accelerated proliferation. However, activation of MAPK does not always lead to cellular proliferation, for example, in a PC-12 cell line, NGF activates MAPK, and induces PC-12 cell differentiation other than proliferation. This suggests that MAPK is one of several pathways that regulates cellular proliferation. Activated MAPK translocates into the nucleus and increases DNA synthesis by regulating the formation of transcription factors, c-fos, c-jun, and AP-1 complex. MAPK also regulates the G0/G1 transition of the cell cycle in fibroblasts.

Growth factors induce activation of MAPK and DNA synthesis in human neuroma fibroblasts.

We used growth factors (bFGF, EGF, PDGF, NGF, and IL-1, TNF-a) to stimulate human neuroma fibroblasts which were cultured in D-MEM medium, grown to confluence, and serum starved for 24 hours. Myelin basic protein was taken as substrate, and the activity of MAPK in the

lysis from stimulated cells was measured. We compared the increase in production of MAPK by increasing concentration of growth factors with phorbol 12-myristate 13-acetate (PMA), which is a potent activator for MAPK. Our results showed that all of these factors increased MAPK activity in human neuroma fibroblasts (Fig. 1). The mitogenic assay demonstrated ³H-thymidine uptake which significantly increased after incubation of the cells in the medium containing these factors (Fig. 2). Previous reports have described that those factors appear in injury sites of nerves. Our data suggests after peripheral nerves are injured, the break-down of the blood-nerve barrier can allow inflammatory cells to migrate to the area of injury and secrete growth factors which bind to their receptors on the membrane of the fibroblasts. Activation of MAPK signal transduction pathway will then induce the quiescent cells to proliferate as part of the repair process.

PREVENTION OF GROWTH FACTOR INVOLVED MITOGENIC EFFECTS BY INHIBITION OF MAPK PATHWAY

MAP kinase kinase or MAPKK is a dual-function upstream kinase that phosphorylates MAPK on threonine and tyrosine. In order to further confirm that MAPK is closely related to neuroma fibroblast proliferation and to find a potential therapeutic way to accelerate nerve regrowth to distal stumps by inhibiting fibroblast proliferation and reducing formation neuroma, is a major barrier for axon growth. A chemical compound, PD98059 is specific MEK inhibitor. Inhibition of MEK would produce decreased activity of MAPK and may block mitogenic effects of some growth factors and stop cell cycle transition from G₀/G₁ which requires activation of MAPK. We used PD98059 pretreated the cells for one hour, MAPK activity and ³H thymidine uptake was decreased to control levels (Fig.3 and 4). This inhibitor blocks bFGF, EGF, PDGF, NGF, PMA, and IL-1,

TNF- α mitogenic effects in the cells.

Although IL-1 and TNF- α are able to activate three intracellular pathways in fibroblasts. We have confirmed two pathways, MAPK and SAPK, were activated in human neuroma fibroblasts after treating the cells with TNF- α and IL-1 (*Tumor necrosis factor alpha and interleukin-1 induce activation of MAP kinase and SAP kinase in human neuroma fibroblast; in press*). Now we find that blocking MAP kinase pathway, DNA synthesis in fibroblasts treated with TNF- α and IL-1 also decreases. To our knowledge, we are first to demonstrate that TNF- α and IL-1 induce fibroblast proliferation through activation of MAPK. TNF- α and IL-1 activate three pathways in fibroblasts, which indicates that those pathways coordinate cell proliferation. The chemical (PD-98059) potential usefulness needs further study in vivo. Another pathway, P40 in human cells, or P38 in murine cells, and MAPkinase activated protein kinase-2 (MAPKAP kinase-2) is also under study. At present, we are trying to confirm the activation of this pathway after treating the cells with TNF- α and IL-1 to test the events after blocking RK, P40 or P38, MAPKAP kinase-2 pathway with another new inhibitor, SB203580.

WOUNDING A FIBROBLAST MONOLAYER INDUCES A RAPID ACTIVATION OF MAP KINASE (*mimicking the early stages of injury nerves*)

The fibroblast monolayer was wounded by crossed lines with a plastic pipette tip and 30 minutes later, the cells were harvested and MAPK was measured. The activity of MAPK is higher after scratching four lines than after making two lines and is not much different in serum free media or in media supplemented with 10% FBS. This suggests that the activity is related with the number of wounded cells and is independent of growth factors. The precise mechanisms need to be

elucidated. It is obvious that the wounding is a stress to the cells, and results in alteration of the plasma membrane, disruption of intercellular communication, the change of anion concentration between extra and intra cellular events. What induces rapid activation of MAPK which may be very important for alerting the quiescent fibroblast to respond to extracellular stimuli and lead the cells to proliferation rather than apoptosis is not clear. The further study should focus on MAPK activity kinetic change, and jurisdiction of the margin cells of wounded monolayers which are survivor after injury. Previous studies demonstrate that c-fos protein increases to a peak at 1 and 2 hours and decreases at 3 hours. It almost disappears at 24 hours. Accordingly MAPK regulation by c-fos protein, we believe that the peak of MAPK activity may be within the first two hours following wounding.

MINOXIDIL SUPPRESSES HUMAN NEUROMA FIBROBLAST PROLIFERATION

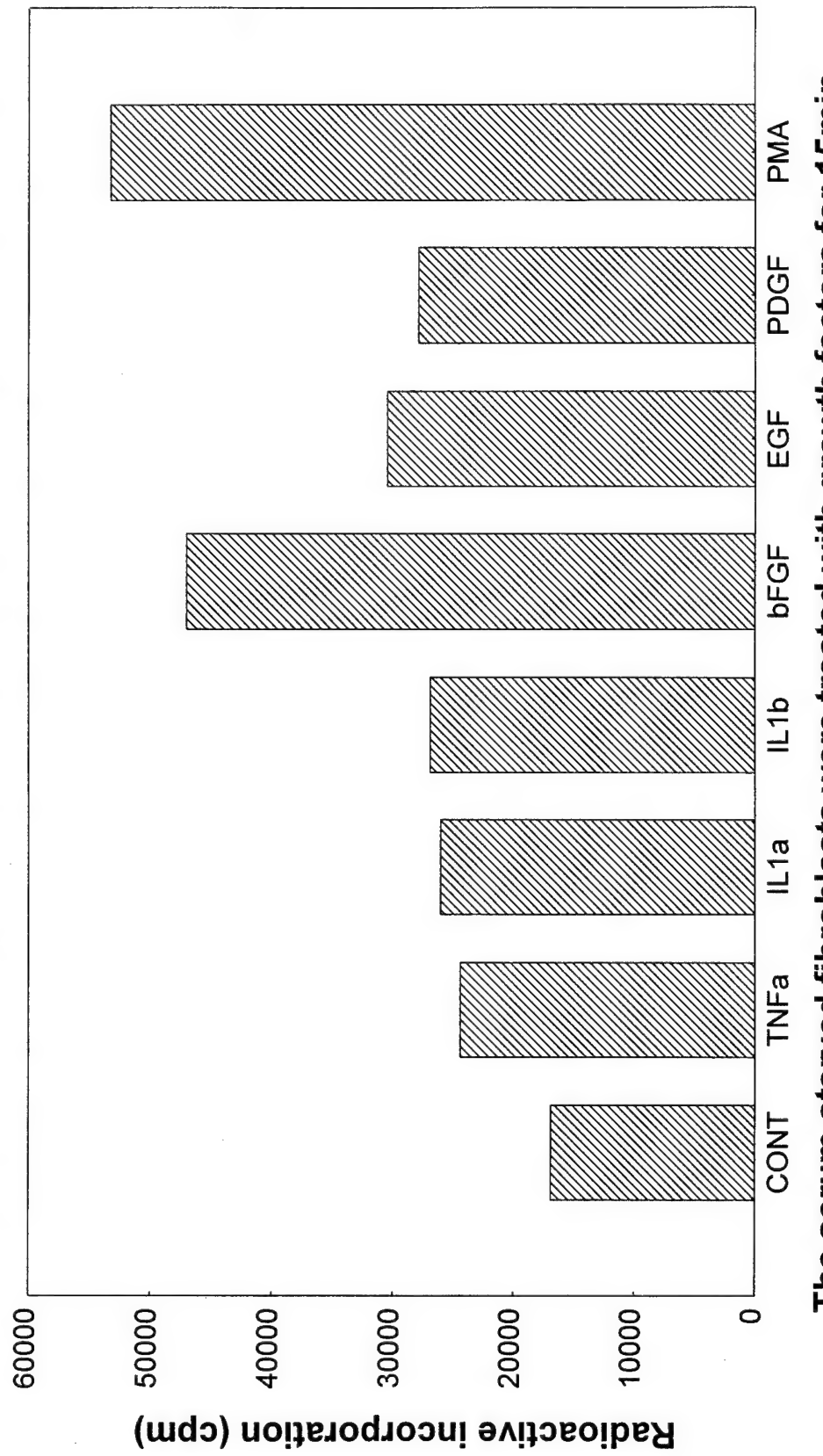
Minoxidil, an antihypertensive pyrimidine oxide and a lysyl hydroxylase inhibitor, has been shown to have functions to inhibit proliferation of human skin fibroblasts and rabbit corneal fibroblasts in culture without cytotoxicity and also blocks collagen production which is closely related to scar formation.

We cultured the human neuroma fibroblasts to 50% of confluence and added 1mM, 2mM, 4mM minoxidil into the medium respectively. 72 hours later, we found that at 2mM and 4mM of dishes, the cell number decreased remarkably compared with the control. The morphology of the cells changed becoming larger and elongated. The cells in the dish containing 1mM minoxidil showed little change. Ninety-six hours after withdrawal of minoxidil, the cells in the dish containing 2mM minoxidil grew well, and finally to confluence, but the cells cultured at higher concentrations

of minoxidil recovered slowly.

Our observations are consistent with previous reports in other cell line studies. This result suggests that the chemical minoxidil may be a useful tool to block neuroma formation.

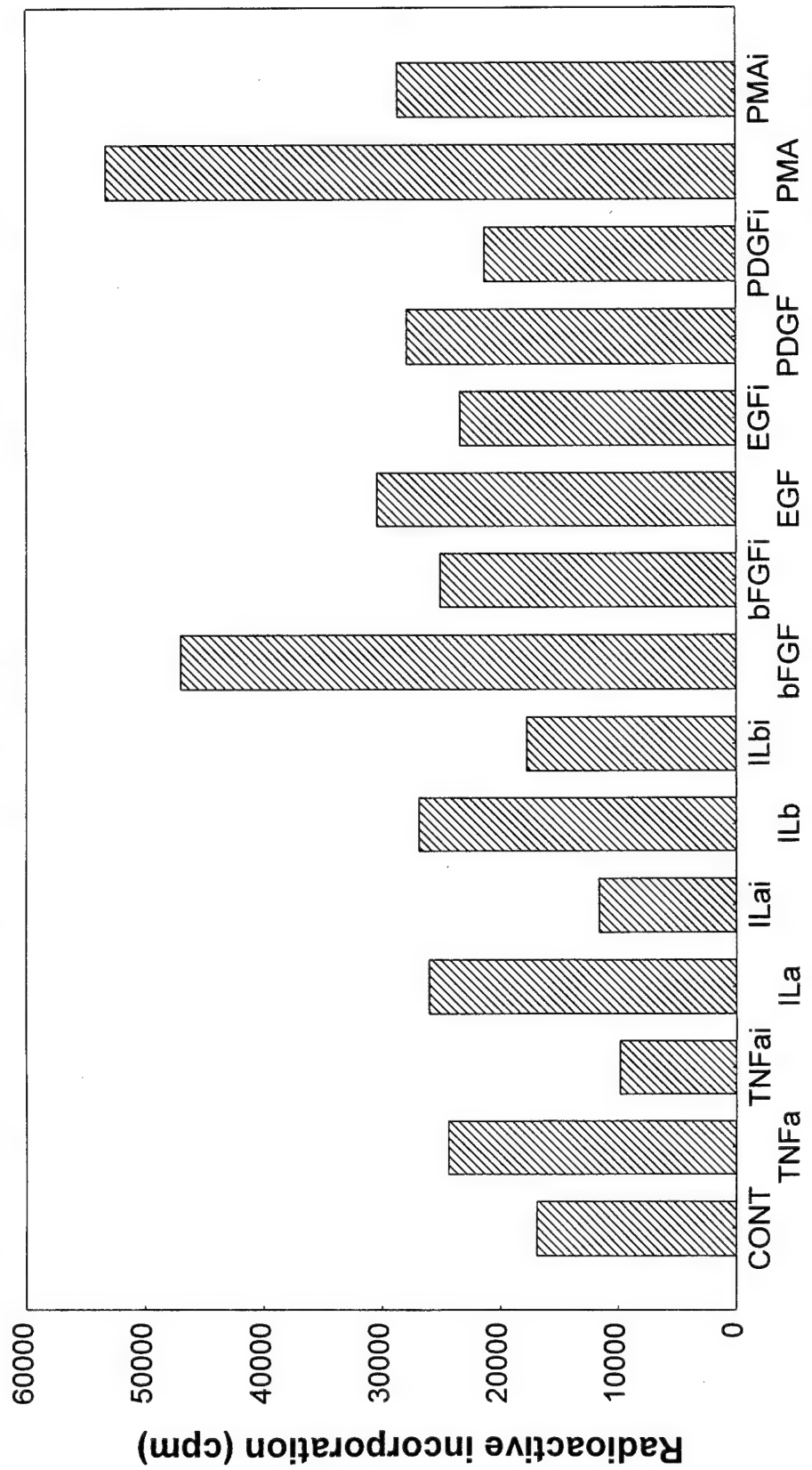
MAP KINASE ACTIVITY IN HUMAN NEUROMA FIBROBLASTS



The serum-starved fibroblasts were treated with growth factors for 15min

Figure 1.

MAP KINASE ACTIVITY IN HUMAN NEUROMA FIBROBLASTS



The fibroblasts were treated with growth factors and inhibitor (i), PD 98059

Figure 2.

GROWTH FACTOR MITOGENIC EFFECTS ON HUMAN NEUROMA FIBROBLASTS

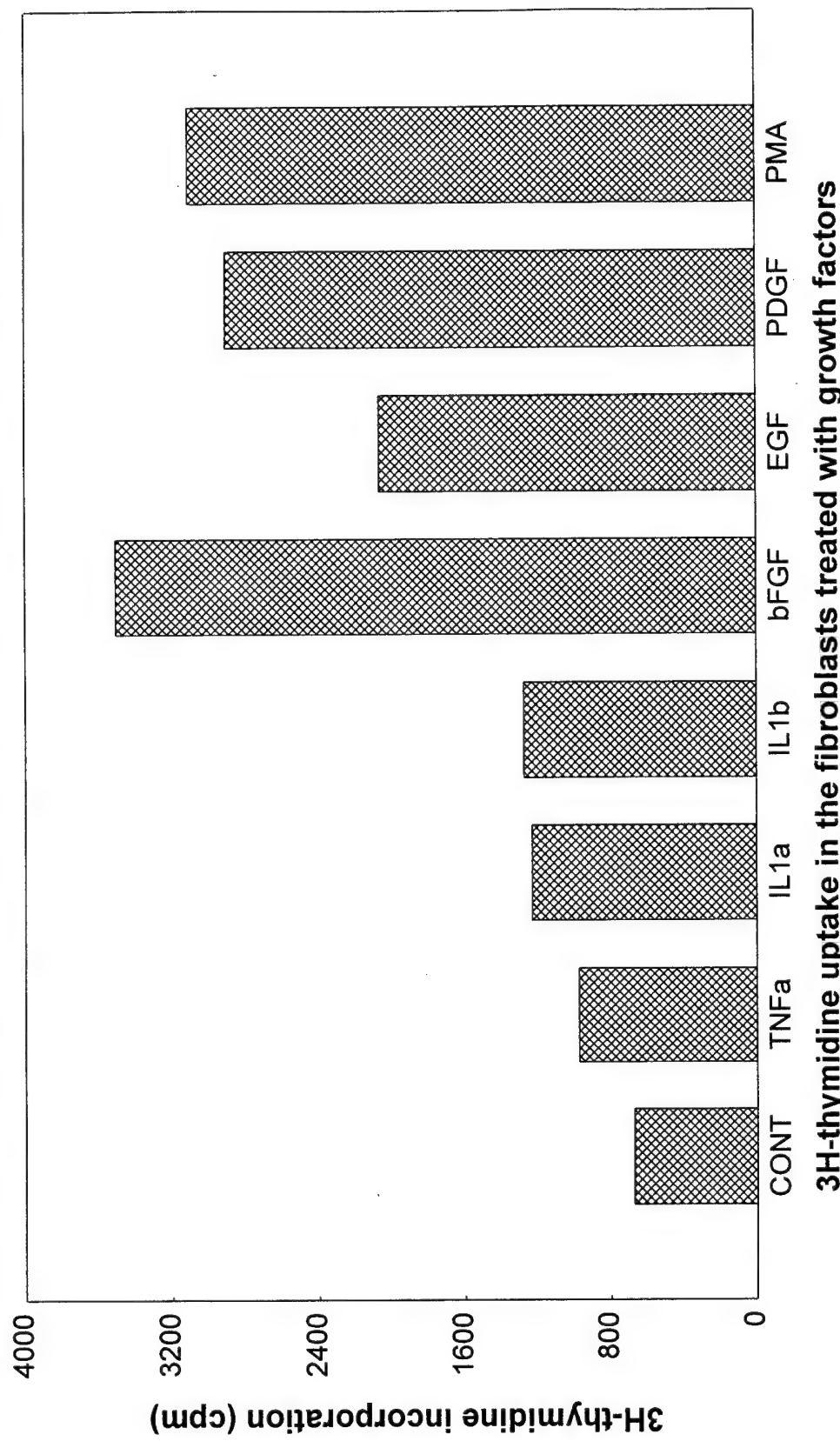
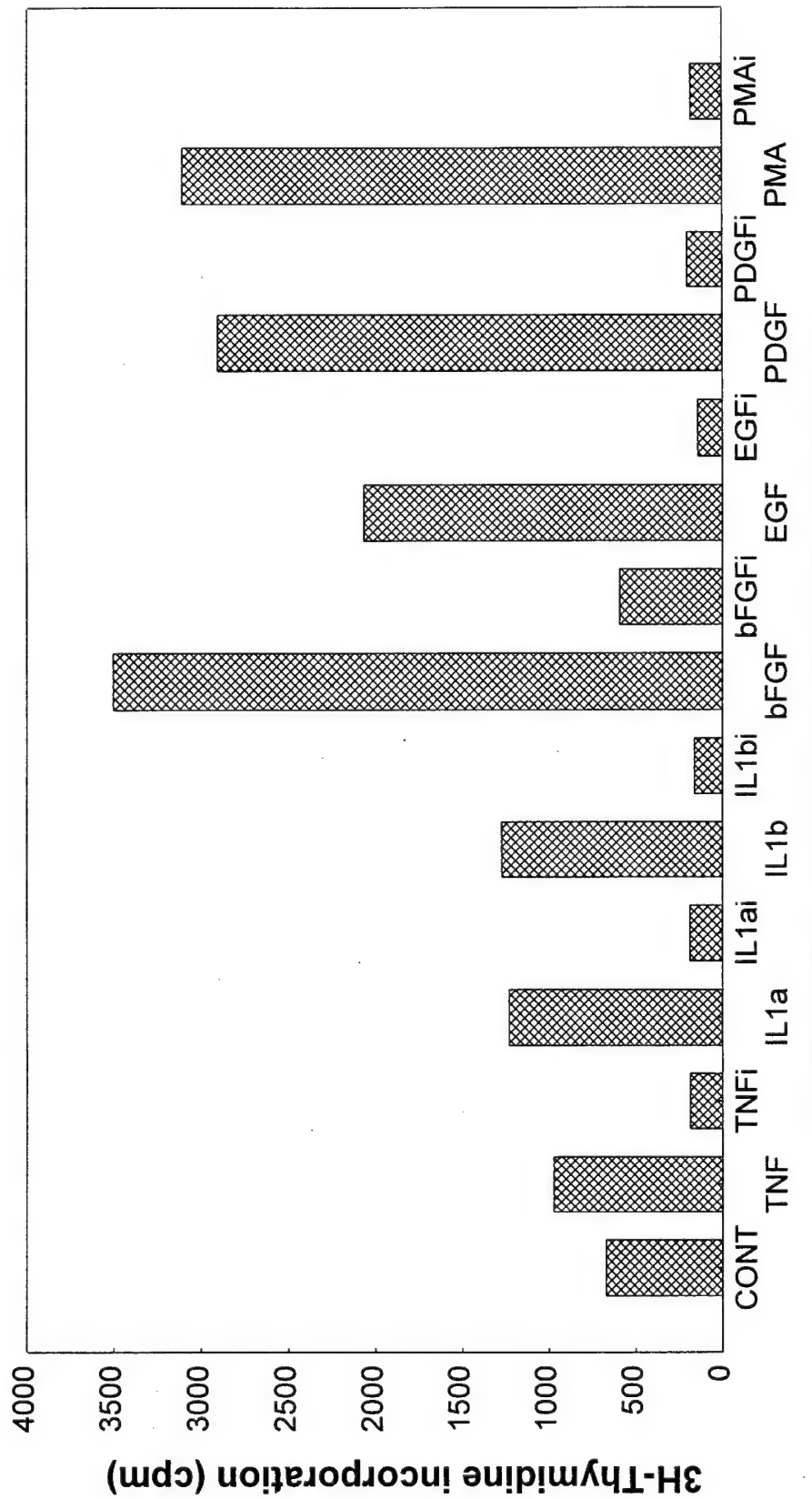


Figure 3.

GROWTH FACTOR MITOGENIC EFFECTS ON HUMAN NEUROFIBROMA FIBROBLASTS



The fibroblasts uptake ^{3}H -thymidine after treatment with
growth factors or combination with inhibitor

Figure 4.

V. INCREASE OF GAP-43 PROTEIN IN SCIATIC NERVE INJURY AND NEUROMA FORMATION

The purpose of this study has been to determine whether a protein associated with nerve injury, GAP-43, increases differently depending on whether or not a nerve injury lead to neuroma or to a non-neuroma condition.

Neuroma is the most common consequence of peripheral nerve injury. After nerve injury or repair, disorganized fibroblasts and Schwann cells form a barrier that the regenerating axons cannot penetrate, forming a bulb-like enlargement which is referred to as an neuroma. While the mechanism of neuroma development is not clear, some growth related factors are considered to be involved in the process. The increase of GAP-43 protein occurs by phosphorylation by protein kinase C (PKC) after injury has been implicated in the release of specific substances from nerve terminals which are important to the process of wound-healing and repair. Previous studies have indicated that nerve ends that have the endoneurium sealed with a bipolar coagulator or that are buried in muscle are less likely to produce a neuroma, compared with the nerve ends that are ligated or untreated. The neuroma can be formed within two weeks in rats after sciatic nerve injury.

The current study was designed to determine if the expression of the neuronal growth-related protein GAP-43, after sciatic nerve lesion and in early stages of neuromal development are different depending on the treatment of these severed ends. The sciatic nerves of adult rats were severed below the sciatic nerve notch and the severed ends were treated in one of three ways: 1) perineurium and endoneurium were sealed by a bipolar coagulator and buried in adjacent muscles; 2) perineurium was tied with a #6 suture and 3) no treatment. The nerves were harvested at two

days, four days, fourteen days and one month post surgery. The nerves were removed and 0.5 cm of the nerve at the severed end from each of the treatment groups. Total proteins were extracted and a SDS gel was run to separate the proteins. The gels were prepared for Western blot using a monoclonal antibody to GAP-43 protein and the nerves were run in groups along with control nerves. It was found that the GAP-43 protein was increased at the ends of all severed nerves when compared with control or with normal nerves. In addition, the nerves that the perineurium was tied with a suture yielded more GAP-43 staining than did nerves with either other treatment group. This finding applied to nerves at 14 days post surgery, the study is continuing to finish the animals at 2 days, 4 days, and 1 month post surgery. At 14 days post surgery the beginning of a neuroma was clearly seen with a growth of bulbous ending following the suturing procedure. However, from this early study appears that the accumulation of GAP-43 protein in the nerve ending is associated with neuroma formation. The study needs to determine if there is a continuous production of the mRNA for GAP-43 protein during this period of time has it feasible that the loss of GAP-43 protein from severed nerve endings inserted into muscle maybe also occurring.

VI. CHANGES OF ENERGY RELATED METABOLITES IN CEREBRO-SPINAL FLUID AFTER BRACHIAL PLEXUS INJURY

It is hypothesized that the severity and type of injury to the spinal cord dorsal roots may be reflected in the change in concentration of energy related metabolites found in the extracellular fluid, the cerebro-spinal fluid.

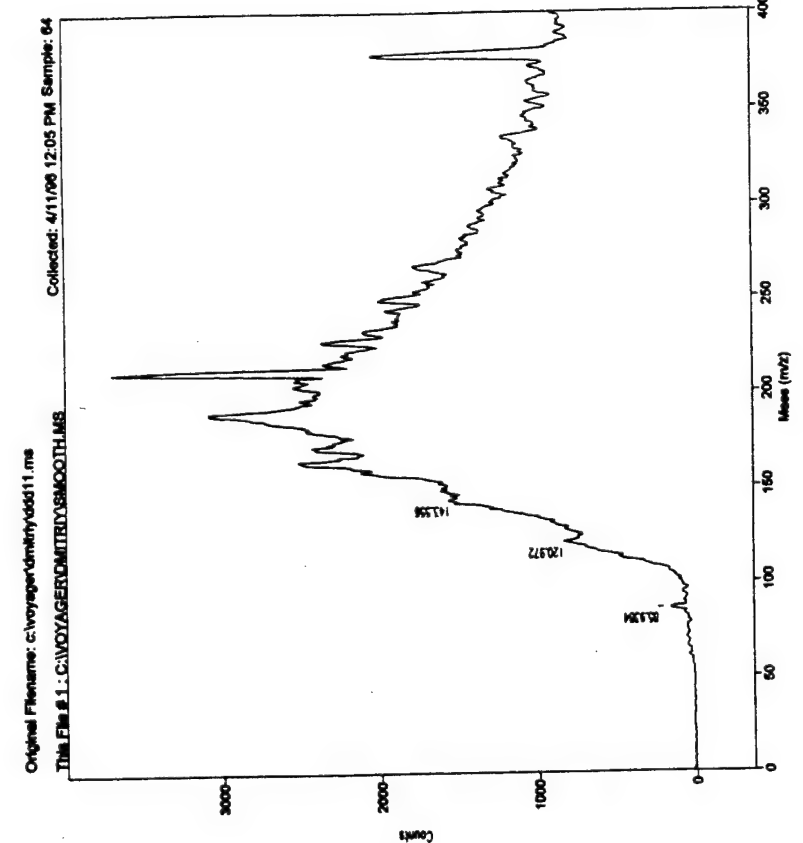
Previous studies have indicated that after spinal cord injury, concentrations of energy related metabolites change in the extracellular fluid (ECF) which has been investigated in a well characterized model of compression trauma to the spinal cord (3-5). Cerebro-spinal fluid (CSF) can communicate freely with the extracellular fluid, and there is no barrier between them as that between blood vessels and extracellular fluid (6). Therefore the concentration of energy related metabolites may be reflected in the level of these metabolites found in the extracellular fluid.

Avulsive injury to the brachial plexus and close to the spinal cord could lead to more severe damage to the neurons in the spinal cord compared to the injury more distal to the spinal cord. This was shown in a previous study where c-fos expression in the spinal cord as well as in higher CNS centers was found to be greatly more pronounced following avulsive injury than in a distal nerve transection (Section B). It has been previously found that avulsive injury close to the spinal cord also can lead to more actual neuron cell death. This current study was designed to investigate the changes of metabolites in the CSF after avulsive injury or brachial plexus in rats. In this study male Sprague-Dawley rats (270-350 gm) were anesthetized by ketamine, ip. The brachial plexus (C4-T1) was exposed and stretched from the spinal cord. The incision was closed with skin clips and the rats were kept in animal care for a various intervals as one day, two days, and one week prior to sacrifice.

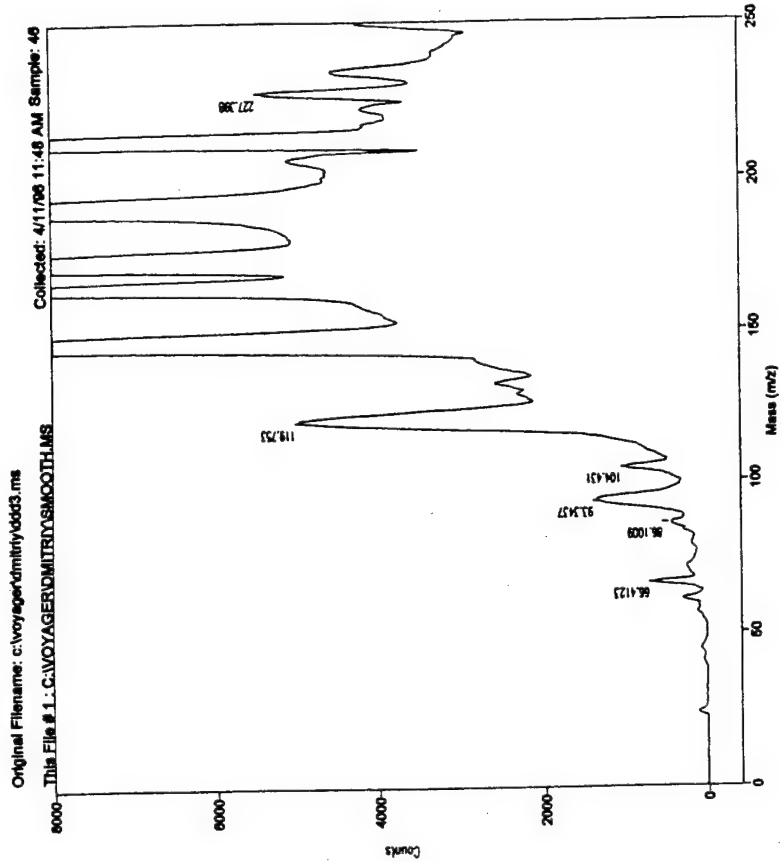
The CSF was removed before sacrifice with a special fire polished, 10 μ l pipette and prepared for analysis using MALDI-TOF mass spectrometry. Initial study showed that one day after avulsion, several peaks between 93 and 200 m/z appeared (Fig. 1B) in contrast to the normal control (Fig. 1A). Further studies to determine what the chemical nature of these peaks and how these correlate with cell death following avulsive injury to the spinal cord.

REFERENCES

1. Zhao S, Zhang D, Kline DG, Beuerman RW, Ma Q, Tran H. Increase in basic fibroblast growth factor and fibroblast growth factor receptor-1 following sciatic nerve injury and neuroma formation. *Soc Neurosci* 21:497, 1995.
2. MA Q, Beuerman RW, Zhao S, Pedroza L, Tran H, Nguyen D, Kline D. Immunolocalization and quantitation of fibroblast growth factor receptor-1 in the human peripheral neuroma. *Soc Neurosci* 21:2050, 1995.
3. Zhang Y, Hillered L, et al. Time course of energy perturbation after compression trauma to the spinal cord: An experimental study in the rat using microdialysis. *Surg Neurol* 1993, 39:297-304.
4. Lui D, Thangnipon W, et al. Excitatory amino acids rise to toxic levels upon impact injury to the rat spinal cord. *Brain Research*, 1991, 547:344-348.
5. Panter SS, Yum SW, et al. Alteration in extracellular amino acids after traumatic spinal cord injury. *Annals of Neurology*, 1990, 27:96-99.
6. Rosenberg GA. *Brain Fluids and Metabolism*. Oxford University Press 1990.



A



B

FIGURE 1

VII. GOALS FOR FOURTH YEAR

The goals for the past year have not changed and are stated in the beginning of this report. We have made progress in determining intracellular pathways that are operational in peripheral nerve inflammation and injury and we have also made progress in determining ways that these pathways can be individually blocked. The fundamental goal of this project has been to develop the basic science to understand these cellular changes that lead to neuroma and then to determine how these may be interfered with in a useful, therapeutic sense.

In pursuing this goal it is necessary to proceed from an intermediate animal model and then to test the approach in monkeys. We have available eight rhesus monkeys that we can ultimately test the therapeutic approach after preliminary testing in rabbits to determine both the concentration and the best method of application. The objective behind this will be to present a therapeutic intervention that can be used at the time of injury or at the time of surgical repair as an adjunct modality to ensure that the optimal conditions for regeneration have been met and that there will be minimal interference from overproduction of fibroblast and matrix accumulation. The immediate objectives of these experiments will be as follows: 1) to test the development of a neuroma and continuity in rabbits sciatic nerve following a crush lesion; 2) to apply the inhibitor of a metabolic intracellular signaling pathway, such as PD98059 (a MAP kinase inhibitor) or SB203580 (a SAP kinase inhibitor) or minoxidil; 3) the progress of nerve regeneration will be followed using electrophysiological methods as well as anatomical methods; and 4) to test the best combination of drug and concentration in our monkey model. We will use several groups of rabbits. The rabbit will be tested in each, six rabbits will be prepared with a crush to both sciatic nerves and the compound

to be tested will be placed in an implantable mini-pump at 0.5 mM to 10 mM concentration. The localization of the application of the test compound will be ensured by putting a loose collagen shield tube around the site of nerve damage. In order to ensure good experimental reliability 12 of the mini-pumps will be prepared, 6 with the test compound, 6 with saline and these will be coded so that the surgeons will not know which side is being treated by the test compound and which one receives the saline placebo. These experiments will be allowed to proceed for 6 weeks, a time period which has been previously found to be sufficient for the development of a neuroma like growth after crush injury. The animals will be tested by nerve conduction velocity studies from the proximal to the distal position and also by muscle conduction. The neuroma will be removed, prepared for electron microscopy, and anatomical studies of the fibroblast and cellular accumulation and also the number and caliber of nerves penetrating the neuroma. We will test these procedures in 6 groups of rabbits, each compound with 2 different concentrations. The concentrations to be used will be based on our *in vitro* studies of neuroma fibroblasts. We expect that it will be necessary to go up at least one magnitude *in vivo* to show efficacy. At the conclusion of the rabbit studies we will carry out 2 monkey studies using the same model as before with the exception that instead of a crush injury on one side and a nerve section on the other side we will carry out a crush injury on both sides and one concentration of the two most promising drugs that we ascertain from the rabbit studies will be used in blinded fashion.

This is an elaborate experiment that will consume the manpower and the laboratory facilities for year four. However, at the conclusion of this period we should have at least one viable compound at a known concentration that is effective at preventing formation of neuromas in continuity. This will be a significant step forward of use in many surgical procedures as well as after

injury.

VIII. CENTRAL NERVOUS SYSTEM CHANGES ASSOCIATED WITH CHRONIC PAIN IN PERIPHERAL NERVE INJURY

ABSTRACT

Pain effects all human beings and acutely, serves as one of the alerting mechanisms to protect us from harm. However, when pain becomes chronic, as is often seen after peripheral nerve trauma, it is frequently intractable and detrimental to the quality of life. The neuronal pathways and the mechanisms by which acute pain is converted to chronic pain are unknown.

HYPOTHESIS. **1.** A critical balance exists between tactile and painful input to sensory thalamus. The connections between and within sensory thalamus and cerebral cortex serve to modulate and suppress noxious signals and thus the perception of pain. **2.** Prolonged reduction of the tactile input produces a disruption of this balanced relationship. The imbalance augments the activity in the nociceptive components of the thalamo-cortico-thalamic relationship. **3.** Prolonged augmentation is thought to initiate mechanisms for neuronal plasticity that result in the permanent changes in neuronal circuitry producing centrally generated pain.

YEAR III GOALS:

The **long-range goals** were to identify the regions within the central nervous system that are likely to be involved in the generation of chronic pain, to determine which, whether and when factors currently thought to be involved in neuroplasticity and excitotoxicity contribute to the establishment of chronic pain and to determine whether a surgical interruption of a somatosensory pathway can avert or terminate a chronic pain state. These studies will provide the foundation for

future work designed to identify potential methods for therapeutic intervention in the treatment and prevention of chronic pain.

To achieve these goals, I conducted a series of experiments designed to:

FIRST SPECIFIC AIM. To demonstrate that interhemispheric connections are necessary for establishing a state of chronic pain. Albino rats were subjected to surgical interruption of the corpus callosum prior to the initiation of a deafferentation stimulus. The rats were then observed for preservation of normal behavior or the onset of autotomy, a constellation of behavioral changes believed to be associated with chronic pain.

SECOND SPECIFIC AIM. To demonstrate that interhemispheric connections are necessary for maintaining a state of chronic pain. A second series of albino rats underwent sectioning of the corpus callosum following the onset of deafferentation-induced autotomy.

THIRD SPECIFIC AIM. To identify the anatomical sites and potential mechanisms that underlie the conversion from a state of acute pain to a state of chronic neuropathic pain.

Immunocytochemical methods will be employed to identify the alterations in early gene expression with the *c-fos* marker, levels of neuronal oxidative metabolism with cytochrome oxidase and in levels of transmitters (glutamate, GABA, serotonin), modulatory neuropeptides (substance P) and modulators of intracellular calcium (calbindin) in two animal models for neuropathic pain; dorsal rhizotomy and chronic inflammation.

RESULTS OF YEAR III GOALS

Behavioral Results. Five albino rats were assigned to each of the study groups. The first 2 groups underwent sectioning of the corpus callosum and were allowed to recover for 2 weeks prior

to either dorsal rhizotomy (5 rats) or complete Freund's adjuvant (CFA) injections into 1 forepaw. The second 2 groups underwent dorsal rhizotomy or received CFA injections prior to any other experimental intervention. Control groups of 5 rats each underwent sham operations. Two groups received sham callosotomy in which the skull was opened and the dura mater was incised followed by either dorsal rhizotomy or CFA injections of a forepaw. Two additional groups underwent corpus callosum sectioning followed by sham dorsal rhizotomy in which a cervical laminectomy and dural incision was performed without sectioning the dorsal roots of cervical nerves or saline injections into the forepaw. It was anticipated that rats undergoing dorsal rhizotomy or CFA injections without callosotomy would begin autotomy (self mutilation - scratching with excoriation, digit and paw amputation) within 2 - 8 weeks. Conversely, those rats with prior callosotomy were not expected to demonstrate autotomy.

The group of rats that received CFA injections reduced the used of the injected forepaw for up to 2 weeks but then returned to normal behavior that was indistinguishable from saline controls. There was no evidence of self mutilating behavior, indeed the alteration of behavior was toward protection of the effected paw. There was a chronic change in the morphology of the CFA-injected forepaws that included erythema, edema and transient skin ulcerations that persisted for as much as 1 year after injection. Corpus callosotomy had no clear effect on the behavior although at times the rats that had undergone callosotomy seemed to have more frequent use of the injected paw.

The group of rats that underwent dorsal rhizotomy showed various degrees of autotomy from mild excoriation of the skin of the forearm and shoulder to self amputation of single phalanges and digits to the destruction of an entire paw and distal forearm. The self destructive behavior occurred between 48 hours and 8 weeks but was observed in only 60% of rats undergoing dorsal

rhizotomy. Autotomy was not observed in any of the sham operated controls. Due to the variable response both in numbers of rats showing any signs of autotomy and in the degree of the mutilation it was not possible to determine at which stage of amputation an animal would spontaneously stop autotomy. It was also not possible to predict which rats would begin autotomy following dorsal rhizotomy. In light of this result, it was not possible to proceed with the experiments planned under the second aim since we would not be able to state whether autotomy stopped as a result of subsequent corpus callosotomy or whether autotomy would have stopped spontaneously.

Rats that underwent corpus callosotomy prior to dorsal rhizotomy seemed to do somewhat better than those without corpus callosum sectioning. No rat having undergone callosotomy demonstrated autonomous behavior within 120 days of dorsal rhizotomy. Three out of the 5 rats in the precallosotomy group survived for 1 year following dorsal rhizotomy without signs of autotomy. One rat excoriated the shoulder at 4 months and 1 rat amputated digits 4 and 5 and the medial forepaw at 120 days. Although suggestive of some potential effect of callosotomy it is not possible to state whether these observations are statistically significant or not. To explore this possibility it would be necessary to significantly increase the sample size in each of the experimental groups to demonstrate a confidence in the effect. Resources to pursue this option are not available.

Preliminary Anatomical Results. Three rats that have been subjected to a component of the CFA protocol have been perfused and their brains have been processed for levels of glutamate, calbindin and *c-fos* activity following single injections into the left forepaw. Post-injection survivals for these animals were 24 hours, 1 week and 4 weeks. Analgesiometry was not performed due to lack of equipment. Within 2 hours of administering CFA, the injected forepaw showed

marked edema and erythema. Following recovery from anaesthesia, the rats' activity was subjectively decreased from pre-injection levels and the use of the left forepaw was avoided. The inflammatory process progressed over the next 24 hours producing moderate to severe erythema and edema that approximately doubled the size of the forepaw. The level of inflammation appeared to stabilize after 24 hours and in the longest surviving rat remained at maximum levels for 12-14 days. The edema and erythema thereafter decreased over the next week and use of the paw increased but the forepaw never returned to its pre-injection condition. Autotomous behavior never developed.

Immunocytochemical labeling of intracellular calbindin was found to be increased in cells and axons of the dorsolateral portion of the substantia gelatinosa and the intermediolateral cell column ipsilateral to the injected forepaw when compared to the contralateral counterparts within 24 hours of administration of CFA. Complementary increases in labeling of glutamate were also observed at similar cord levels in the neuropile of the substantia gelatinosa and intermediolateral cell column. Calbindin activity was also increased in the axons of the medial lemniscus contralateral to the injected forepaw within 24 hours of injection. Although calbindin and glutamate labeling also appeared to be increased at this time in the VB contralateral to the injected forepaw, the preliminary results are equivocal. After a 1 week survival, the labeling of calbindin and glutamate both appeared to decrease in the dorsolateral portion of the substantia gelatinosa and the intermediolateral cell column as shown for calbindin. Labeling in the contralateral spinal cord, medical lemniscus and VB was not changed appreciably from the initial labeling pattern seen following 24 hour survival. Following a 4 week survival, the intensity of calbindin labeling was less in VB contralateral to the injected forepaw when compared to the ipsilateral counterpart.

C-fos labeling was found only in the rat that survived for 4 weeks. Neurons were found to

be labeled bilaterally, but asymmetrically denser contralateral to the injected forepaw, in the posterior thalamus adjacent to the medial border of the ventral lateral geniculate nucleus and extending into the posterior-most aspect of the lateral portion of the posterior nucleus of the thalamus (Pol). The significance of this labeling is unclear. Since the identical dilution of the same batch of antibody was used to label *c-fos* in all of the tissue, the lack of labeling cannot be explained by non-reactive antibodies. Alternatively, it is possible that the pattern of labeled cells is artifactual since similar patterns of labeling have been observed in relation to components of the circadian cycle (Kurkoff, '94). All of the rats, however, were sacrificed within 1 hour of each other, demonstrated no apparent difference in behavior and experienced no difference in manipulation prior to or during anaesthesia and perfusion. The asymmetry of the labeling and the fact that the pattern was only observed in the animal that had survived for 4 weeks therefore suggests a need for further study and clarification.

PRESENT GOALS

In light of the results of the initial studies, coupled with recent observations obtained in the clinical management of peripheral nerve injury and the potential for more active collaboration with Drs. England and Happel an extention of the original study was made to define the role of gabapentin in the treatment of neuropathic pain. Gabapentin (Neurontin®, Parke Davis) is a new antiseizure medication with surprisingly few adverse effects that has recently been approved for use in the treatment of seizures. Because many antiseizure drugs have been used successfully in the treatment of chronic pain, gabapentin has also been tried in the hope of providing greater relief from pain. There are currently several reports in the literature that suggest that gabapentin is helpful in

the treatment of difficult cases of chronic nerve pain of many types such as causalgia and reflex sympathetic dystrophy. Use of gabapentin in our own clinic has also produced dramatic results in cases of polyradiculopathy, diabetic and post-traumatic polyneuropathy, trigeminal neuralgia, paraneoplastic and toxic neuropathies and atypical facial pain. Although gabapentin was conceived as an antiepileptic drug and designed to be a GABA analogue that could cross the blood-brain barrier, it was not found to have affinity for the GABA receptor in binding studies. Indeed, gabapentin's mechanism of action is yet to be determined. Our study plan was therefore modified to attempt to determine the efficacy of gabapentin in altering pain thresholds in animal models for neuropathic pain, e.g., chronic inflammation and peripheral nerve ligation, and to determine the site of action for gabapentin in the treatment of pain.

To begin to achieve these goals, we have conducted a series of experiments designed to determine the effect of gabapentin on the pain threshold of rats with chronic inflammation. Since starting this portion of the project 2 independent laboratories have been able to show the efficacy of gabapentin in both the peripheral nerve ligation and formalin injection models of pain (personal communication).

Our laboratory has completed the following group of experiments and is in the process of analyzing the data.

1. The baseline pain threshold was determined in 100 rats by measuring their response to noxious thermal stimuli according to the protocol of Hargreaves et.al. ('88). For this, the rats were held under a plastic chamber and placed on an elevated glass surface. The forepaw was radiantly warmed from below through the glass plate. The timer and heat source were turned off when the paw was moved. An upper cutoff latency of 10.5 seconds was imposed to prevent tissue

damage. Baseline measurements were made on 3 days prior to experimental manipulation. Each paw was stimulated 4 times during each testing session for a total of 16 trials per session per rat.

2. Rats were then anesthetized with a combination of ketamine (60 mg/kg) and xylazine (8 mg/kg) and the left forepaw of each rat received a subcutaneous injection of 0.25 ml of complete Freund's adjuvant (CFA; *Mycobacterium tuberculosis*; Sigma) suspended in an oil:saline (1:1) emulsion (0.5mg *Mycobacterium*/ml emulsion) using a sterile tuberculin syringe. The rats then recovered from anaesthesia.

3. The pain threshold was again determined on 2 separate days following CFA injections.

4. Gabapentin was administered by subcutaneous injection to 56 rats in doses ranging from 20-160 mg/kg. Twelve control rats received subcutaneous injects of comparable volumes of saline. The pain threshold was measured on 3 successive days following determination of post-CFA pain threshold.

5. Carbamazepine (40 mg/kg) and ibuprofen (100 mg/kg) was administered to 2 groups of 12 rats as a treatment controls. Pain thresholds were measured as in Step 4.

6. Rats were then euthanized.

7. Portions of the brains and peripheral nerves of 10 rats were removed and will be analyzed for gabapentin binding to determine regions in which gabapentin acts.

CURRENT RESULTS

The data from the outlined experiments are being analyzed at the present time. Conclusions based on the yet incomplete evaluation are that unlike peripheral nerve ligation and formalin injections the response to gabapentin in the model for chronic inflammation was not significantly different from controls in the injected paw. Interestingly, however, the response latency in the uninjected paws was consistently shorter in the gabapentin-treated rats when compared to control responses. In control rats the latency to paw withdrawal in the uninjected paws was longer than the baseline response. Treatment with gabapentin resulted in unusually aggressive behavior that was not observed in either treated or untreated controls and seemed to be dose dependant. This observation is interesting in the context of anecdotal clinical reports of increased irritability in some patients taking gabapentin. This data is currently being prepared for publication and presentation at the regional meeting of the American Federation for Clinical Research and at the American Academy of Neurology.

Tissue samples have only been collected at this time. These samples will be analyzed in collaboration with Dennis Paul, Ph.D., Department of Pharmacology, in competitive binding assays to determine regional activity of gabapentin with specific interest in nociceptive pathways. Of particular interest is peripheral nerve, dorsal root ganglia, spinal cord and brain stem.

GOALS FOR YEAR 4

The mechanism by which gabapentin produces its effect remains unknown, however, its efficacy in the treatment of pain associated with peripheral nerve injury suggests that a clear indication of its mechanism of action is likely to provide significant insight into our understanding of pain and how it can be treated. We would propose to continue this line of research by utilizing our baseline immunohistochemical data in the central nervous system to determine the effects of gabapentin on *c-fos/fra*, substance P and GABA immunohistochemistry in normal rats and in rats with peripheral nerve ligation.

IX. ION CHANNELS IN INJURED PERIPHERAL NERVES

1. Specific Aims

- I. To determine if nerve injury alters the distribution/quantity of sodium channels.
- II. To determine whether the sodium channel population is altered in human neuromas.
- III. To determine whether the potassium channel population is altered in human neuromas.
- IV. To determine how sodium channel distribution is altered in acute demyelinative nerve injury.

2. Studies and Results

I. The study of sodium channels in nerve injury induced by toxins has been described previously. Peripheral nerve fibers of *Carassius auratus* (goldfish) were acutely and focally injured by exposure to the neurotoxic agent, potassium tellurite (K_2TeO_3). Using a polyclonal antibody directed against the α -subunit of the sodium channel, the injured nerves were examined using immunocytochemical and radioimmunoassay (RIA) methods. Identical studies were performed on contralateral control nerves from the same fish. These studies showed a focal accumulation of sodium channels within the tips of injured axons. The major increase in sodium channel concentration occurred between 7 and 11 days after toxin exposure; however, excess sodium channels persisted chronically in several axonal endings. These studies indicate that nerve injury which is severe enough to cause wallerian axonal degeneration can alter the sodium channel population in a subpopulation of injured axons.

II. The study of sodium channels within human painful neuromas has also proceeded well. Seventeen painful neuromas from 16 patients have now been examined using a site-specific anti-sodium channel antibody. This antibody is directed against an 18-mer peptide which corresponds to a region highly conserved in all known vertebrate sodium channels. Normal sural nerves from 6 of these patients served as controls. All specimens were examined using the same antibody in both immunocytochemical and radioimmunoassay (RIA) methods. Immunocytochemistry showed abnormal segmental accumulation of sodium channels within many axons in the neuromas. Dense immunolocalization was especially apparent within axonal tips. Contrastingly, in sural nerves focal accumulation of sodium channels was restricted to nodes of Ranvier. RIA confirmed a significantly ($P = 0.0075$) greater sodium channel density in neuromas (median = 28.6; mean \pm SEM = 32.5 ± 3.7 pM per g) as compared to sural nerves (median = 18.2; mean \pm SEM = 17.1 ± 2.2 pM per g).

The degree of painfulness of individual neuromas was correlated with the sodium channel density. Further analysis showed a clear trend in the direction of greater pain for neuromas with greater concentrations of sodium channels. These data indicate that sodium channels accumulate abnormally within the axons of human painful neuromas. Additionally, they suggest a positive correlation between the density of sodium channels within neuromas and their degree of pain.

In order to refine these studies of sodium channels in injured axons, we are continually developing new and highly specific anti-sodium channel antibodies. In collaboration with Dr. S. Rock Levinson at the University of Colorado, we have over the past year developed another site-specific anti-sodium channel antibody. This antibody (1384.1) is now affinity purified and is ready for immunocytochemical and radioimmunoassay studies. This new antibody will be utilized to study

more human neuromas as well as experimental neuromas in rhesus monkeys, which are being created by Dr. David Kline's group (see Dr. Kline's section for details of this model).

III. We have begun examining human neuromas with a highly specific anti-potassium channel antibody. This antibody is specifically directed against a voltage-gated, delayed rectifier potassium channel. Comparison control studies are being made using normal human sural nerve and normal rat sciatic nerve. Thus far, we have examined ten human neuromas with this antibody utilizing immunocytochemical techniques. Abnormal axonal distributions of these potassium channels within the neuromas is evident. These potassium channels appear to accumulate abnormally within some axonal segments but not others. The details and spatial distribution of these channels are being evaluated by confocal microscopy.

This study has only just started, and the specific potassium channel abnormalities within these neuromas is not yet worked out. We are planning to simultaneously examine the neuromas with both the anti-potassium channel antibody and the new anti-sodium channel antibody (1384.1) by utilizing double-labeling immunocytochemistry. These experiments will allow us to determine directly the relationship of potassium channel distribution with the sodium channel distribution within the neuromas.

IV. Over the past year we have also investigated the changes which occur along nerves injured acutely by demyelination. The posterior lateral line nerves of *Carassius auratus* were demyelinated acutely by intraneuronal microinjection of lysolecithin. These nerves were then examined immunocytochemically using the anti-sodium channel antibodies. Demyelination developed rapidly, and by 7-8 days postinjection many axons exhibited long stretches of demyelination. At 8-9 days occasional isolated patches of sodium channels were seen along

demyelinated axons. These sodium channel clusters were 10-20 microns in length and were not associated with Schwann cells. At 10-11 days, proliferating Schwann cells adhered to demyelinated axons. The patches of sodium channels which persisted were seen only along bare axons, but many of the sodium channel clusters were increasingly associated with the edges of the Schwann cells. As the Schwann cells elongated, the clusters of sodium channels appeared to be pushed along the axon by the Schwann cells. Eventually, as Schwann cell elongation and remyelination proceeded, the remaining clusters of sodium channels became increasingly more localized and restricted to new nodes of Ranvier.

These observations again emphasize that demyelination results in a reorganization of axonal sodium channels. They suggest that sodium channel clusters along axons arise *de novo* and independently of Schwann cells; however, if reinvestment of axons by Schwann cells occurs, the final localization of sodium channels is controlled by or linked to Schwann cell localization. In certain nerve injuries (such as neuromas) where neurites may remain unmyelinated, abnormal accumulations of sodium channels may remain indefinitely because of the lack of controlling factors associated with such cells.

3. Significance

Peripheral nerve trauma is often associated with dysesthesia and painful impulses arising from injured axons. This is especially the case with neuromas, which because of their painfulness may cause considerable distress for patients. The complete explanation for the pain of peripheral nerve trauma is not known, but ectopic axonal hyperexcitability is likely a major factor. Since the axolemmal distribution of voltage-gated ion channels largely determines the regions of electrical

excitability in normal axons, an altered distribution or quantity of such channels could cause ectopic impulse generation in injured axons. The accumulation of sodium channels within injured axons is a likely cause of such ectopic axonal hyperexcitability and pain. Modification of sodium channel distribution or function may prove a particularly fruitful approach to the treatment of pain in diseases of the peripheral nervous system.

Of course, potassium channels are also important in maintaining axonal resting potential and preventing ectopic and repetitive action potential generation. It will be very important to investigate the distribution and function of potassium channels within injured nerves, and specifically within neuromas. Complex interactions between sodium and potassium channels are likely to occur within injured axons.

4. Plans

Over the next year we plan to investigate the functionality of sodium channels within neuromas by utilizing patch-clamp techniques on axonal membrane. Although our studies to date have shown immunological evidence of excess sodium channels within the axons of neuromas, we have no direct evidence of their functional properties. It will be important to demonstrate their electrical properties, density, and ability to generate action potentials.

We also plan to extend our immunologic and electrical studies to experimental neuromas developed in monkeys. The monkey neuroma model has been developed by Dr. David Kline in the Department of Neurosurgery and is already underway. Study of these experimental neuromas will allow elucidation of the timing and sequence of the development of sodium channel abnormalities. It will also allow potential therapeutic trials aimed at modifying the sodium channel population and

the development of pain.

Finally, we now have site-specific anti-potassium channel antibodies, which will be useful in exploring the potassium channel population of neuromas. This is important since an abnormal distribution or downregulation of the quantity or function of potassium channels could contribute to abnormal axonal excitability. The simultaneous investigation of sodium channel and potassium channel distributions and functionality should provide more information on the basis of axonal hyperexcitability in neuromas.

5. Human Subjects

There are no changes in the protocol.

6. Vertebrate Animals

There are no changes in the protocol.

X. PUBLICATIONS

England JD, Happel LT, Kline DG, Gamboni F, Thouron C, Liu ZP, Levinson SR. Sodium channel accumulation in human painful neuromas. *Neurology* 47:272-276, 1996.

England JD, Levinson SR, Shranger P. Immunocytochemical investigations of sodium channels along nodal and internodal portions of demyelinated axons. *Microscopy Research Technique* 33:445-451, 1996.

Lu G, Beuerman RW, Zhao S, Sun G, Nguyen DH, Ma S, Kline DG. Tumor Necrosis Factor Alpha and Interleukin-1 Induce Activation of MAP Kinase and SAP Kinnase in Human Neuroma Fibroblasts. *Neurochemistry International: Cytokine*, in press.

Varnell RJ, Freeman JY, Maitchouk D, Beuerman RW, Gebhardt BM. Detection of Substance P in Human Tears By Laser Desorption Mass Spectrometer and Immunoassay. *Neuroscience Letters*, in press.

Zhao S, Beuerman RW, Kline DG. Neurotization of motor nerves innervating lower extremity by utilizing lower intercostal nerves. *Reconstructive Microsurgery*, in press.

Sodium channel accumulation in humans with painful neuromas

Article abstract—Painful neuromas from 16 patients were examined using site-specific antisodium channel antibodies employed in immunocytochemical and radioimmunoassay methods. Normal sural nerves from six of these patients served as controls. Immunocytochemistry showed abnormal segmental accumulation of sodium channels within many axons in the neuromas. Dense immunolocalization was especially apparent within the axonal tips. Radioimmunoassay confirmed a significantly greater density of sodium channels in the neuromas as compared with the sural nerves. Thus, sodium channels accumulate abnormally within the axons of neuromas in humans. This alteration of the sodium channels may underlie the generation of axonal hyperexcitability and the resulting abnormal sensory phenomena (pain and paresthesias), which frequently occur after peripheral nerve injury.

NEUROLOGY 1996;47:272-276

J.D. England, MD; L.T. Happel, PhD; D.G. Kline, MD; F. Gamboni, PhD; C.L. Thouron; Z.P. Liu, MD; and S.R. Levinson, PhD

Peripheral nerve trauma may result in the formation of a neuroma, a tangled mass of regenerating axons embedded within the connective tissue of a nerve trunk. The axons within a neuroma not only fail to reinnervate their original targets, but may also develop abnormal electrical hyperexcitability.^{1,2}

In human neuromas, the development of ectopic hyperexcitability within sensory axons is likely to be a major cause of neuroma-associated pain and dysesthesias. Clinical evaluation of patients with painful neuromas and routine histologic analysis of excised neuromas have not identified the factors responsible for this pain. Because the ability of an axon to generate an action potential depends ultimately on the distribution and properties of voltage-gated ion channels, especially voltage-gated sodium channels, a potential cause of ectopic axonal hyperexcitability could be an abnormal redistribution of ion channels within injured axons. A particularly attractive hypothesis is that aberrant axonal electrical hyperexcitability is, in part, caused by an abnormal accumulation of sodium channels along injured or regenerating axons.²⁻⁵

This report describes the changes in the sodium channels which characterize painful neuromas in humans. These findings are correlated with what is currently known about the remodeling of axonal membranes within neuromas.

Methods. Patients. The study group consisted of 16 patients with painful traumatic neuromas selected from a large population of patients with peripheral nerve injuries seen at the Louisiana State University School of Medicine, New Orleans. Each patient was evaluated clinically and electrophysiologically (EMG/nerve conduction study) by a team of neurologists and neurosurgeons. The pain of each patient's nerve injury was graded subjectively on a scale from 1+ to 4+ (table). For each of the 16 patients in this study, surgical treatment of the neuroma was believed to offer the best chance for pain relief or nerve regeneration. Thus, each patient underwent surgical excision of the neuroma. In some cases, sural nerve autografts were interposed within the resected nerve segment.

Preparation of antisodium channel antibody. A site-directed antibody was raised to a highly conserved region found in all known vertebrate sodium channels, including those of human neuronal tissues. This segment (TE-EQKKYYNAMKKLGSKK) resides in a putative intracellular loop connecting domains III and IV in the alpha subunit of the sodium channel. The synthetic peptide coding for this segment was conjugated to a keyhole-limpet hemocyanin carrier and used to immunize rabbits through regular injections. The resultant high-titer antisera were processed using an immunoaffinity column to which the immunizing peptide had been immobilized, yielding a highly pure and concentrated preparation of antisodium channel antibodies. The specificity of the antibody preparation was demonstrated by the quantitative elimination

Table Sodium channel density and painfulness of neuromas

Patient	Specimen	NaCh*	Pain	
1	C5 neuroma	23.5	+	
2	Normal nerve	23.7	-	
3	Middle trunk neuroma	25.8	+	
4	C5-upper trunk neuroma	26.3	+	
5	Femoral neuroma and normal nerve	28.6 9.6	+	-
6	Upper trunk neuroma	30.1	+	
7	Axillary neuroma and normal nerve	30.6 12.6	+	-
8	C6 neuroma	31.0	+	
9	C5 neuroma	31.0	++	
10	C7 neuroma	31.2	+	
11	Superficial radial neuroma	32.7	++	
12	Brachial plexus neuroma	32.9	+++	
13	Medial cord neuroma and normal nerve	48.3 20.4	++ -	
14	Sural neuroma	48.3	+++	
15	Sciatic neuroma (distal segment)	67.2	++++	
	Sciatic neuroma (proximal segment) and normal nerve	25.4 16.2	++++ -	
16	Sciatic neuroma and normal nerve	74.2 20.1	+	-

* Sodium channel density in picomol per gram of wet weight.

- = no pain; + = mild pain; ++ = moderate pain; +++ = severe pain; ++++ = very severe pain.

of antibody binding by preincubation with either pure sodium channel or synthetic peptide in a sensitive radioimmunoassay (RIA)⁶ and in immunocytochemical preparations (figure 1d).

Immunocytochemistry. Immunocytochemical methods were performed in accordance with described procedures.^{5,6} After reaction with tissue, the antisodium channel antibody was visualized with lissamine rhodamine-labeled goat antirabbit immunoglobulin G. For control slides, the primary antisodium channel antibody was preblocked with the peptide antigen (1 µl of peptide per 2 µl of antibody overnight at 4°C). Labeled specimens were examined with either an Olympus BH2 epifluorescence microscope or a Leica laser scanning confocal microscope.

Radioimmunoassay. Neuroma or sural nerve specimens were weighed and then homogenized in 0.1 mol/liter sodium phosphate buffer (pH 7.5) and 1% Lubrol PX. They were then centrifuged at 45,700g for 25 min, and the pellets were discarded. The supernatants were denatured by adding 1% SDS and 2.5% betamercaptoethanol and boiling for 2 min. After cooling, they were dialyzed against 0.1 mol/liter sodium phosphate buffer at room temperature for 24 hr. The extracts were retrieved and diluted in 0.1 mol/liter sodium phosphate buffer (pH 7.5), 1% bovine serum

albumin, 0.1% Lubrol, and 0.021% egg phosphatidylcholine (Sigma, grade V) to a concentration of <10 mg wet tissue per 100 µl. Samples (100 µl per tube) were incubated with the antisodium channel antibody diluted to 1:2,000 for 1 hr at room temperature. Twenty microliters of iodine-125-labeled purified eel sodium channel (17 fmol or 30,000 cpm; specific activity = 1.06 mCi/nmol; 1 Ci = 37 GBq) was then added to each tube and incubated another 2 hr at room temperature. Antibody-antigen complexes were solid phase precipitated by adding 100 µl of Tachisorb-R (Calbiochem #575544) and incubating with gentle shaking for 2 hr at room temperature. Samples were washed with 0.1 mol/liter sodium phosphate buffer, 1% bovine serum albumin, 0.1% Lubrol, and 0.02% egg phosphatidylcholine (Sigma, grade V) (1.25 ml per tube) and then centrifuged at 3,700g for 5 min. The pellets were resuspended in the same buffer and recentrifuged at 3,700g for another 5 min. The supernatants were discarded, and the radioactivity of the pellets was determined using a gamma counter. Concentrations of sodium channels were calculated with reference to a standard curve determined by using known quantities of highly purified eel sodium channel.

Results. Immunocytochemistry. Seventeen neuromas from 16 patients (one patient had two specimens) and six sural nerves from six of these patients were examined immunocytochemically.

In the sural nerves, sodium channel-specific immunoreactivity (IR) was seen only at nodes of Ranvier. Unmyelinated axons exhibited no specific IR anywhere along their axolemma. These results in human sural nerves are identical to those found using similar immunohistochemical studies in fish posterior lateral line nerves.^{5,6} Although electrophysiologic and biochemical studies demonstrate some voltage-gated sodium channels along normal unmyelinated and internodal axolemma, the density of these sodium channels is too low to be visualized immunocytochemically with antisodium channel antibodies.^{5,6}

All neuromas showed abnormally intense sodium channel-specific IR within many axons. This IR was seen in large-diameter (>1 µm) and small-diameter (<1 µm) axons, although larger axons with dense IR were more frequently encountered. The IR was always nonuniform in distribution, occurring in patches of variable density along the axons. Of special note, this dense specific IR usually appeared along demyelinated or unmyelinated segments of axolemma. When myelinated fibers were seen, focal accumulation of sodium channels was observed only at normal nodes of Ranvier. Some of the most intense immunolabeling was seen at the neurite tips, and these axonal endings were always devoid of a myelin sheath. Within neuromas there was considerable individual axon variability of IR, with some axons showing many patches of intense IR and other axons (even neighbors) showing no IR. Even in the most intensely labeled neuromas, no more than 30 to 40% of all axons showed sodium channel-specific IR. Although all neuromas exhibited abnormal sodium channel-specific IR within many axons, there was considerable variability in terms of the number and intensity of axons stained within individual neuromas. Only minimal nonspecific immunofluorescence was seen when the primary antisodium channel antibody was preblocked with peptide, confirming the specificity of the above-noted IR. Figure 1 provides examples of these immunocytochemical observations.

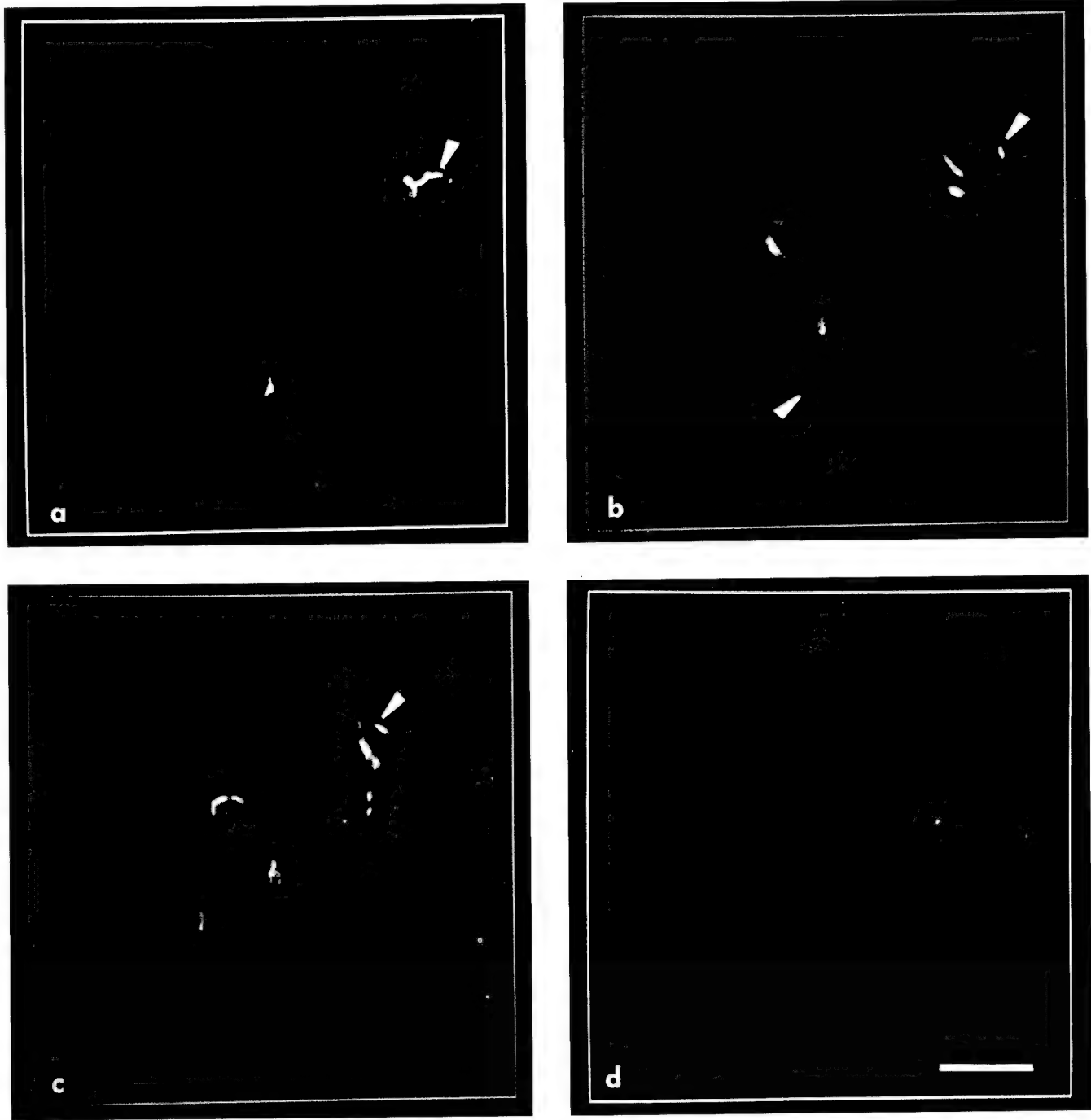


Figure 1. Sodium channel immunocytochemistry of neuromas. (a, b, c) Distinct segments of sodium channel-specific immunoreactivity are present throughout the axons of these neuromas. Also note the intense immunoreactivity present in several axonal tips (arrowheads). (d) Control showing the nonspecific immunofluorescence that occurs when the primary antisodium channel antibody is preblocked with peptide. Scale bar = 10 μ m.

Radioimmunoassay. Sixteen neuromas from 15 of the patients (one patient had two specimens) and six sural nerves were examined using RIA. Portions of all of these specimens had been examined immunocytochemically (see prior discussion). For each specimen the concentration of sodium channels was calculated and expressed as picomol per gram of wet weight. The Mann-Whitney U test was used for statistical analysis of the two populations. RIA data demonstrated a significantly greater ($p = 0.0075$) sodium channel density in neuromas (median = 28.6; mean

\pm SEM = 32.5 ± 3.7 picomol per gram) as compared with sural nerves (median = 18.2; mean \pm SEM = 17.1 ± 2.2 picomol per gram). The true density of axonal sodium channels within these neuromas was probably even greater because neuromas contain far more nonneuronal tissue than normal nerve. Figure 2 graphically illustrates the sodium channel density for each specimen. The variance of the normal nerves was much less than that of the neuromas, and there was very little overlap between the two populations. These population differences are consistent

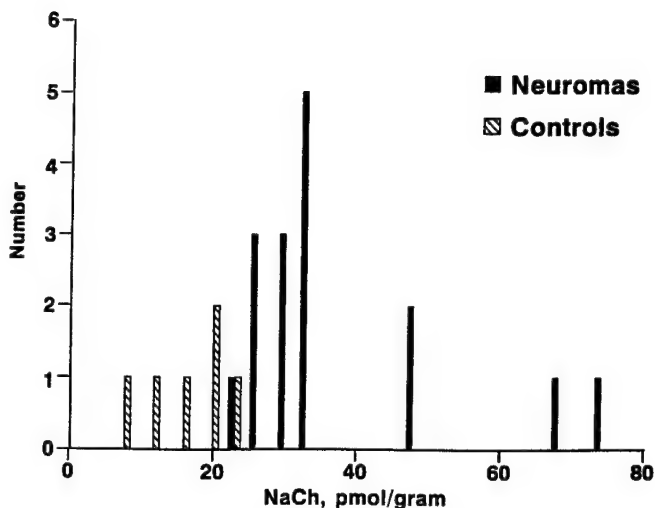


Figure 2. Frequency histogram of the sodium channel density in neuromas and control nerves. The neuromas, as a group, had a significantly greater concentration of sodium channels as compared with the control nerves (see text).

with the expected biologic variability of the sodium channel density, which was greater for the neuromas. Matched pairs of specimens were available from five patients (i.e., neuroma and sural nerve from the same patient). In each case, the neuroma contained a significantly greater density of sodium channels than the sural nerve. All RIA data are provided in the table, in which the neuromas are ordered according to their sodium channel density (i.e., from lowest to highest) and their degree of pain is provided. By inspection, one can ascertain a trend in the direction of greater pain for neuromas with greater concentrations of sodium channels. These data suggest a positive correlation between the density of sodium channels within neuromas and their degree of pain.

Discussion. This study shows that sodium channels accumulate abnormally within the axons of human painful neuromas. This work extends and corroborates the findings of several animal studies of nerve injury.³⁻⁵ Immunocytochemical analysis of neuromas of the lateral line nerve of the fish *Apteronotus*³ and focally injured nerve fibers of the lateral line nerve of *Carassius auratus* (goldfish)⁵ have shown sodium channel accumulation at the endings of injured axons. Devor et al.⁴ immunolocalized sodium channels at the electron microscopic level in neuromas produced in rats. Sodium channel accumulation occurred in preterminal axolemma, which was either demyelinated or unmyelinated, as well as in neuroma end bulbs. The large-diameter ($>1 \mu\text{m}$) axons within the neuromas acquired excess sodium channels only after myelin was stripped from their internodal axolemma. Many of these axons contained distinct patches of heavy sodium channel immunolabeling. These findings are concordant with our observations in human neuromas and, thus, may be a general feature of neuromas.

The accumulation of sodium channels within the

axons of neuromas may be due to several factors. Sodium channels are synthesized in neuron cell bodies and transported down axons by microtubule-based fast axoplasmic transport.^{5,7} When the cell bodies of the squid giant fiber lobe are dissociated from their giant axons and maintained in culture, sodium channels amass within the somata.⁷ This observation suggests that the axonal membrane normally serves as a "sink" for sodium channels synthesized within the cell body and that its removal by axotomy causes sodium channels to accumulate in the remaining viable membrane. After injury to axons, sodium channels, which are continuously transported down axons, would be expected to accumulate at the nerve fibers' distal segments. Concordant with this hypothesis are studies demonstrating that block of fast axoplasmic transport decreases ectopic electrical activity in injured peripheral nerves.²

Local demyelination of axons within neuromas may be another factor that permits focal accumulation of sodium channels. In our study and previous studies³⁻⁵ of traumatic nerve injury, when sodium channels were found in large axons ($>1 \mu\text{m}$ diameter), the axolemma was devoid of myelin. Demyelination of axons, even when not accompanied by axotomy, permits the insertion of sodium channels along previously internodal axolemma.⁶ Taken together, these observations indicate that changes of the regional axonal environment at the site of injury may act to change the distribution of sodium channels.

An important question regarding the accumulation of sodium channels within neuromas is whether this accumulation is relevant to the pathophysiology of pain associated with neuromas. Neuromas certainly may serve as a generator of painful impulses.^{1,2} Wall and Gutnick¹ were the first to demonstrate that some afferent fibers originating in a neuroma develop spontaneous electrical hyperexcitability. This axonal spontaneous hyperexcitability and the sensitivity of neuromas to mechanical and chemical stimuli are now indisputable facts.^{2,8} The prevalence of such ectopic axonal hyperexcitability varies with nerve fiber type and with the time since nerve injury, but it is nearly always present. At peak activity, an average of 28% of all injured fibers fire spontaneously and an even higher percentage exhibit abnormal mechanosensitivity.² Because the axolemmal distribution of sodium channels largely determines the regions of electrical excitability in normal axons, an altered distribution or quantity of such channels is a likely cause of ectopic impulse generation in injured axons.^{2-5,8}

Besides the immunologic evidence supporting abnormal accumulation of sodium channels within neuromas, pharmacologic and mathematical models support this concept. Local anesthetics such as lidocaine and mexiletine, which selectively block sodium channels, have been studied in animals and humans with peripheral nerve injury. In humans with neuromas, pain can be decreased by local infiltration of lidocaine into the subcutaneous tissues surrounding the

neuroma.⁹ In rats with experimental neuromas, intravenous infusion of both lidocaine and mexiletine can completely abolish the spontaneous afferent activity arising within neuromas without blocking nerve conduction itself.¹⁰ Matzner and Devor⁸ showed that the sodium channel blockers tetrodotoxin and lidocaine stop neuroma firing by suppressing the process of impulse initiation without blocking impulse propagation. In contrast, veratridine, which increases sodium conductance, accelerates ectopic firing.⁸ Taken together, these pharmacologic studies provide strong evidence that the generator potential associated with ectopic neuroma firing sites is encoded into an impulse train by a process that depends on voltage-sensitive sodium channels. Mathematic models suggest that excess membrane sodium conductance plays a major role in promoting axonal hyperexcitability. The Hodgkin-Huxley equation was used to predict the effects of altering maximal sodium conductance (g_{Na+max}) on the process of repetitive neuronal firing.² This model shows that increasing g_{Na+max} , without changing any other membrane variable, decreases the threshold current necessary to evoke repetitive firing. This change in membrane properties renders the membrane hyperexcitable. Although changes in other membrane properties may occur in the axons within neuromas, these data indicate that accumulation of excess sodium channels is sufficient to cause ectopic axonal hyperexcitability.

The accumulation of sodium channels within injured axons may be a feature common to all varieties of peripheral nerve trauma, especially those which give rise to neuromas. It is likely to be a major cause of ectopic axonal hyperexcitability. When injured sensory fibers develop hyperexcitability, the perception of pain and paresthesias likely occurs^{2,4,5}; however, the entire explanation for neuroma-associated pain is, undoubtedly, more complicated than this. The membrane remodeling that allows a redistribution of sodium channels probably causes changes in other membrane-associated proteins, as well. In particular, other ion channels may undergo changes in distribution, quantity, or function. If alterations of voltage-sensitive potassium channels or calcium channels occur, axonal membrane electrical properties could be affected in a complex manner. Peripheral nerve injury should also trigger changes in the CNS such as postsynaptic amplification of afferent barrages and central sensitization, in which normally nonpainful afferent input is perceived as painful.² These other factors notwithstanding, further investigation of ion channel distribution and function within damaged axons should provide a better understanding of the basis for the abnormal electrical

excitability that frequently develops after peripheral nerve trauma. Modification of ion channel distribution or function may prove to be a particularly fruitful approach to the treatment of pain in diseases of the peripheral nervous system.

From the Departments of Neurology (Drs. England, Happel, and Liu), Neurosurgery (Drs. Happel and Kline), and Anatomy (Ms. Thouron), Louisiana State University School of Medicine, New Orleans, LA; and the Department of Physiology (Drs. Gamboni and Levinson), University of Colorado School of Medicine, Denver, CO.

Supported by grants from the National Institutes of Health (NS15879 to S.R.L.), the United States Department of Defense (DAMD 17-93-V-3013 to J.D.E., L.T.H., and D.G.K.), and a Neuroscience Incentive Grant from the Louisiana State University Neuroscience Center (J.D.E. and L.T.H.).

Presented in part at the 47th Annual Meeting of the American Academy of Neurology, Seattle, WA, May 1995.

Received August 29, 1995. Accepted in final form November 13, 1995.

Address correspondence and reprint requests to Dr. John D. England, Department of Neurology, Louisiana State University School of Medicine, 1542 Tulane Avenue, New Orleans, LA 70112-2822.

References

- Wall PD, Gutnick M. Properties of afferent nerve impulses originating from a neuroma. *Nature* 1974;248:740-743.
- Devor M, Lomazov P, Matzner O. Sodium channel accumulation in injured axons as a substrate for neuropathic pain. In: Boivie J, Hansson P, Lindblom U, eds. *Touch, temperature, and pain in health and disease: mechanisms and assessments, progress in pain research and management*. Vol 3. Seattle: IASP Press, 1994:207-230.
- Devor M, Keller CH, Deerinck TJ, Levinson SR, Ellisman MH. Na^+ channel accumulation on axolemma of afferent endings in nerve end neuromas in *Apterodonotus*. *Neurosci Lett* 1989; 102:149-154.
- Devor M, Govrin-Lippmann R, Angelides K. Na^+ channel immunolocalization in peripheral mammalian axons and changes following nerve injury and neuroma formation. *J Neurosci* 1993;13:1976-1992.
- England JD, Gamboni F, Ferguson MA, Levinson SR. Sodium channels accumulate at the tips of injured axons. *Muscle Nerve* 1994;17:593-598.
- England JD, Gamboni F, Levinson SR, Finger TE. Changed distribution of sodium channels along demyelinated axons. *Proc Natl Acad Sci USA* 1990;87:6777-6780.
- Brismar T, Gilly WF. Synthesis of sodium channels in the cell bodies of squid giant axons. *Proc Natl Acad Sci USA* 1987;84: 1459-1463.
- Matzner O, Devor M. Hyperexcitability at sites of nerve injury depends on voltage-sensitive Na^+ channels. *J Neurophysiol* 1994;72:349-359.
- Chabal C, Jacobson L, Russell LC, Burchiel KJ. Pain responses to perineuronal injection of normal saline, gallamine, and lidocaine in humans. *Pain* 1989;36:321-325.
- Chabal C, Russell LC, Burchiel KJ. The effect of intravenous lidocaine, tocainide, and mexiletine on spontaneously active fibers originating in rat sciatic neuromas. *Pain* 1989;38:333-338.

Immunocytochemical Investigations of Sodium Channels Along Nodal and Internodal Portions of Demyelinated Axons

JOHN D. ENGLAND, S. ROCK LEVINSON, AND PETER SHRAGER

Department of Neurology, Louisiana State University School of Medicine, New Orleans, Louisiana 70112 (J.D.E.); Department of Physiology, University of Colorado School of Medicine, Denver, Colorado 80262 (S.R.L.); Department of Physiology, University of Rochester Medical Center, Rochester, New York 14642 (P.S.)

KEY WORDS Ion channels, Neural conduction, Antibodies, Schwann cell, Doxorubicin, Lysolecithin

ABSTRACT Voltage-gated sodium channels are largely localized to the nodes of Ranvier in myelinated axons, providing the physiological basis for saltatory conduction. Studies using anti-sodium channel antibodies have shown that along demyelinated axons sodium channels form new distributions. The nature of this changed distribution appears to vary with the time course and mechanism of demyelination. In chronic demyelination, sodium channels increase in number and redistribute along previously internodal axon segments. In chronic demyelination produced by doxorubicin, the increase in sodium channels appeared independently of Schwann cells, suggesting increased neuronal synthesis. In acute demyelination produced by lyssolecithin new clusters of sodium channels developed but only in association with the edges of remyelinating Schwann cells, which appeared to control the distribution and mobility of the channels. These findings affirm the plasticity of sodium channels in demyelinated axons and are relevant to understanding how these axons recover conduction. © 1996 Wiley-Liss, Inc.

INTRODUCTION

The sodium channel is a transmembrane protein which mediates the voltage-dependent sodium permeability of electrically excitable membranes. The presence of sodium channels is of obvious importance for the generation and propagation of action potentials along axolemma. The distribution of sodium channels along myelinated axons is nonuniform since they are largely localized to the nodes of Ranvier (Chiu, 1980; Ellisman and Levinson, 1982; Neumcke and Stampfli, 1982; Ritchie and Rogart, 1977; Waxman and Ritchie, 1993). This nodal localization of sodium channels provides one of the physiological bases for saltatory conduction. In contrast to these unchallenged observations regarding the localization of sodium channels in myelinated axons, little is known regarding the distribution of sodium channels in demyelinated axons. Such information is important because the resumption of axonal conduction appears the basis for recovery in many demyelinating diseases (Albers et al., 1985; Smith and Hall, 1980; Sumner, 1981). The recent availability of antibodies specifically directed against sodium channels has provided new and refined methods for examining sodium channels along demyelinated axons.

DISTRIBUTION OF SODIUM CHANNELS ALONG MYELINATED AXONS

In normal myelinated axons sodium channels are largely localized to the axolemma at nodes of Ranvier. The most recent electrophysiological and biochemical studies demonstrate an axolemmal sodium channel density of ~1,000 to 2,000/ μm^2 at the nodes of Ranvier compared with a density of 40 to 80/ μm^2 in the internodal segments (Chiu, 1980, 1987; Ellisman and Levin-

son, 1982; Neumcke and Stampfli, 1982; Ritchie and Rogart, 1977; Shrager, 1989; Waxman and Ritchie, 1993). Immunocytochemical studies such as those illustrated in Figures 1 and 2a have provided clear-cut proof of the nodal clustering of sodium channels.

The mechanisms underlying the segregation of sodium channels at nodes of Ranvier are not well understood. The observation that nodal-specific axolemmal specialization can develop independently of myelination suggests that intrinsic axonal factors immobilize sodium channels at nodes of Ranvier, perhaps independently of glial cell contact (Ellisman, 1979; Wiley-Livingston and Ellisman, 1980). Of particular interest in this regard is the protein, ankyrin, which links certain transmembrane proteins with the cytoskeleton in several types of cells, including erythrocytes and neurons (Baines, 1990). One isoform of ankyrin not only localizes to nodes of Ranvier (Kordeli et al., 1990) but also binds to the voltage-gated sodium channel (Srinivasan et al., 1988). These findings provide indirect support for the hypothesis that sodium channels are restricted to the node by their linkage to ankyrin, which associates with the internal cytomatrix via spectrin (Baines, 1990). The particular role played by glial cells in determining or refining nodal clustering of sodium channels is not known, but in one experimental model using co-cultures of sensory neurons and Schwann cells, the clustering of sodium channels on axons appeared to be related to Schwann cell contact (Joe and Angelides,

Received February 13, 1995; accepted in revised form March 20, 1995.

Address reprint requests to John D. England, M.D., Department of Neurology, Louisiana State University Medical Center, 1542 Tulane Avenue, New Orleans, LA 70112.

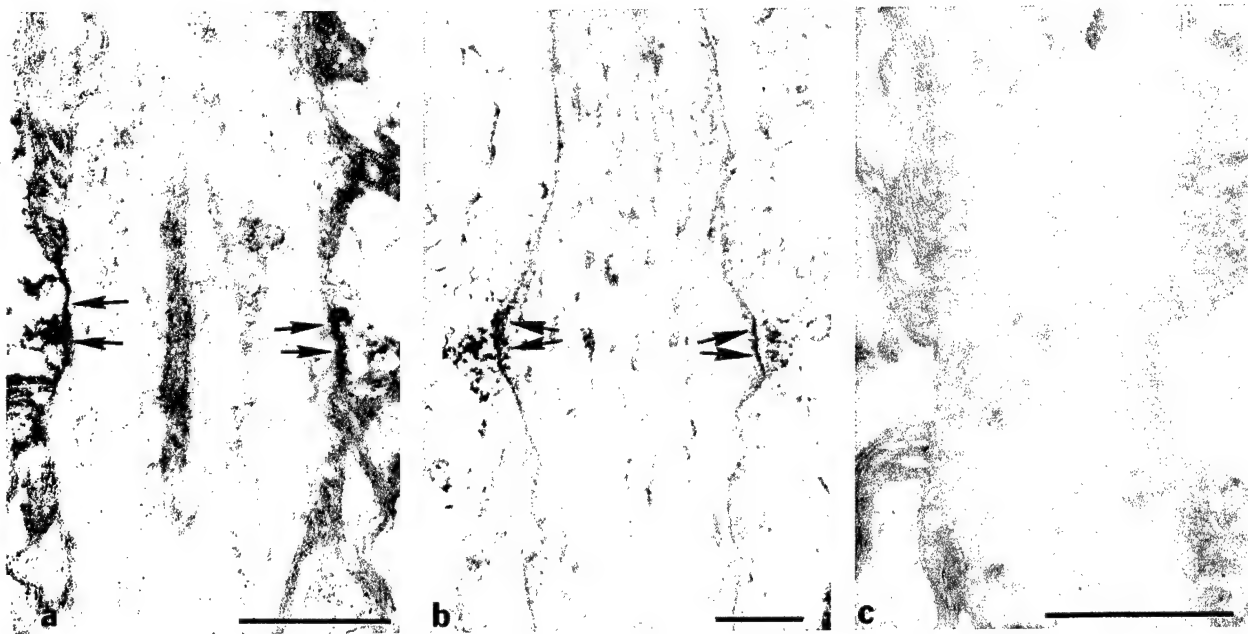


Fig. 1. Sodium channel localization along myelinated axons from the dorsal column of eel (*Electrophorus electricus*) spinal cord using a polyclonal anti-sodium channel antibody. **a:** Partially mechanically desheathed myelinated fiber showing sodium channel-specific immunostaining at the node of Ranvier (arrows). Bar = 1 μm . **b:** Completely mechanically desheathed fiber showing that sodium channel-specific immunostaining is still restricted to the nodal zone despite

antibody access to internodal axolemma (arrows). Bar = 1 μm . **c:** Myelinated fiber reacted with antibody pre-adsorbed with purified sodium channel. The lack of immunostaining confirms antibody specificity for sodium channels. Bar = 1 μm . (Reproduced from Ellisman and Levinson, 1982, with permission of the authors and National Academy of Sciences.)

1992). Even if initial nodal clustering of sodium channels can occur independently of glial cell contact, glial cell-axon interactions could reshape and refine the final distribution of sodium channels. A major possibility is that the density of sodium channels could be suppressed along axolemma ensheathed by Schwann cells.

In the peripheral nervous system Schwann cell processes are closely apposed to the axolemma at nodes of Ranvier, and in the central nervous system astrocyte processes have a similar perinodal anatomy (Berthold and Rydmark, 1983; Hildebrand, 1971; Raine, 1984; Sims et al., 1991; Waxman and Black, 1984). These relationships are so specific that Schwann cell processes (in the PNS) and perinodal astrocyte processes (in the CNS) should be considered integral parts of the node of Ranvier. Thus, in the central nervous system, perinodal astrocytes are important components of the node of Ranvier even though oligodendrocytes provide myelin for the central axons. Both Schwann cells and astrocytes contain sodium channels. Glial sodium channels were documented first in cultured Schwann cells and astrocytes (Bevan et al., 1985; Chiu et al., 1984; Nowak et al., 1987; Shrager et al., 1985), but recent immunohistochemical studies have confirmed that sodium channels are expressed *in situ* by astrocytes and Schwann cells (Black et al., 1989a,b; Ritchie et al., 1990). Why sodium channels exist within these glial cells is not known. One theory is that these satellite cells may function as ancillary sites for the synthesis of sodium channels, which are then transferred to nodal axolemma (Bevan et al., 1985; Gray and

Ritchie, 1985; Shrager et al., 1985). Since neurons produce and transport sodium channels independently of glial cells (Brismar and Gilly, 1987; England et al., 1994; Lombet et al., 1985), axonal sodium channels most likely do not arise exclusively or primarily from satellite cells. Thus, the significance of glial associated sodium channels is currently unknown.

DISTRIBUTION OF SODIUM CHANNELS ALONG DEMYELINATED AXONS

Demyelination is the primary pathophysiologic process in several important diseases of the nervous system. Examples include multiple sclerosis and the demyelinating peripheral neuropathies. In these diseases, at least acutely, most of the symptoms and signs are due to demyelinative conduction block along affected axons. Although remyelination and the re-establishment of saltatory conduction can restore function, many of these diseases are characterized by incomplete remyelination. This is especially true for demyelinative diseases of the central nervous system such as multiple sclerosis where limited remyelination occurs (McDonald, 1974, 1977). The well-established fact that patients with multiple sclerosis often exhibit considerable remission after an attack (despite persistent central nervous system demyelination) suggests that some chronically demyelinated axons can recover conduction, perhaps in a continuous manner (McDonald, 1974, 1977). In view of this possibility, several investigators have been interested in exploring how sodium channels might be reorganized along demyelinated ax-

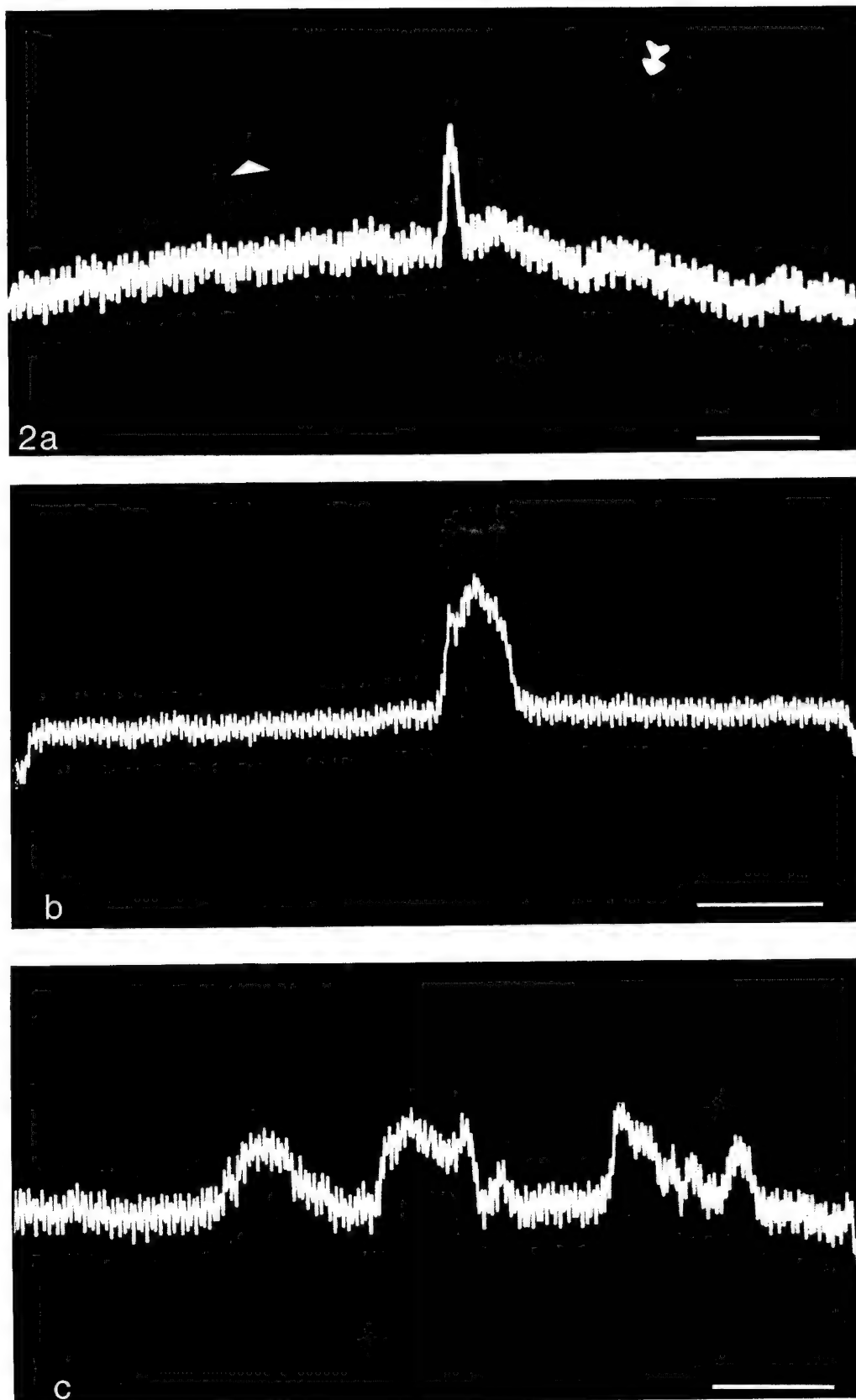


Fig. 2. Sodium channel localization along lateral line nerve axons from *Carassius auratus* using a polyclonal anti-sodium channel antibody. In a, b, and c the top image is the fluorescence photomicrograph and the bottom image is the digitized representation showing the relative pixel intensity along the axons. **a:** Normal myelinated axon. Note the discrete peak of immunoreactivity at the node of Ranvier, and

the virtually undetectable nonspecific fluorescence of mechanically desheathed internodal axon (arrowhead). **b:** Demyelinated axon at 14 days after injection of doxorubicin with one segment of intense immunoreactivity. **c:** Demyelinated axon at 21 days after injection of doxorubicin with multiple segments of intense immunoreactivity. Bars = 50 μm . (Reproduced from England et al., 1990, with permission of the authors and National Academy of Sciences.)

ons. Knowing how these channels are affected by demyelination is important to understanding why demyelinated axons fail to conduct impulses or, conversely, how some might recover conduction.

SUBACUTE AND CHRONIC DEMYELINATION

Several toxins which specifically demyelinate nerve are known. Using them, one can create a well-defined *in vivo* experimental model of demyelinated nerve which is well suited for investigating the resulting modulations of axonal sodium channels.

In vivo intraneuronal microinjection of doxorubicin, a DNA intercalating agent, causes delayed subacute demyelination by killing Schwann cells (England et al., 1988, 1990). In the posterior lateral line nerve of *Carassius auratus* (goldfish) this agent results in extensive segmental demyelination of axons starting at 12 to 14 days postinjection. Using a well-characterized polyclonal antibody directed against sodium channels, immunocytochemical studies have revealed new distributions of sodium channels along some of these demyelinated axons (England et al., 1990). The formation of the new distributions of sodium channels occurred concomitantly with the evolution of segmental demyelination, being evident by days 14 and 21 after injection. The segments of immunoreactivity specific for sodium channels ranged in length from 35 to 72 μm , much longer than nodes of Ranvier, which are approximately 1 μm in length. Several demyelinated axons (especially at days 21 to 28 after injection) showed multiple regions of specific immunoreactivity, each extending over relatively long stretches of bare axolemma (Fig. 2). These changes occurred along axons surrounded only by Schwann cell basal lamina without Schwann cell cytoplasm or myelin, implying that the new patches of sodium channels arose from within the axons themselves. Additionally, the length and location of the sodium channels indicated placement into previously internodal axolemma.

An important issue is whether such new distributions of sodium channels arise from the redistribution of already existing sodium channels at nodes of Ranvier or from the synthesis of new sodium channels. Evidence in favor of the synthesis of new sodium channels is available from radioimmunoassay (RIA) studies. RIA demonstrated a significant increase in the number of sodium channels in doxorubicin-demyelinated lateral line nerves of *C. auratus* (England et al., 1990, 1991). At days 14 and 28 after doxorubicin treatment there was approximately a three- to four-fold increase of sodium channels in the demyelinated nerves (Fig. 3). The time course of this phenomenon exactly paralleled that of the sodium channel distribution changes seen immunocytochemically (England et al., 1990). Taken together, these studies strongly suggest that new sodium channels are inserted into demyelinated axolemma.

Other studies have suggested a redistribution of sodium channels along demyelinated axons. For instance, Bostock and Sears demonstrated short segments of continuous conduction along axons demyelinated by diphtheria toxin (Bostock and Sears, 1976, 1978), and ferric ion-ferrocyanide (FeFCN) staining

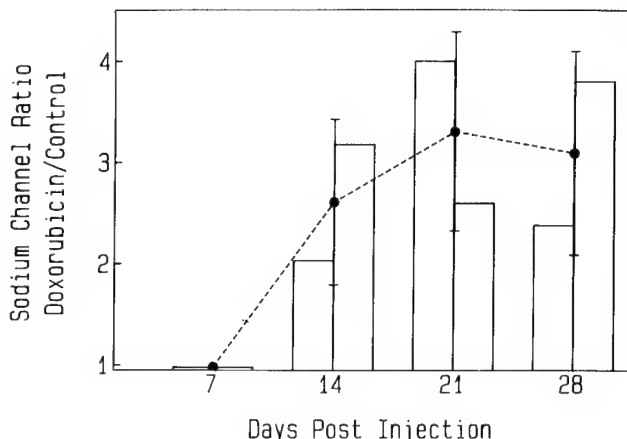


Fig. 3. Time course of the change in sodium channel quantity in nerves demyelinated by doxorubicin. Each column represents the ratio of the sodium channel concentration per wet weight demyelinated nerve/sodium channel concentration per wet weight control nerve for pooled nerve preparations. A total of 88 demyelinated nerves and an equal number of control nerves were analyzed by radioimmunoassay. The mean ratios (●) \pm S.D. are shown. (Reproduced from England et al., 1991, with permission of the authors and Elsevier Science B.V.)

suggested a reorganization of axon membrane in rat demyelinated peripheral nerve fibers (Foster et al., 1980). More recently, increased sodium channel densities (assessed by tritiated saxitoxin binding) have been documented in the hypomyelinated brain of the mutant mouse *shiverer*, which has a deletion of the myelin basic protein gene (Noebels et al., 1991), as well as within the demyelinated brain lesions of human multiple sclerosis (Moll et al., 1991). Interestingly, the magnitude of these increases in sodium channels (two- to four-fold) closely approximates the values found in the RIA studies of doxorubicin-demyelinated nerves (England et al., 1991). Collectively, these data suggest that chronic demyelination in general causes a similar increase in the number of axonal sodium channels.

Although the above-noted studies are all consistent with the placement of new sodium channels along chronically demyelinated axons, the source of these channels is not known. The two major possibilities are that these sodium channels are synthesized within the neuron cell bodies or within glial cells. Sodium channels are quite clearly synthesized in neuron cell bodies (Brisman and Gilly, 1987) and transported within axons by fast axoplasmic transport (Lombet et al., 1985). In nerves demyelinated by doxorubicin, sodium channels increase despite the fact that Schwann cells die, suggesting a neuronal source for the new channels (England et al., 1990, 1991). Closely related work has demonstrated that excess sodium channels accumulate in afferent endings in nerve end neuromas (Devor et al., 1989) and within the tips of injured axons (England et al., 1994), further implying that new sodium channel distributions can arise solely from neuronal mechanisms. Since some astrocytes and Schwann cells contain sodium channels (Bevan et al., 1985; Black et al., 1989a,b; Chiu et al., 1984; Nowak et al., 1987; Ritchie

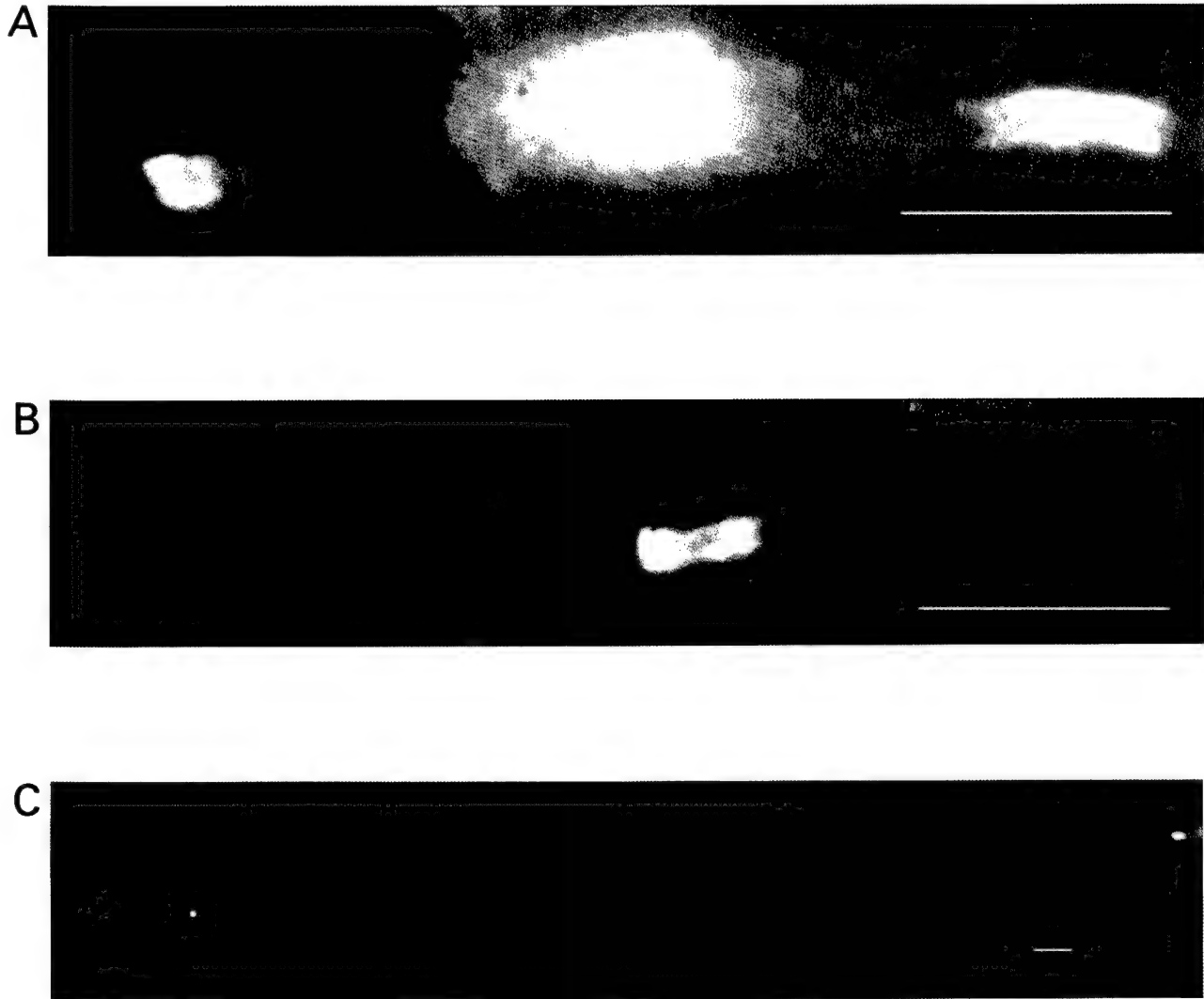


Fig. 4. Sodium channel clustering in remyelinating axons following intraneuronal microinjection of lyssolecithin. **A:** Aggregates of sodium channels form at the edges of a Schwann cell, 14 days postinjection. **B:** Two sodium channel clusters associated with different Schwann cells appear to fuse, forming a new node of Ranvier, also at

14 days postinjection. **C:** Two new nodes of Ranvier separated by a short internode, 60 days postinjection. Bars = 10 μm . (Panel C reproduced from Dugandzija-Novakovic et al., 1995, with permission of the Society for Neuroscience.)

et al., 1990; Shrager et al., 1985), one must, at the least, consider the possibility that these glial cells provide demyelinated axons with new sodium channels. Additionally, neuronal synthesis of sodium channels and glial transport of sodium channels to axons may both occur. Using a polyclonal anti-sodium channel antibody, Black et al. have demonstrated patches of increased sodium channel density along rat spinal cord axons demyelinated by ethidium bromide/irradiation (Black et al., 1991); however, this immunostaining occurred only at axonal sites in contact with astrocyte or Schwann cell processes. The association of astrocytes with sodium channels along demyelinated central nervous system axons is somewhat surprising since it is

the oligodendrocytes which provide myelin in the central nervous system. But, as previously noted, some astrocytes are normally closely apposed to central axons at the perinodal region. Astrocytes, instead of oligodendrocytes, appear to have an intimate association with sodium channels in central axons. In a few other experimental systems the development of sodium channel clusters in axolemma appeared to depend upon glial-axonal contact (Black et al., 1985; Hildebrand and Waxman, 1983; Rosenbluth, 1985; Rosenbluth and Blakemore, 1984). Thus, glial cells may provide or promote the expression of sodium channels along some chronically demyelinated axons. Their exact contribution requires further study.

ACUTE DEMYELINATION

Intraneuronal microinjection of lysolecithin causes acute demyelination (Hall and Gregson, 1971). The initial damage to myelin is visible within a few hours postinjection, progressing to complete demyelination of some axons within a few days. Proliferation of Schwann cells also occurs within a few days, and remyelination is evident by 9 to 10 days postinjection. This acute demyelination and rapid remyelination is, thus, much different than the chronic demyelination and incomplete remyelination which follows doxorubicin injection (England et al., 1988).

Using a site-directed polyclonal anti-sodium channel antibody, sodium channel clustering has been studied along rat sciatic axons demyelinated by intraneuronal injection of lysolecithin (Dugandzija-Novakovic et al., 1995). Demyelination developed rapidly, and by 7 days postinjection many axons exhibited long stretches of complete demyelination. At this stage clusters of sodium channels were rarely seen, appearing only at heminodes (marking the transition from myelinated to demyelinated axon at the injection site) and occasionally in the middle of a demyelinated axonal segment (presumably representing original nodal clusters). Beginning at approximately 8 days, proliferating Schwann cells adhered to demyelinated axons, and clusters of sodium channels were found at the edges of the Schwann cells (Fig. 4A). When the Schwann cells elongated, the clusters of sodium channels seemed to move with them along the axon. As the Schwann cells continued to move toward one another, their associated clusters of sodium channels were forced together in the ever decreasing length of axon separating the Schwann cell processes. Eventually the clusters of sodium channels associated with two apposing Schwann cells appeared to fuse, forming new nodes of Ranvier (Fig. 4B and C). Thus, at least in this model of acute demyelination, sodium channel aggregation and mobility are presumably linked to or controlled by remyelinating Schwann cells.

Previous investigators have studied the electrophysiological changes which occur along axons after acute demyelination. Rat ventral root axons were demyelinated by lysolecithin and examined using the electrophysiological technique of external longitudinal current analysis (Smith et al., 1982). New discrete foci of inward axonal current were seen as early as 4 days after application of lysolecithin, at which time remyelination or other morphological evidence of nodal formation were not yet present. These investigators suggested that these discrete foci of inward current were destined to become new nodes of Ranvier; therefore, they named them "phi" biological nodes or "phi"-nodes. Perhaps these "phi" nodes are the electrophysiological correlate of the sodium channel clusters seen immunocytochemically (Dugandzija-Novakovic et al., 1995) although why the electrophysiological foci were seen earlier (4 days) than the immunocytochemical clusters (8 days) is not known. Whether "phi" nodes require Schwann cell influence for their formation or arise de novo is also not known.

Entirely different electrophysiological results were

documented along rat ventral root axons acutely demyelinated by diphtheria toxin (Bostock and Sears, 1976, 1978). Using the same technique of external longitudinal current analysis, Bostock and Sears recorded inwardly directed membrane currents over relatively long stretches of demyelinated axons, suggesting continuous conduction. Why axons acutely demyelinated by lysolecithin should develop discrete foci of inward current (suggesting discrete foci of sodium channels), whereas axons acutely demyelinated by diphtheria toxin should develop long segments of continuous conduction (suggesting long segments of internodal sodium channels) is an unresolved issue.

Sodium channel redistribution in demyelination may vary not only with the time course of this process (acute, subacute, and chronic) but also with the mechanism of demyelination. Resolution of these issues will require complementary electrophysiological and immunocytochemical studies. Understanding these processes in full will also require identification of the molecular interactions which determine aggregation of sodium channels within the axonal membrane.

ACKNOWLEDGMENTS

We thank Ms. Cathy A. England for secretarial assistance. This work was supported by grants from the National Institutes of Health (NS01272 to J.D.E., NS15879 to S.R.L., and NS17965 to P.S.) and the United States Department of Defense (DAMD17-93-V-3013 to J.D.E.).

REFERENCES

- Albers, J.W., Donofrio, P.D., and McGonagle, T.K. (1985) Sequential electrodiagnostic abnormalities in acute inflammatory demyelinating polyradiculopathy. *Muscle Nerve*, 8:528–539.
- Baines, A.J. (1990) Ankyrin and the node of Ranvier. *TINS*, 13:119–121.
- Berthold, C., and Rydmark, M. (1983) Electron microscopic serial section analysis of nodes of Ranvier in lumbosacral spinal roots of the cat: Ultrastructural organization of nodal compartments in fibres of different sizes. *J. Neurocytol.*, 12:475–505.
- Bevan, S., Chiu, S.Y., Gray, P.T.A., and Ritchie, J.M. (1985) The presence of voltage-gated sodium, potassium and chloride channels in rat cultured astrocytes. *Proc. R. Soc. Lond. (Biol.)*, 225:229–313.
- Black, J.A., Sims, T.J., Waxman, S.G., and Gilmore, S.A. (1985) Membrane ultrastructure of developing axons in glial cell deficient rat spinal cord. *J. Neurocytol.*, 14:79–104.
- Black, J.A., Friedman, B., Waxman, S.G., et al. (1989a) Immuno-ultrastructural localization of sodium channels at nodes of Ranvier and perinodal astrocytes in rat optic nerve. *Proc. R. Soc. Lond. (Biol.)*, 238:38–57.
- Black, J.A., Waxman, S.G., Friedman, B., et al. (1989b) Sodium channels in astrocytes of rat optic nerve in situ: Immuno-electron microscopic studies. *Glia*, 2:353–369.
- Black, J.A., Felts, P., Smith, K.J., Kocsis, J.D., and Waxman, S.G. (1991) Distribution of sodium channels in chronically demyelinated spinal cord axons: Immuno-ultrastructural localization and electrophysiological observations. *Brain Res.*, 544:59–70.
- Bostock, H., and Sears, T.A. (1976) Continuous conduction in demyelinated mammalian nerve fibres. *Nature*, 263:786–787.
- Bostock, H., and Sears, T.E. (1978) The internodal axon membrane: Electrical excitability and continuous conduction in segmental demyelination. *J. Physiol.*, 280:273–301.
- Brismar, T., and Gilly, W.F. (1987) Synthesis of sodium channels in the cell bodies of squid giant axons. *Proc. Natl. Acad. Sci. U.S.A.*, 84:1459–1463.
- Chiu, S.Y. (1980) Asymmetry currents in the mammalian myelinated nerve. *J. Physiol.*, 309:499–519.
- Chiu, S.Y. (1987) Sodium and potassium currents in acutely demyelinated internodes of rabbit sciatic nerves. *J. Physiol.*, 391:631–649.

Chiu, S.Y., Shrager, P., and Ritchie, J.M. (1984) Neuronal-type Na^+ - and K^+ -channels in rabbit cultured Schwann cells. *Nature*, 311: 156–157.

Devor, M., Keller, C.H., Deerinck, T.J., Levinson, S.R., and Ellisman, M.H. (1989) Na^+ channel accumulation on axolemma of afferent endings in nerve end neuromas in Apterous. *Neurosci. Lett.*, 102:149–154.

Dugandzija-Novakovic, S., Koszowski, A.G., Levinson, S.R., and Shrager, P. (1995) Clustering of Na^+ channels and node of Ranvier formation in remyelinating axons. *J. Neurosci.*, 15:492–503.

Ellisman, M.H. (1979) Molecular specializations of the axon membrane at nodes of Ranvier are not dependent upon myelination. *J. Neurocytol.*, 8:719–735.

Ellisman, M.H., and Levinson, S.R. (1982) Immunocytochemical localization of sodium channel distributions in the excitable membranes of Electrophorus electricus. *Proc. Natl. Acad. Sci. U.S.A.*, 79:6707–6711.

England, J.D., Rhee, E.K., Said, G., and Sumner, A.J. (1988) Schwann cell degeneration induced by doxorubicin (Adriamycin). *Brain*, 111: 901–913.

England, J.D., Gamboni, F., Levinson, S.R., and Finger, T.E. (1990) Changed distribution of sodium channels along demyelinated axons. *Proc. Natl. Acad. Sci. U.S.A.*, 87:6777–6780.

England, J.D., Gamboni, F., and Levinson, S.R. (1991) Increased numbers of sodium channels form along demyelinated axons. *Brain Res.*, 548:334–337.

England, J.D., Gamboni, F., Ferguson, M.A., and Levinson, S.R. (1994) Sodium channels accumulate at the tips of injured axons. *Muscle Nerve*, 17:593–598.

Foster, R.E., Whalen, C.C., and Waxman, S.G. (1980) Reorganization of the axon membrane in demyelinated peripheral nerve fibers: Morphological evidence. *Science*, 210:661–663.

Gray, P.T., and Ritchie, J.M. (1985) Ion channels in Schwann and glial cells. *Trends Neurosci.*, 8:411–415.

Hall, S.M., and Gregson, N.A. (1971) The in vivo and ultrastructural effects of injection of lysophosphatidyl choline into myelinated peripheral nerve fibres of the adult mouse. *J. Cell Sci.*, 9:769–789.

Hildebrand, C. (1971) Ultrastructural and light-microscopic studies of the nodal region in large myelinated fibres of the adult feline spinal cord white matter. *Acta Physiol. Scand. (Suppl.)*, 364:43–71.

Hildebrand, C., and Waxman, S.G. (1983) Regional node-like membrane specializations in non-myelinated axons of rat retinal nerve fiber layer. *Brain Res.*, 258:23–32.

Joe, E., and Angelides, K. (1992) Clustering of voltage-dependent sodium channels on axons depends on Schwann cell contact. *Nature*, 356:333–335.

Kordeli, E., Davis, J., Trapp, B., and Bennett, V. (1990) An isoform of ankyrin is localized at nodes of Ranvier in myelinated axons of central and peripheral nerves. *J. Cell Biol.*, 110:1341–1352.

Lombet, A., Laduron, P., Mourre, C., Jacomet, Y., and Lazdunski, M. (1985) Axonal transport of the voltage-dependent Na^+ channel protein identified by its tetrodotoxin binding site in rat sciatic nerves. *Brain Res.*, 345:153–158.

McDonald, W.I. (1974) Remyelination in relation to clinical lesion of the central nervous system. *Br. Med. Bull.*, 30:186–189.

McDonald, W.I. (1977) Acute optic neuritis. *Br. J. Hosp. Med.*, 18:42–48.

Moll, C., Mourre, C., Lazdunski, M., and Ulrich, J. (1991) Increase of sodium channels in demyelinated lesions of multiple sclerosis. *Brain Res.*, 556:311–316.

Neumcke, B., and Stampfli, R. (1982) Sodium currents and sodium-current fluctuations in the rat myelinated nerve fibers. *J. Physiol.*, 329:163–184.

Noebels, J.L., Marcom, P.K., and Jalilian-Tehrani, M.H. (1991) Sodium channel density in hypomyelinated brain increased by myelin basic protein gene deletion. *Nature*, 352:431–434.

Nowak, L., Ascher, P., and Berwald-Netter, Y. (1987) Ionic channels in mouse astrocytes in culture. *J. Neurosci.*, 7:101–109.

Raine, C.S. (1984) On the association between perinodal astrocyte processes and the node of Ranvier in the CNS. *J. Neurocytol.*, 13: 21–27.

Ritchie, J.M., and Rogart, R.B. (1977) Density of sodium channels in mammalian myelinated nerve fibers and nature of the axonal membrane under the myelin sheath. *Proc. Natl. Acad. Sci. U.S.A.*, 74: 211–215.

Ritchie, J.M., Black, J.A., Waxman, S.G., and Angelides, K.J. (1990) Sodium channels in the cytoplasm of Schwann cells. *Proc. Natl. Acad. Sci. U.S.A.*, 87:9290–9294.

Rosenbluth, J. (1985) Intramembranous particle patches in myelin-deficient rat mutant. *Neurosci. Lett.*, 62:19–24.

Rosenbluth, J., and Blakemore, W.F. (1984) Structural specializations in cat of chronically demyelinated spinal cord axons as seen in freeze-fracture replicas. *Neurosci. Lett.*, 48:171–177.

Shrager, P. (1989) Sodium channels in single demyelinated mammalian axons. *Brain Res.*, 483:149–154.

Shrager, P., Chiu, S.Y., and Ritchie, J.M. (1985) Voltage-dependent sodium and potassium channels in mammalian cultured Schwann cells. *Proc. Natl. Acad. Sci. U.S.A.*, 82:948–952.

Sims, T.J., Gilmore, S.A., and Waxman, S.G. (1991) Radial glia give rise to perinodal processes. *Brain Res.*, 549:25–36.

Smith, K.J., and Hall, S.M. (1980) Nerve conduction during peripheral demyelination and remyelination. *J. Neurol. Sci.*, 48:201–219.

Smith, K.J., Bostock, H., and Hall, S.M. (1982) Saltatory conduction precedes remyelination in axons demyelinated with lysophosphatidyl choline. *J. Neurol. Sci.*, 54:13–31.

Srinivasan, Y., Elmer, L., Davis, J., Bennett, V., and Angelides, K. (1988) Ankyrin and spectrin associate with voltage-dependent sodium channels in brain. *Nature*, 333:177–180.

Sumner, A.J. (1981) The physiological basis for symptoms in Guillain-Barré syndrome. *Ann. Neurol. (Suppl.)*, 9:28–30.

Waxman, S.G., and Black, J.A. (1984) Freeze-fracture ultrastructure of the perinodal astrocyte and associated glial junctions. *Brain Res.*, 308:77–87.

Waxman, S.G., and Ritchie, J.M. (1993) Molecular dissection of the myelinated axons. *Ann. Neurol.*, 33:121–136.

Wiley-Livingston, C.A., and Ellisman, M.H. (1980) Development of axonal membrane specializations defines nodes of Ranvier and precedes Schwann cell myelin elaboration. *Dev. Biol.*, 79:334–355.

Neurochemistry International: Cytokine

Date submitted/Revision: May 17, 1996

TUMOR NECROSIS FACTOR ALPHA AND INTERLEUKIN-1 INDUCE ACTIVATION
OF MAP KINASE AND SAP KINASE IN HUMAN NEUROMA FIBROBLASTS

GANG LU,¹ ROGER W. BEUERMAN,^{1*} SHURUM ZHAO,² GUANG SUN,¹
DOAN H. NGUYEN,¹ SUSAN MA,¹ and DAVID G. KLINE²

¹LSU Eye Center and ²Department of Neurosurgery,
Louisiana State University Medical Center School of Medicine,
New Orleans, Louisiana, U.S.A.

*Author to whom all correspondence should be addressed:

Roger W. Beuerman, Ph.D., LSU Eye Center, 2020 Gravier Street,
Suite B, New Orleans, LA 70112
Fax: 504-568-4210

Abstract— Two cytokines, tumor necrosis factor alpha (TNF- α) and interleukin-1 (IL-1), which are released by macrophages during the early inflammatory phase of nerve injury, are known to induce activation of mitogen-activated protein kinase (MAPK) and stress-activated protein kinase (SAPK), which locate at different signal transduction pathways and are involved in cell cycle G₀/G₁ transition and cellular proliferation in human fibroblasts. Activation of these two protein kinases by the cytokines may stimulate fibroblast proliferation in damaged nerves and thereby play a role in the formation of a neuroma, a disorganized mass of tissue that interferes with neural regeneration and repair. To investigate the possibility that this mechanism is operative in neuroma formation, we used cultured, serum-starved fibroblasts from surgically removed human neuromas stimulated with TNF- α and/or IL-1 α and IL-1 β , and measured the activation of MAPK and SAPK using myelin basic protein (MBP) and human c-Jun (1-169) glutathione S-agarose transferase (GST) fusion protein as substrates. For comparison, neuroma fibroblast cultures were also stimulated with phorbol 12-myristate 13-acetate (PMA) and platelet-derived growth factor-AB (PDGF-AB), a potent activator for MAPK. TNF- α and both forms of IL-1 produced a rapid activation of MAPK, with a peak at 15 minutes for TNF- α stimulation, and a peak at 30 minutes for IL-1 stimulation. TNF- α combined with either IL-1 α or IL-1 β produced a synergistic effect on the activation of MAPK. The increases in MAPK induced by TNF- α and IL-1 were similar to the increases induced by PMA and PDGF-AB. To confirm the presence of MAPK, immunoprecipitation and immunoblotting were carried out on experimental and control lysates. TNF- α and IL-1 also increased activation of SAPK, but to a lesser extent than MAPK. PMA and PDGF-AB were also much less effective in stimulating activation of SAPK. Our findings indicate that TNF- α and IL-1 activate parallel signal transduction pathways in

human neuroma fibroblasts, and that they are relatively stronger activators of MAPK than of SAPK. Previous studies have convincingly demonstrated that MAPK and SAPK are involved in human fibroblast proliferation (Brach *et al.*, 1993; Meloche, 1995; Pagès *et al.*, 1993). The results of our study suggest that TNF- α and IL-1 may play a role in frustrating functional nerve regeneration after injury by stimulating these two kinases which, in turn, leads to fibroblast proliferation and neuroma formation.

Injury to peripheral nerve initiates a series of cellular reactions that include invasion of the injury site by inflammatory cells and activation and transformation of the neural fibroblasts and Schwann cells. Interruption of the vascular supply and the associated cellular damage allow macrophages and other cells of immune origin to gain easy access to the interior of the nerve (Frisén *et al.*, 1993; Venezie *et al.*, 1995). Macrophages secrete large amounts of cytokines, in particular tumor-necrosis factor alpha (TNF- α). The environment in which this occurs (the interior of the damaged nerve) is somewhat sequestered from the extra-neuronal space and there is ample opportunity for the fibroblasts and Schwann cells therein to be exposed to cytokines or other cell signaling molecules.

An undesirable consequence of nerve damage is the development of a neuroma, which prevents neural growth and functional recovery. A neuroma consists of a disorganized mass of connective tissue made up largely of fibroblasts and their collagen products. Cytokines, which can be damaging or stimulatory to fibroblasts, may be involved in neuroma formation, but their role, if any, is unclear. The purpose of this study was to examine the response of human neuroma fibroblasts to cytokines and to determine if a growth or proliferative response could be identified.

TNF- α (cachectin), a product of stimulated monocytes and macrophages, is a 17-kDa polypeptide that binds to two specific receptors (55 kDa and 80 kDa) and mediates a wide range of biological activities (Vilcek and Lee, 1991). In human fibroblasts, the 55-kDa receptor is the major functional receptor for TNF- α (Tartaglia and Goeddel, 1991). Interleukin-1 occurs in the form of two polypeptides, IL-1 α and IL-1 β , which are distinct gene products with molecular weights of 17 kDa. However, they recognize the same cell surface receptors and share various biologic activities. There are two types of receptors for

IL-1. Receptor type I is a major functional receptor; the 25-kDa cytoplasmic portion is essential for signaling. Receptor type II is a smaller protein and is unimportant in signal transduction (Sims *et al.*, 1993). Both TNF- α and IL-1 are proinflammatory cytokines and induce some similar biological effects, particularly those associated with local and systemic inflammatory processes, but they share only 3% of their primary amino acid structure and have entirely different receptors (Dinarello, 1991). TNF- α and IL-1 have been shown to stimulate fibroblast proliferation, modulate reparative functions following tissue injury, and accelerate wound healing (Dinarello, 1991; Schmidt *et al.*, 1982; Sugarman *et al.*, 1985; Vilcek *et al.*, 1986; Vilcek and Lee, 1991).

Previous studies have demonstrated that TNF- α and IL-1 activate several protein kinases, including MAPK, in human fibroblasts, indicating that these two cytokines may share a cytoplasmic component of a signal transduction pathway (Guy *et al.*, 1991). Activation of MAPK is an absolute requirement for triggering the fibroblast proliferative response and cell cycle progression (Meloche, 1995, Pagès, 1993). Recent studies have confirmed that, in some types of cells, TNF- α and IL-1 also induce activation of a novel protein kinase, stress-activated protein kinase (SAPK), which is part of a signal transduction cascade related to, but distinct from, the MAPK pathway (Brach *et al.*, 1993; Kyriakis *et al.*, 1994; Sánchez *et al.*, 1994; Sluss *et al.*, 1994; Westwich *et al.*, 1994; Whitmarsh *et al.*, 1995). Activated MAPK and/or SAPK can translocate into the nucleus and regulate the early response genes *c-jun* and *c-fos*, which are activated prior to the G₀/G₁ cell cycle transition. Neutralizing antibodies to *c-jun* or *c-fos* are capable of abolishing cell cycle progression in human fibroblasts.

In the present study, we stimulated fibroblasts cultured from human neuroma tissues

with TNF- α and IL-1 and found that both protein kinases, MAPK and SAPK, were activated in the stimulated cells. For activation of MAPK, the effect of a combination of TNF- α and either IL-1 α or IL-1 β was synergistic. PMA and PDGF-AB increased activation of MAPK, but had only weak effects on SAPK. These results suggest that TNF- α and IL-1 may trigger fibroblast proliferation and accelerate the early stages of neuroma formation after injury to peripheral nerve.

EXPERIMENTAL PROCEDURES

Materials

Human recombinant TNF- α (3.3×10^4 units/ μ g), IL-1 α (1×10^4 units/ μ g), IL-1 β (1×10^4 units/ μ g), and platelet-derived growth factor isoform AB (PDGF-AB) were purchased from Upstate Biotechnology Incorporated (UBI, Lake Placid, NY). Anti-MAPK rabbit polyclonal antibody covalently coupled to protein A agarose by dimethylpimelimidate; anti-human MAPK polyclonal antibody, which recognizes 42-kDa and 44-kDa isoforms of MAPK; and human c-Jun (1-169) GST fusion protein were also purchased from UBI. Protein transfer membrane was obtained from Amersham (England). [γ - 32 P]ATP (800 Ci/mmol) and 125 I-protein A (58.67 mCi/mg) were obtained from ICN (Irvine, CA). Sodium pyrophosphate, trichloroacetic acid, b-glycerolphosphate, and b-mercaptoethanol were purchased from Aldrich Chemical Co. (Milwaukee, WI). Dulbecco's Modified Eagle Medium (D-MEM) and fetal bovine serum were obtained from Gibco BRL, Life Technologies, Inc. (Grand Island, NY). PMA and all other reagents were purchased from Sigma (St. Louis, MO).

Cell culture and cytokine treatment

Human neuroma tissues obtained from surgical patients were cut into pieces and cultured in D-MEM containing 20% fetal bovine serum, 100 units/ml penicillin, and 100 µg/ml streptomycin, and maintained at 37°C in a humidified atmosphere of air with 5% CO₂. The cells were used at passages 2 to 6. In each passage, about 1 x 10⁶ cells were seeded in 100 mm polystyrene tissue culture dishes and allowed to grow to confluence. The medium was changed to serum-free medium for 24 hr prior to experimental manipulation. The quiescent cells were stimulated by adding 10 ng/ml TNF-α, 3 ng/ml IL-1α, or 3 ng/ml IL-1β or a combination of TNF-α and IL-1α or IL-1β. In another experiment, PDGF-AB (10 ng/ml) was added to the culture medium, and the cells were incubated for 15 min at 37°C, or PMA (300 ng/ml) was added to the medium and the cells were incubated for 10 min at 37°C. Control cells were cultured in the same fashion but were not stimulated with cytokines.

MAPK in vitro assay

Experimental and control cells were washed three times in ice-cold phosphate-buffered saline, then scraped into 500 µl of ice-cold lysis buffer containing 50 mM b-glycerolphosphate (pH 7.4), 7 mM NaF, and 0.3 mM EDTA. The cell lysate was collected into a pellet pestle tube (Kontes) and centrifuged at 5000 rpm for 5 min at 4°C. The pellets were ground, then centrifuged again at 12,000 rpm for 15 min at 4°C. The supernatant was collected into Eppendorf microcentrifuge tubes and stored at -70° C for analysis. The protein concentration was measured with BCA protein assay reagent (Pierce, Rockford, IL).

MAPK activity was determined with the use of myelin basic protein (MBP) as substrate. In this procedure, 15 µl of cell extract, 10 µl (2 µg/µl) MBP, 15 µl reaction buffer

mixture containing 70 mM b-glycerolphosphate, 10 mM NaF, 0.6 mM EDTA, 15 mM MgCl₂, 2 mM dithiothreitol, 2 µCi [γ -³²P]ATP, and 10 µM ATP were added. The tubes were vortexed gently and incubated for 10 min at 30°C. The reaction was stopped by placing 20-µl aliquots of the kinase assay mixture onto 2 × 2 cm squares of P81 phosphocellulose papers, which were then washed in 0.75% phosphoric acid for 15 min with three changes of buffer. After the papers were rinsed in acetone for 5 min, each paper was transferred into a scintillation vial and radiolabel incorporation was determined by liquid scintillation counting. The remaining reaction mixture was mixed with 15 µl of 2X Laemmli's sample buffer, boiled for 5 min, and subjected to 10% SDS-PAGE. The gel was washed extensively in a washing buffer containing 1% sodium pyrophosphate and 5% trichloroacetic acid, then dried for autoradiography.

Immunocomplex MAPK assay

Experimental and control cells were washed three times with ice-cold phosphate-buffered saline, then lysed in 500 µl of lysis buffer containing 50 mM b-glycerolphosphate (pH 7.4), 7 mM NaF, 0.3 mM EDTA, 10 µg/ml pepstatin, and 10 µg/ml aprotinin. The cell lysates were centrifuged at 12,000 rpm in an Eppendorf microcentrifuge tube for 15 min at 4°C. The supernatant (300 µl) was collected and incubated with protein A-agarose rabbit polyclonal antibody to MAPK for 2 hr at 4°C. After centrifugation, the supernatant was removed, the bead-antibody-antigen complex was washed twice with lysis buffer, and the complex was resuspended in 20 µl of substrate (MBP, 2 µl/ml). The reaction was started by adding 20 µl of the reaction buffer mixture containing 5 µCi [γ -³²P]ATP and 10 µM ATP, and the samples were incubated for 10 min at 37°C. The reaction was stopped by the addition

of 20 μ l of 2X Laemmli's sample buffer. The samples were boiled for 5 min and subjected to 10% SDS-PAGE. After electrophoresis, the gel was dried and autoradiography was performed. Band densities were determined by scanning with a StrataScan 7000 (StrataGene, CA).

Immunoblotting

Equal volumes of lysate were subjected to 10% SDS-PAGE. After electrophoresis, the proteins were transferred to a membrane using transfer buffer containing 20 mM Trisma (base) (pH 8.6), 120 mM glycine, and 20% (V/V) methanol. The membrane was washed with PBS (pH 7.4), blocked with freshly prepared PBS containing 3% nonfat dry milk, and subsequently probed with rabbit polyclonal antibody to MAPK diluted 1:200 in PBS nonfat milk buffer overnight at 4°C. The next day, the membrane was washed with PBS buffer. For detection of antibody, the membrane was incubated in PBS nonfat milk buffer containing 125 I-protein A (1 μ Ci/ml) for 2 hr at room temperature, washed three times in PBS buffer, dried, and exposed to x-ray film at -70°C.

Solid-phase JNK assay

A previously described method (Hibi *et al.*, 1993) was modified slightly and adapted for this experiment. Briefly, cultured cells were lysed with a buffer containing 25 mM HEPES (pH 7.7), 0.3 M NaCl, 1.5 mM MgCl₂, 0.2 mM EDTA, 0.1% Triton X-100, 0.5 mM DTT, 20 mM b-glycerolphosphate, 0.1 mM Na₃VO₄, 2 μ g/ml leupeptin, and 100 μ g/ml PMSF. The lysates were diluted in buffer containing 25 mM HEPES (pH 7.7), 75 mM NaCl, 2.5 mM MgCl₂, 0.1 mM EDTA, 0.05% Triton X-100, 0.5 mM DTT, 20 mM b-glycerolphosphate, 0.1

mM Na₃VO₄, 2 µg/ml leupeptin, and 100 µg/ml PMSF. Diluted cell lysates (300 µl with 30 µg protein) were mixed with 5 µl of c-Jun GST agarose suspension and incubated with gentle agitation for 2 hr at 4°C, then pelleted by centrifugation. The complexes were washed three times with HEPES binding buffer [20 mM HEPES (pH 7.7), 50 mM NaCl, 2.5 mM MgCl₂, 0.1 mM EDTA, and 0.05% Triton X-100], resuspended in 20 µl of kinase buffer [20 mM HEPES (pH 7.6), 20 mM MgCl₂, 20 mM b-glycerolphosphate, 20 mM p-nitrophenyl phosphate, 0.1 mM Na₃VO₄, 2 mM DTT] containing 20 µM ATP and 3 µCi [γ -³²P]ATP, and incubated for 20 min at 30°C. The reaction was terminated by adding 20 µl of 2X Laemmli's sample buffer and the samples were subjected to 10% SDS-PAGE. After electrophoresis the gel was washed with washing buffer for staining and autoradiography. The band density of phosphorylated c-Jun GST fusion protein was determined by scanning densitometry.

RESULTS

Kinetics of MAPK activation

MAPK phosphorylates MBP *in vitro* as a specific substrate. By measuring the ability of lysates from experimental and control cells to phosphorylate MBP, we determined the ability of cytokines alone and in combination to activate MAPK in human neuroma fibroblasts. To determine optimal concentrations and contact time for stimulation, we initially measured the activity of MAPK in a concentration series following stimulation by TNF- α and IL-1. In this system, a peak of MAPK activation was reached for TNF- α at 10 ng/ml (Fig. 1A). This concentration is consistent with previous reports that cytokines in low concentration can stimulate proliferation and mediate various cellular functions of fibroblasts (Hattori *et al.*, 1993; Sugarman *et al.*, 1985; Vilcek *et al.*, 1986). The profile for IL-1 α appeared to have two

peaks, one at 1 ng and one at 100 ng; however, in preliminary experiments involving stimulation with IL-1 α and TNF- α in combination, 3 and 6 ng of IL-1 α gave similar results, and, therefore, 3 ng was chosen for use in subsequent experiments. As seen in Fig. 1-C, the peak at 6 ng was only slightly and non-significantly greater than the value at 3 ng. (Although we also saw a peak at 100 ng, this concentration is probably not physiological.) The time-dependent study of MAPK activation showed that TNF- α induced a rapid activation of MAPK; the level was maximal at 15 min, then declined to control level at 1 hr (Fig. 1D). For IL-1 α and IL-1 β stimulation, MAPK activity was maximal at 30 min (a slight delay from the peak with TNF- α), and declined by 60 minutes (Fig. 1E, F).

TNF- α and IL-1 activation of MAPK in human neuroma fibroblasts

We evaluated MAPK activation produced by TNF- α and IL-1, individually and in combination, using a 15-min stimulation period. PMA and PDGF-AB, two known activators of MAPK, were selected as positive controls. PMA is a potent activator of MAPK, exerting its effect by phosphorylation of protein kinase C and Raf-1 signal transduction pathways. We used 300 ng/ml of PMA, which produced maximal stimulation in the human neuroma fibroblasts (data not shown). PDGF-AB, a major functional isoform of platelet-derived growth factor that also stimulates fibroblast proliferation (Meyer-Ingold and Eichner, 1995), was used at a concentration of 10 ng/ml. PDGF-AB is an intrinsic tyrosine MAPK activator and the signal transduction pathway and mitogenic effects are well documented (Lubinus *et al.*, 1994; Marshall, 1995; Valius and Kazlauska, 1993). Following the 15-min stimulation period, the lysates from experimental and control cells were reacted with substrate (MBP) and reaction buffer containing [γ - 32 P]ATP for 10 min. Phosphorylation of MBP was used as the measure

of MAPK activity in the lysates.

The results showed that treatment with either TNF- α or IL-1 alone increased activation of MAPK nearly 2.5-fold, compared with control. Samples treated with a combination of TNF- α and IL-1 showed a 3.5-fold increase in the phosphorylation of MBP, an increase greater than that produced by either cytokine alone (Fig. 2). The increase resulting from stimulation by the two cytokines together was also greater than that produced by PDGF-AB and was similar to that produced by PMA, which was the most potent activator used in our study. These results demonstrated that TNF- α and IL-1 are individually capable of activating MAPK and also that stimulation with the two cytokines together produces a synergistic effect that further enhances MAPK activation. Statistical analysis of the results from 8 to 11 independent repetitions showed that activation by TNF- α and IL-1 α together was significantly greater than activation by either one alone ($p < 0.0001$). Activation by TNF- α and IL-1 β was also greater than activation by TNF- α alone ($p < 0.001$), but was not significantly different from activation by IL-1 β ($p = 0.051$).

We undertook to demonstrate activation of MAPK more specifically, in that it is possible that some other protein kinase could potentially phosphorylate MBP, the substrate used in this study. To this end, immunoprecipitation of MAPK from experimental and control lysates was carried out with protein A-agarose bound to rabbit polyclonal antibody to MAPK, and the resulting immunocomplex was reacted with MBP and reaction buffer containing [γ -³²P]ATP. Following electrophoresis, the densities of the phosphorylated MBP bands were calculated. It was found that, after stimulation with TNF- α , IL-1 α , and IL-1 β , MAPK levels were 4.5-, 2.3- and 3-fold higher than control levels, respectively. The combination of TNF- α and IL-1 α and the combination of TNF- α and IL-1 β produced 5.5- and 6-fold higher levels,

respectively, compared with controls. PMA stimulation produced 7-fold higher levels, and PDGF-AB produced 5-fold higher levels, compared with controls (Fig. 3). Thus, activation of MAPK and the synergistic effect the combination of TNF- α and IL-1 were confirmed in these experiments.

We analyzed MAPK by immunoblotting with a polyclonal antibody that recognizes both the 42-kDa and the 44-kDa isoforms. Activation of MAPK requires phosphorylation on the threonine and serine residues, which changes the electrophoretic mobility. In untreated control cells, the 42-kDa band was seen, but the 44-kDa band was somewhat stronger. In the lysate from the cytokine-treated cells (Fig. 4), however, the 44-kDa band was considerably more intense than the 42-kDa band. This type of molecular weight shift is consistent with MAPK activation.

TNF- α and IL-1 activation of JNK/SAPK signaling pathway

Recent studies have found that in some cell types, TNF- α and IL-1 activate a distinct signal transduction pathway, the JNK/SAPK signaling pathway, which is thought to be responsible for phosphorylation of the transactivating domain of the c-Jun protein *in vivo* and is an upstream regulator of activation of the *c-jun* gene. Phosphorylated c-Jun homodimers have potent AP-1 activity and control the expression of a number of genes.

To determine if TNF- α and IL-1 induce activation of the JNK pathway in human neuroma fibroblasts, solid-phase protein kinase assays were carried out using a GST fusion protein containing amino acids 1-169 of c-Jun. This c-Jun GST fusion protein is bound through its GST moiety to glutathione (GSH)-agarose beads to generate an affinity matrix for identification of c-Jun binding proteins. The c-Jun amino-terminal kinase binds to a specific

region within the c-Jun transactivation domain and phosphorylates serine 63 and serine 73.

After binding and SDS-PAGE, an increase in phosphorylated c-Jun GST was found in lysates treated with TNF- α , IL-1 α , or IL-1 β . IL-1 β alone and IL-1 β in combination with TNF- α phosphorylated the protein more efficiently than any of the other cytokines or combinations used in this study. Control lysates, as well as those involving PMA and PDGF stimulation, showed only weak phosphorylation of c-Jun GST (Fig. 5).

DISCUSSION

Our results demonstrate that TNF- α and IL-1 activate MAPK in human neuroma fibroblasts. Previous studies have shown that these cytokines share many common biological activities, despite the fact that they are structurally unrelated and bind to different cell surface receptors (Dinarello, 1991). This phenomenon could be explained by sharing of a common segment of a signal transduction pathway. Two-dimensional gel electrophoresis has demonstrated that both TNF- α and IL-1 increase phosphorylation of a specific group of at least 23 proteins and decrease phosphorylation of 10 additional proteins, whereas other cytokines do not exhibit this effect (Guy *et al.*, 1991; 1992). Because the TNF- α and IL-1 receptors lack intrinsic kinase activity, the cytokines bind to their receptors and initiate a signaling cascade by phosphorylation of intracellular protein kinases, including protein kinase C, protein kinase A, phospholipase C, MAPK, and SAPK (Brenner *et al.*, 1989; Mizel, 1990; Saklatvala, 1995; Sluss *et al.*, 1994; Vietor *et al.*, 1993; Vilcek and Lee, 1991; Whitmarsh *et al.*, 1995). The receptor for PDGF-AB does have intrinsic tyrosine kinase activity (Lubinus *et al.*, 1994; Valius and Kazlauska, 1993), and PMA is a potent tumor promoter and strong

MAPK activator (Gause *et al.*, 1993; Srinivasan and Begum, 1994). In our study, both induced a large increase in activation of MAPK, but only weak activation of SAPK, and the increase in MAPK activation stimulated by TNF- α and IL-1 was similar to that produced by PMA and PDGF-AB. These results indicate that TNF- α and IL-1 are relatively potent stimulators of MAPK in these cells.

MAPK can phosphorylate a large number of proteins after they are activated. These proteins, which include c-Fos, Elk-1, and c-Myc, are often regulatory in nature and are located in the cytoplasm and the nucleus (Saklatvala, 1995). Moreover, upstream proteins of the MAPK cascade, including NGF receptor, EGF receptor, PTP2C, SOS, Raf-1, and MEK, are also good substrates for MAPK (Cano and Mahadevan, 1995; Seger and Krebs, 1995). Cytoskeletal elements, such as MAP-1, MAP-2, and MAP-4, are also substrates for MAPK (Saklatvala, 1995; Seger and Krebs, 1995); phosphorylation of these proteins regulates cytoskeletal rearrangements and cellular morphology.

Usually, activation of MAPK is involved in the cell cycle G₀/G₁ transition and is directly correlated with cellular proliferation (Boulton *et al.*, 1990; Meloche, 1995). However, in some types of cells, such as neurons, activation of MAPK is unrelated to cell proliferation (Qui and Green, 1992; Traverse *et al.*, 1992). MAPK activation in PC12 cells causes cellular differentiation that is frequently accompanied by cessation of proliferation (Cowley *et al.*, 1994). Some forms of PDGF are potent activators of MAPK in human fibroblasts; the isoforms PDGF-AB and PDGF-BB elicit a strong mitogenic response, whereas PDGF-AA is not a major functional isoform and does not have a significant effect on DNA synthesis in the cells (Lubinus *et al.*, 1994; Meyer-Ingold and Eichner, 1995). Both TNF- α and IL-1 have

been shown to promote MAPK activation and also to promote DNA synthesis in fibroblasts. In fact, these activities of the two cytokines have been most convincingly demonstrated in studies of fibroblasts (Guy *et al.*, 1991; Vietor *et al.*, 1993; Vilcek *et al.*, 1986; Schmidt *et al.*, 1982). Data from our study substantiate the finding that TNF- α and IL-1 may accelerate cell proliferation following activation of MAPK. However, our study also shows that TNF- α and IL-1 activate MAPK synergistically, which may be due to binding of the cytokines to different receptors affecting a common target kinase. TNF- α and IL-1 show many synergistic functions (Dinarello, 1991; Vilcek and Lee, 1991), and these cytokines have been found in wound fluid and plasma after injury (Grayson *et al.*, 1993; Wells *et al.*, 1992), which suggests that they have intrinsic secondary relationships to one another.

TNF- α and IL-1 activate SAPK in human neuroma fibroblasts, a signal transduction pathway thought to be distantly related to the MAPK pathway. Two SAPK isoforms (46-kDa SAPK₁ and 55-kDa SAPK₂) have been identified. SAPK can activate transcriptional activity of *c-jun* by phosphorylation of the c-Jun NH₂-terminal domain at serine 63 and 73 (Hibi *et al.*, 1993; Kyriakis *et al.*, 1994) MAPK and SAPK are similar in that both require dual phosphorylation at threonine and serine within subdomain VIII for activation (Cano and Mahadevan, 1995). However, upstream protein kinases are distinct. For downstream substrates, although MAPK also phosphorylates c-Jun, phosphopeptide mapping has indicated that phosphorylation occurs at a C-terminal site on Ser-243 that is inhibitory (Minden *et al.*, 1994). In our study, activation of SAPK was induced by TNF- α and IL-1 binding to their receptors and mediating a distinct signaling transduction pathway.

Cytokines affect both MAPK and SAPK (Saklatvala, 1995); however, the

transcriptional control site is thought to be a physiologically significant target of their signaling transduction pathways (Whitmarsh *et al.*, 1995). Several studies have demonstrated that MAPK induces activation of *c-fos* and SAPK activates *c-jun*. Both *c-fos* and *c-jun* are components of the AP-1 transcription factor complex, which is capable of forming homodimers and heterodimers with various other members of the Jun-Fos family (Angel and Karin, 1991). TCF and Elk-1 can also be substrates for both MAPK and SAPK. Phosphorylation of Elk-1 by these kinases leads to increased TCF at SRE (serum response element) and increased transcriptional activity, which contributes to increased *c-fos* expression by activating the *c-fos* promoter associated with SRE (Whitmarsh *et al.*, 1995). Increased expression of Fos and Jun proteins is essential for activation of AP-1. Studies have also demonstrated that TNF- α -stimulated fibroblast proliferation requires activation of *c-jun*/AP-1 (Brach *et al.*, 1993). In our study, TNF- α and IL-1 increased activation of MAPK and SAPK, which would, in turn, promote fibroblast proliferation by increasing *c-fos* and *c-jun* activity.

TNF- α and IL-1 are secreted by macrophages in the peripheral and central nervous systems, and the levels of these cytokines have been shown to increase dramatically in plasma 24 to 48 hrs after peripheral nerve injury (Wells *et al.*, 1992). In addition, cytokines can induce non-neuronal cells such as astrocytes, Schwann cells, and fibroblasts to produce NGF, which may facilitate the regeneration of injured axons (Carman-Krzan *et al.*, 1991; Lindholm *et al.*, 1987, 1988; Hattori *et al.*, 1993). Our results indicate that TNF- α and IL-1 induce activation of MAPK and SAPK in human neuroma fibroblasts and that these activated protein kinases may act to accelerate fibroblast proliferation, which clearly has a central role in neuroma formation. The results of this and other studies suggest that early inflammatory

events may have an important role in the initiation of cellular events that could lead to neuroma formation. However, additional events, possibly including the lingering presence of inflammatory cells and the continued release of cytokines, must occur to maintain the activation of the fibroblasts beyond the role required for repair.

Acknowledgement —This work was supported in part by Department of the Army, Cooperative Agreement DAMD17-93-V-3013 (This does not necessarily reflect the position or the policy of the government, and no official endorsement should be inferred.) and U.S. Public Health Service grants EY04074 (Dr. Beuerman) and EY02377 (Departmental Core Facility) from the National Eye Institute, National Institutes of Health, Bethesda, Maryland.

REFERENCES

Angel P. and Karin M. (1991) The role of Jun, Fos and the AP-1 complex in cell-proliferation and transformation. *Biochim. Biophys. Acta* **1072**, 129-157.

Boulton T. G., Yancopoulos G. D., Gregory J. S., Slaughter C., Moomaw C., Hsu J. and Cobb M. H. (1990) An insulin-stimulated protein kinase similar to yeast kinases involved in cell cycle control. *Science* **249**, 64-67.

Brach M. A., Gruss H. J., Sott C. and Herrmann F. (1993) The mitogenic response to tumor necrosis factor alpha requires c-Jun/AP-1. *Mol. Cell. Biol.* **13**, 4284-4290.

Brenner D. A., O'Hara M., Angel P., Chojkier M. and Karin M. (1989) Prolonged activation of jun and collagenase genes by tumor necrosis factor-a. *Nature* **337**, 661-663.

Cano E. and Mahadevan L. C. (1995) Parallel signal processing among mammalian MAPKs. *Trends Biochem. Sci.* **20**, 117-122.

Carman-Krzan M., Vig'e X. and Wise B. C. (1991) Regulation by interleukin-1 of nerve growth factor secretion and nerve growth factor mRNA expression in rat primary astroglial cultures. *J. Neurochem.* **56**, 636-643.

Cowley S., Paterson H., Kemp P. and Marshall C. J. (1994) Activation of MAP kinase is necessary and sufficient for PC12 differentiation and for transformation of NIH 3T3 cells. *Cell* **77**, 841-852.

Dinarello C. A. (1991) Interleukin-1 and interleukin-1 antagonism. *Blood* **77**, 1627-1652.

Frisén J., Risling M. and Fried K. (1993) Distribution and axonal relations of macrophages in a neuroma. *Neuroscience* **55**, 1003-1013.

Gause K. C., Homma M. K., Licciardi K. A., Seger R., Ahn N. G., Peterson M. J., Krebs E.

C. and Meier K. E. (1993) Effects of phorbol ester on mitogen-activated protein kinase activity in wild-type and phorbol ester-resistant EL4 thymoma cells. *J. Biol. Chem.* **268**, 16124-16129.

Grayson L. S., Hansbrough J. F., Zapata-Sirvent R. L., Dore C. A., Morgan L. J. and Nicholson M. A. (1993) Quantitation of cytokine levels in skin graft donor site wound fluid. *Burns* **19**, 401-405.

Guy G. R., Chua S. P., Wong N. S., Ng S. B. and Tan Y. H. (1991) Interleukin 1 and tumor necrosis factor activate common multiple protein kinases in human fibroblasts. *J. Biol. Chem.* **266**, 14343-14352.

Guy G. R., Coa X., Chua S. P. and Tan Y. H. (1992) Okadaic acid mimics multiple changes in early protein phosphorylation and gene expression induced by tumor necrosis factor or interleukin-1. *J. Biol. Chem.* **267**, 1846-1852.

Hattori A., Tanaka E., Murase K., Ishida N., Chatani Y., Trujimoto M. N., Hayashi K. and Kohno M. (1993) Tumor necrosis factor stimulates the synthesis and secretion of biologically active nerve growth factor in non-neuronal cells. *J. Biol. Chem.* **268**, 2577-2582.

Hibi M., Lin A., Smeal T., Minden A. and Karin M. (1993) Identification of an oncoprotein- and UV-responsive protein kinase that binds and potentiates the c-Jun activation domain. *Genes Dev.* **7**, 2135-2148.

Kyriakis J. M., Banerjee P., Nikolakaki E., Dai T., Rubie E. A., Ahmad M. F., Avruch J. and Woodgett J. R. (1994) The stress-activated protein kinase subfamily of c-Jun kinases. *Nature* **369**, 156-160.

Lindholm D., Heumann R., Meyer M. and Thoenen H. (1987) Interleukin-1 regulates synthesis of nerve growth factor in non-neuronal cells of rat sciatic nerve. *Nature* **330**, 658-659.

Lindholm D., Heumann R., Hengerer B. and Theonen H. (1988) Interleukin 1 increases stability and transcription of mRNA encoding nerve growth factor in cultured rat fibroblasts. *J. Biol. Chem.* **263**, 16348-16351.

Lubinus M., Meier K. E., Smith E. A., Gause K. C., LeRoy E. C. and Trojanowska M. (1994) Independent effects of platelet-derived growth factor isoforms on mitogen-activated protein kinase activation and mitogenesis in human dermal fibroblasts. *J. Biol. Chem.* **269**, 9822-9825.

Marshall C. J. (1995) Specificity of receptor tyrosine kinase signaling: transient versus sustained extracellular signal-regulated kinase activation. *Cell* **80**, 179-185.

Meloche S. (1995) Cell cycle reentry of mammalian fibroblasts is accompanied by the sustained activation of p44mapk and p42mapk isoforms in the G₁ phase and their inactivation at the G1/S transition. *J. Cell. Physiol.* **163**, 577-588.

Meyer-Ingold W. and Eichner W. (1995) Platelet-derived growth factor. *Cell. Biol. Int.* **19**, 389-398.

Minden, A., Lin A., Smeal T., Dérijard B., Cobb M., Davis R. and Karin M. (1994) c-Jun N-terminal phosphorylation correlates with activation of the JNK subgroup but not the ERK subgroup of mitogen-activated protein kinases. *Mol. Cell. Biol.* **14**, 6683-6688.

Mizel S. B. (1990) Cyclic AMP and interleukin 1 signal transduction. *Immunology Today* **11**, 390-391.

Pagés G., Lenormand P., L' Allemand G., Chambard J. C., Meloche S. and Pouysségur J. (1993) Mitogen-activated protein kinases p42mapk and p44mapk are required for fibroblast proliferation. *Proc. Natl. Acad. Sci. U.S.A.* **90**, 8319-8323.

Qui, M. S. and Green, S. H. (1992) PC12 cell neuronal differentiation is associated with prolonged p21^{ras} activity and consequent prolonged ERK activity. *Neuron* **9**, 705-717.

Saklatvala J. (1995) Intracellular signalling mechanisms of interleukin 1 and tumor necrosis factor: possible targets for therapy. *Br. Med. Bull.* **51**, 402-418.

Sánchez I., Hughes R. T., Mayer B. J., Yee K., Woodgett J. R., Avruch J., Kyriakis J. M. and Zon L. I. (1994) Role of SAPK/ERK kinase-1 in the stress-activated pathway regulating transcription factor c-Jun. *Nature* **372**, 794-798.

Schmidt J. A., Mizel S. B., Cohen D. and Green I. (1982) Interleukin 1, a potential regulator of fibroblast proliferation. *J. Immunol.* **128**, 2177-2182.

Seger R. and Krebs E. G. (1995) The MAPK signaling cascade. *FASEB J.* **9**, 726-735.

Sims J. E., Gayle M. A., Slack J. L., Alderson M. R., Bird T. A., Giri J. G., Colotta F., Re F., Mantovani A., Shanebeck K., Grabstein K. H. and Dower S. K. (1993) Interleukin 1 signalling occurs exclusively via the type I receptor. *Proc. Natl. Acad. Sci. U.S.A.* **90**, 6155-6159.

Sluss H. K., Barett T., Dérijard B. and Davis R. J. (1994) Signal transduction by tumor necrosis factor mediated by JNK protein kinases. *Mol. Cel. Biol.* **14**, 8376-8384.

Srinivasan M. and Begum N. (1994) Stimulation of protein phosphatase-1 activity by phorbol esters. *J. Biol. Chem.* **269**, 16662-16667.

Sugarman B. J., Aggarwal B. B., Hass P. E., Figari I. S., Palladino M. A., Jr. and Shepard H.

M. (1985) Recombinant human tumor necrosis factor-a: effects on proliferation of normal and transformed cells in vitro. *Science* **230**, 943-945.

Tartaglia L. A. and Goeddel D. V. (1991) Two TNF receptors. *Immunology Today* **13**, 151-153.

Traverse, S., Gomez, N., Paterson, H., Marshall, C. and Cohen, P. (1992) Sustained activation of the mitogen-activated protein (MAP) kinase cascade may be required for differentiation of PC12 cells: comparison of the effects of nerve growth factor and epidermal growth factor. *Biochem. J.* **288**, 351-355.

Valius M. and Kazlauska A. (1993) Phospholipase C-rl and phosphatidylinositol 3 kinase are the downstream mediators of the PDGF receptor's mitogenic signal. *Cell* **73**, 321-334.

Venezie R. D., Toews A. D. and Morell P. (1995) Macrophage recruitment in different models of nerve injury: Lysozyme as a marker for active phagocytosis. *J. Neurosci. Res.* **40**, 99-107.

Vietor I., Schwenger P., Li W., Schlessinger J. and Vileck J. (1993) Tumor necrosis factor-induced activation and increased tyrosine phosphorylation of mitogen-activated protein (MAP) kinase in human fibroblasts. *J. Biol. Chem.* **268**, 18994-18999.

Vilcek J., Palombella V. J., DeStefano D. H., Swenson C., Feinman R., Hirai M. and Tsujimoto M. (1986) Fibroblast growth enhancing activity of tumor necrosis factor and its relationship to other polypeptide growth factors. *J. Exp. Med.* **163**, 632-643.

Vilcek J. and Lee T. H. (1991) Tumor necrosis factor-new insights into the molecular mechanisms of its multiple actions. *J. Biol. Chem.* **266**, 7313-7316.

Wells M. R., Racis S. P., Jr. and Vaidya U. (1992) Changes in plasma cytokines associated

with peripheral nerve injury. *J. Neuroimmunol.* **39**, 261-268.

Westwick J. K., Weitzel C., Minden A., Karin M. and Brenner D. A. (1994) Tumor necrosis factor α stimulates AP-1 activity through prolonged activation of the c-Jun kinase. *J. Biol. Chem.* **269**, 26396-26401.

Whitmarsh A. J., Shore P., Sharrocks A. D. and Davis R. J. (1995) Integration of MAP kinase signal transduction pathways at the serum response element. *Science* **269**, 403-407.

FIGURE LEGENDS

Fig. 1. TNF- α and IL-1 activation of MAPK in human neuroma fibroblasts. (A) TNF- α , (B) IL-1 α , and (C) IL-1 β concentration-dependent responses. (D) TNF- α , (E) IL-1 α , and (F) IL-1 β time kinetics. Human neuroma fibroblasts were grown to confluence and incubated in serum-free medium for 24 hr, then stimulated for 15 min with TNF- α or IL-1 in doses ranging from 0.5 to 100 ng/ml. For the time kinetics studies, cells were treated with 10 ng/ml TNF- α or 3 ng/ml IL-1 and harvested at different time points. The activity of MAPK in the lysates was determined as described in *Experimental Procedures*. Three independent tests were repeated in each experiment. Values are expressed as means \pm standard errors. CONT, control.

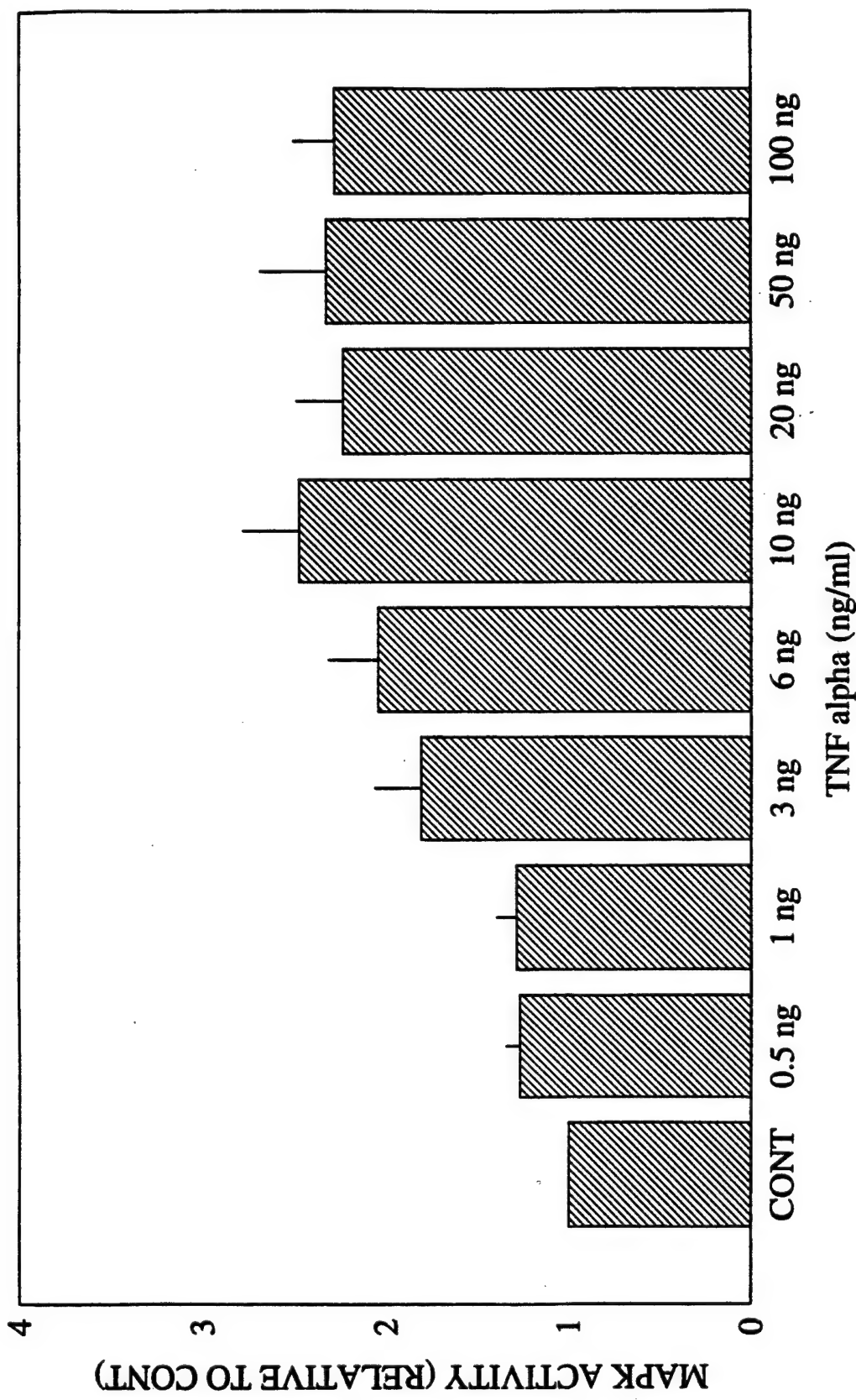
Fig. 2. MAPK activation of activity in human neuroma fibroblasts treated with either TNF- α , IL-1, or a combination of the two; PMA; or PDGF-AB. Serum-starved cells were treated with 10 ng/ml TNF- α and/or 3 ng/ml IL-1 for 15 min, 300 ng/ml PMA for 10 min, or 10 ng/ml PDGF-AB for 15 min. Eight to 11 independent experiments were repeated with TNF- α and IL-1, and three with PMA and PDGF-AB. The lysates from experimental and control cells were reacted with substrate (MBP) and reactivation buffer containing [γ - 32 P]ATP for 10 min. Phosphorylation of MBP was measured to determine MAPK activity in the lysates. The combination of TNF- α and IL-1 α produced significantly greater MAPK activation than either one alone ($P < 0.0001$). Activation by TNF- α and IL-1 β combined was significantly greater than that produced by TNF- α alone ($p < 0.001$), but not significantly different from that produced by IL-1 β alone ($p = 0.051$). Values are expressed as means \pm standard errors. CONT, control; T_IL1a, TNF- α plus IL-1 α ; T_IL1b, TNF- α plus IL-1 β .

Fig. 3. Immunoprecipitation analysis of MAPK activity. (A) The lysates from experimental and control cells were immunoprecipitated with protein A-agarose bound to rabbit polyclonal antibody to MAPK, and the resulting immunocomplexes were washed, resuspended, and mixed with reaction buffer containing MBP and [γ -³²P]ATP for 10 min at 30°C. The reaction was stopped by the addition of 2X Laemmli's sample buffer, after which the samples were boiled for 3 min and subjected to 10% SDS-PAGE. (B) The phosphorylated MBP bands were scanned and the densities of the bands were calculated and plotted as a histogram. CONT, control; T_IL1a, TNF- α plus IL-1 α ; T_IL1b, TNF- α plus IL-1 β .

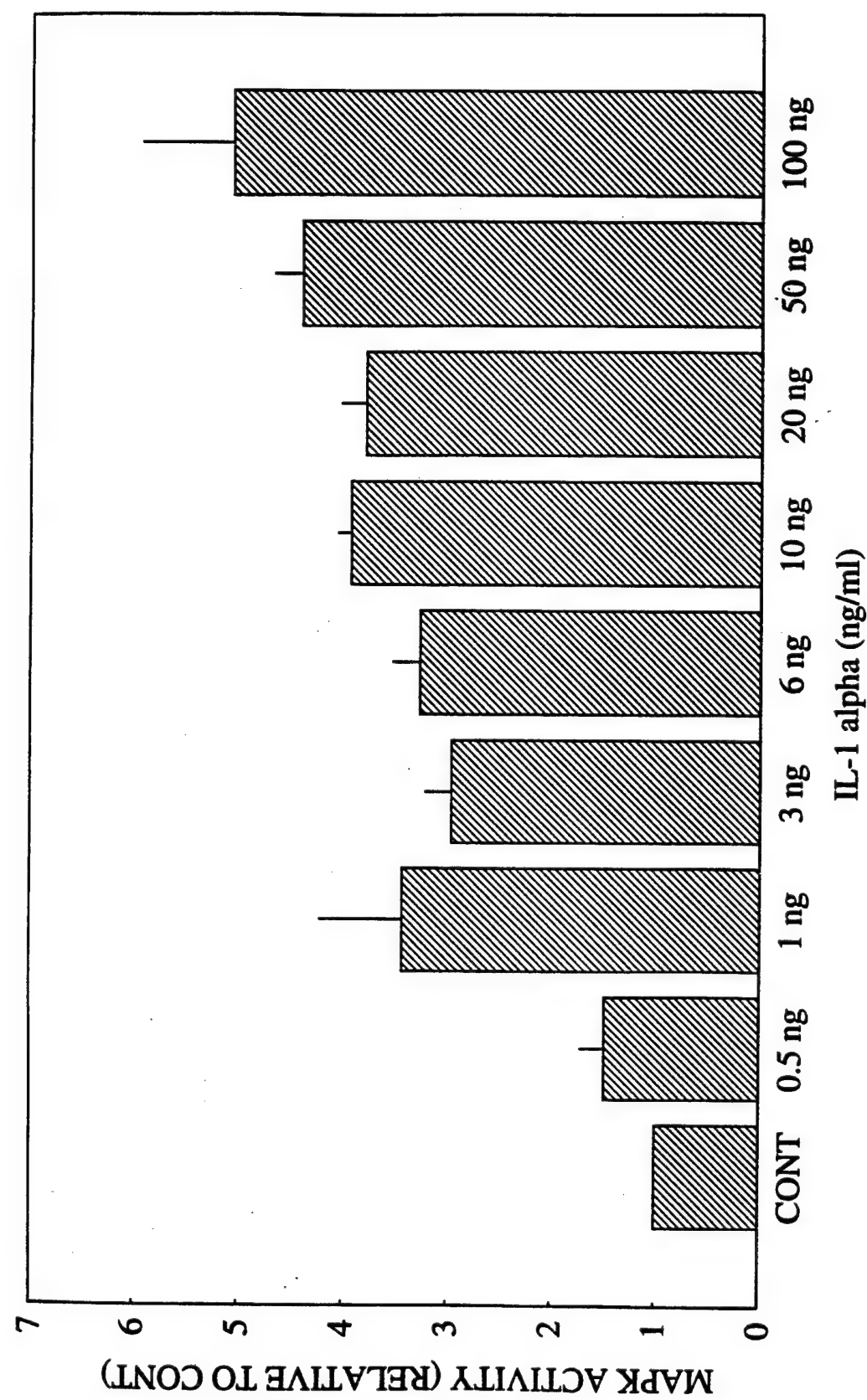
Fig. 4. Immunoblot analysis of human neuroma fibroblast lysates. Lysates from experimental and control cells were analyzed as previously described. Equal volumes of the lysates were subjected to 10% SDS-PAGE. After electrophoresis, the protein was transferred onto nitrocellulose membranes then probed with an anti-MAPK antibody that recognizes both the 44-kDa and the 42-kDa isoforms of MAPK. The immunocomplexes on the membrane were detected with ^{125}I -labeled protein A and imaged by autoradiography. CONT, control.

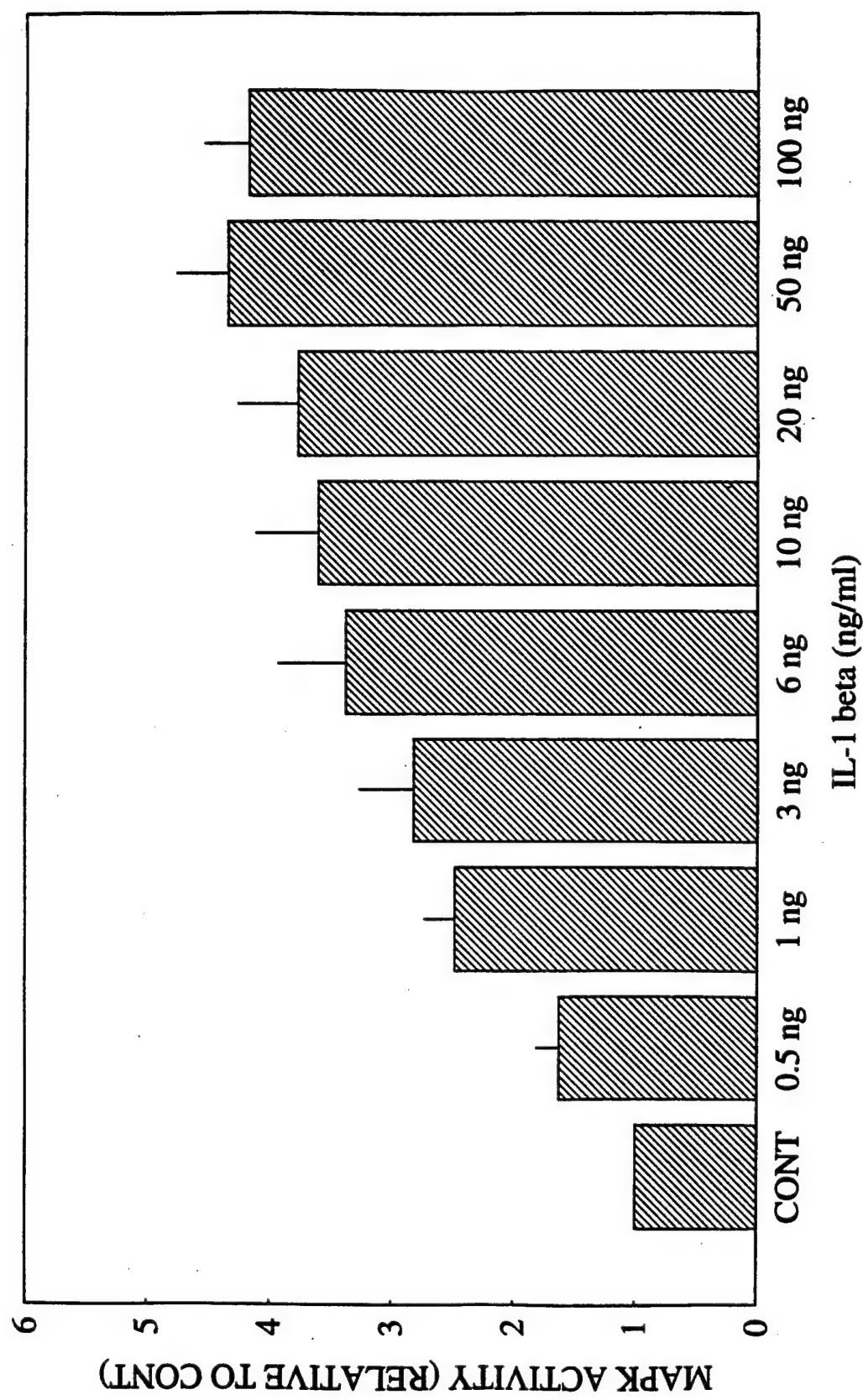
Fig. 5. Determination of SAPK activity with solid-phase protein kinase assay.

(A) Experimental and control cell lysates were diluted to a volume of 300 μ l containing 30 μ g protein. The lysate solution was mixed with agarose-conjugated human c-Jun (1-169) GST fusion protein and incubated with gentle agitation for 2 hr at 4°C, then pelleted. After washing, the pellets were resuspended and incubated in kinase buffer containing [γ -³²P]ATP for 20 min at 30°C. The reaction was terminated by adding 2X Laemmli's sample buffer and the samples were subjected to 10% SDS-PAGE. Following electrophoresis, the gel was washed and imaged by autoradiography. (B) Radioactivity incorporated into the bands of c-Jun GST was measured by densitometry and the results were plotted as a histogram. CONT, control; T_IL1a, TNF- α plus IL-1 α ; T_IL1b, TNF- α plus IL-1 β .

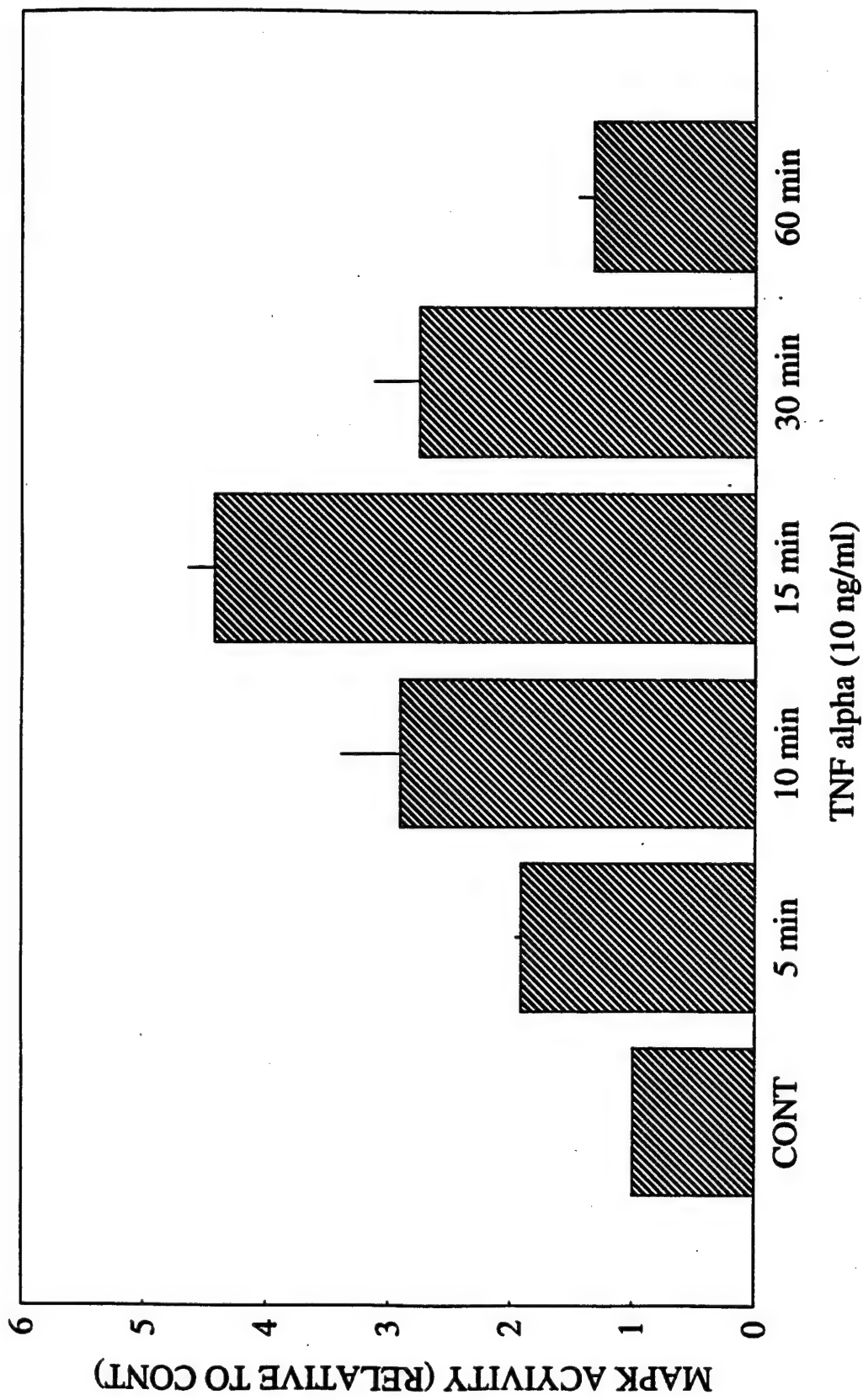


Lu et al
Figure 1 A
TOP ↑

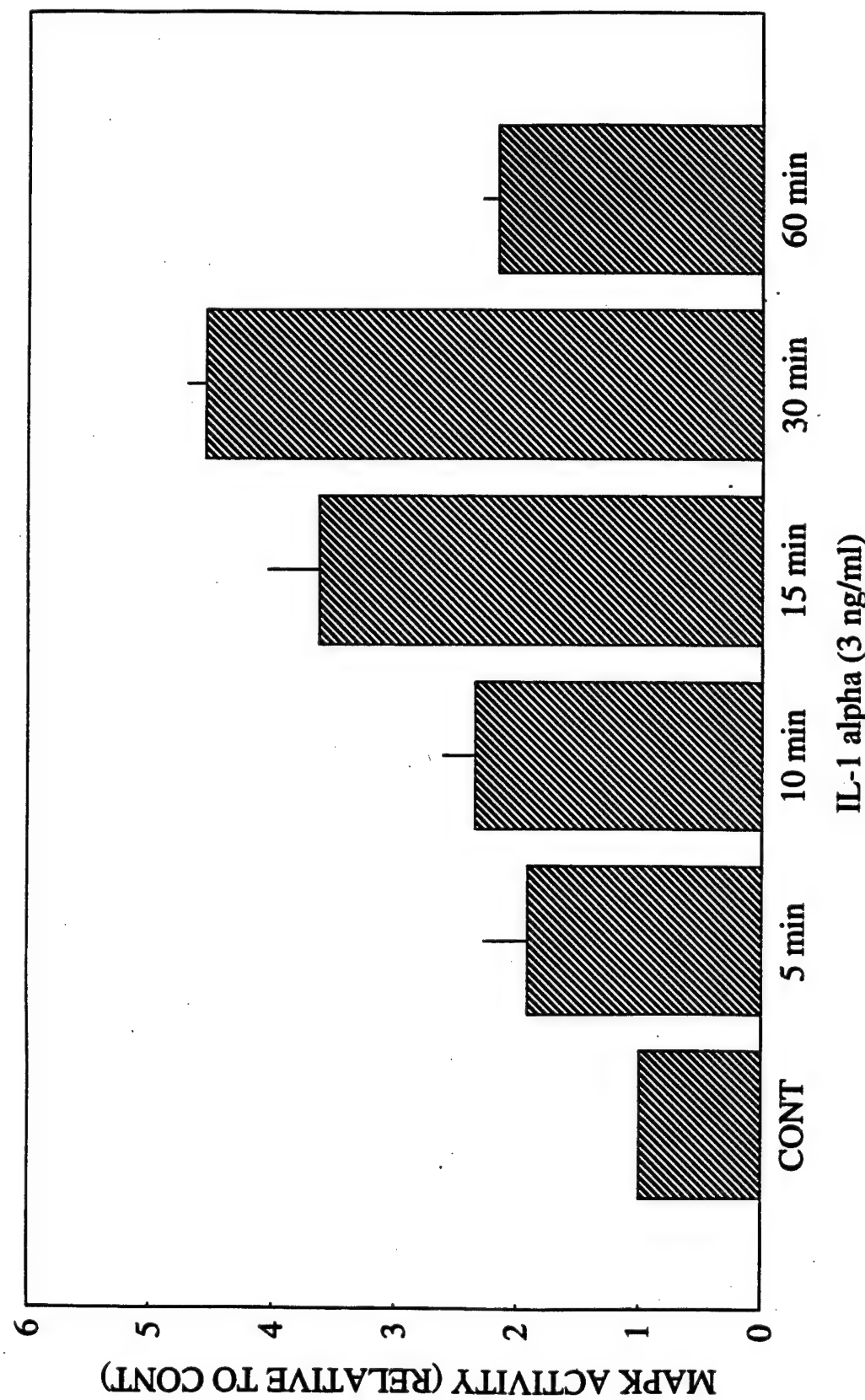




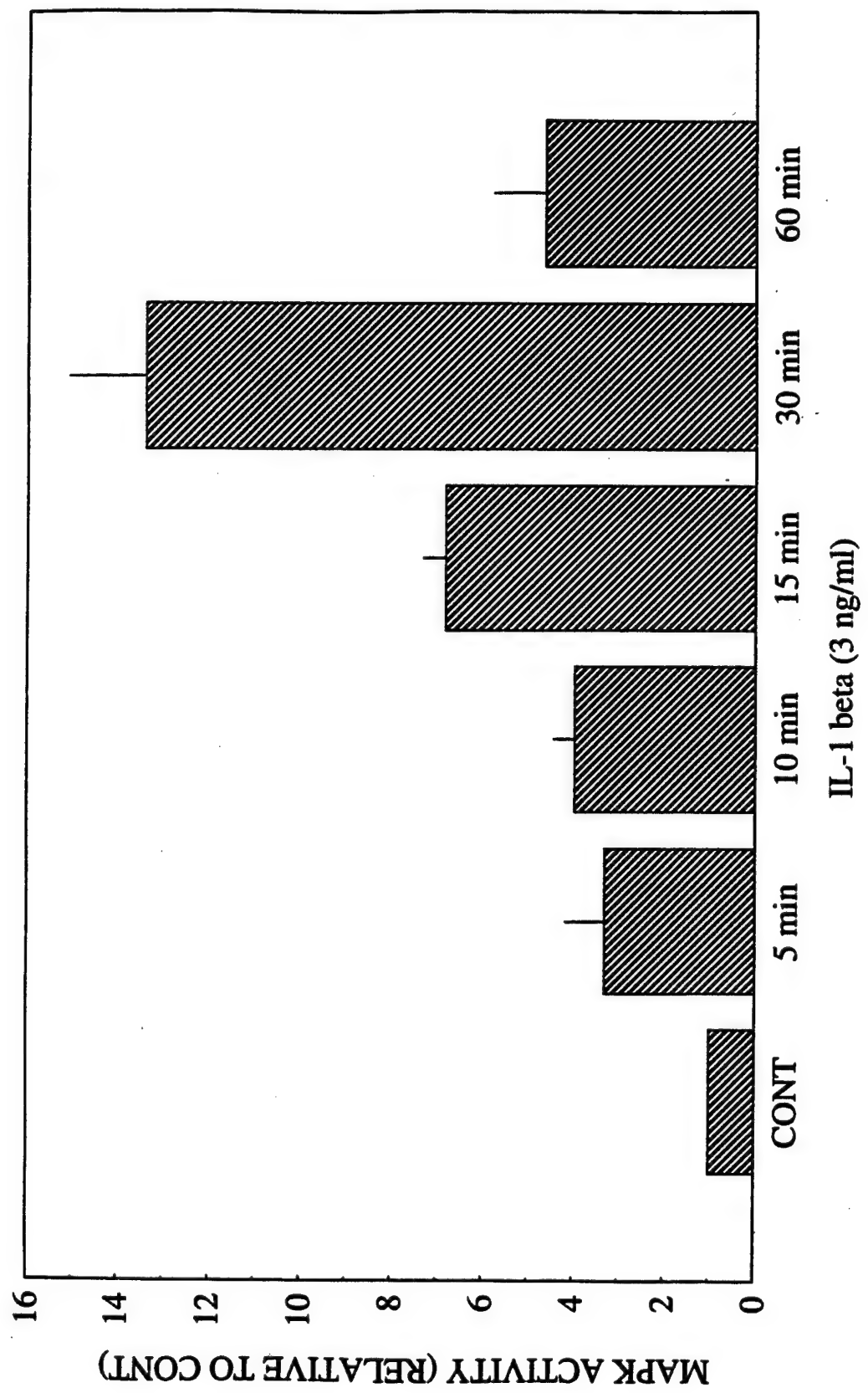
Lu et al
Figure 1 C
TOP ↑



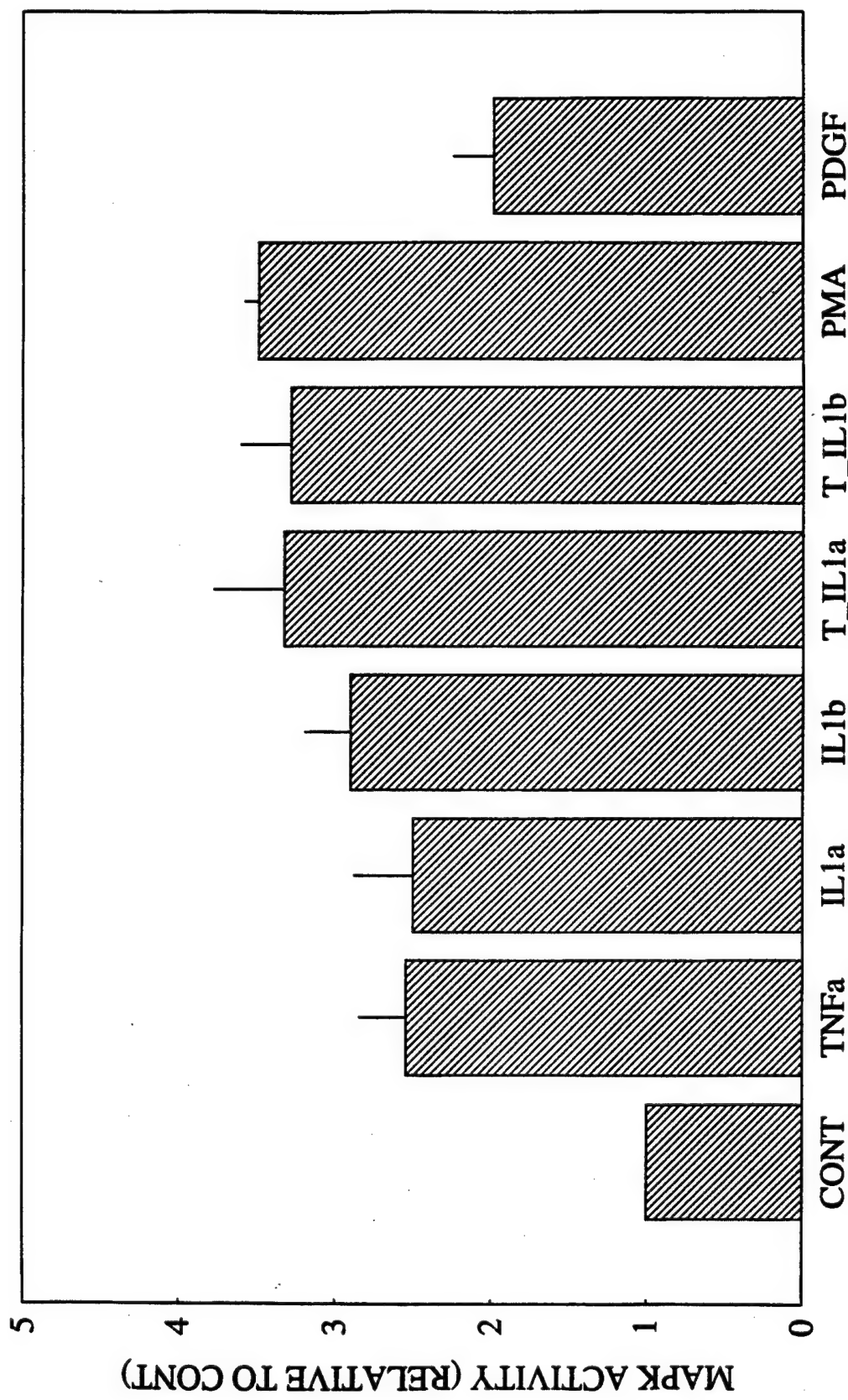
Lu et al
Figure 1 D
TOP ↑



Lu et al
Figure 1 E
TOP ↑



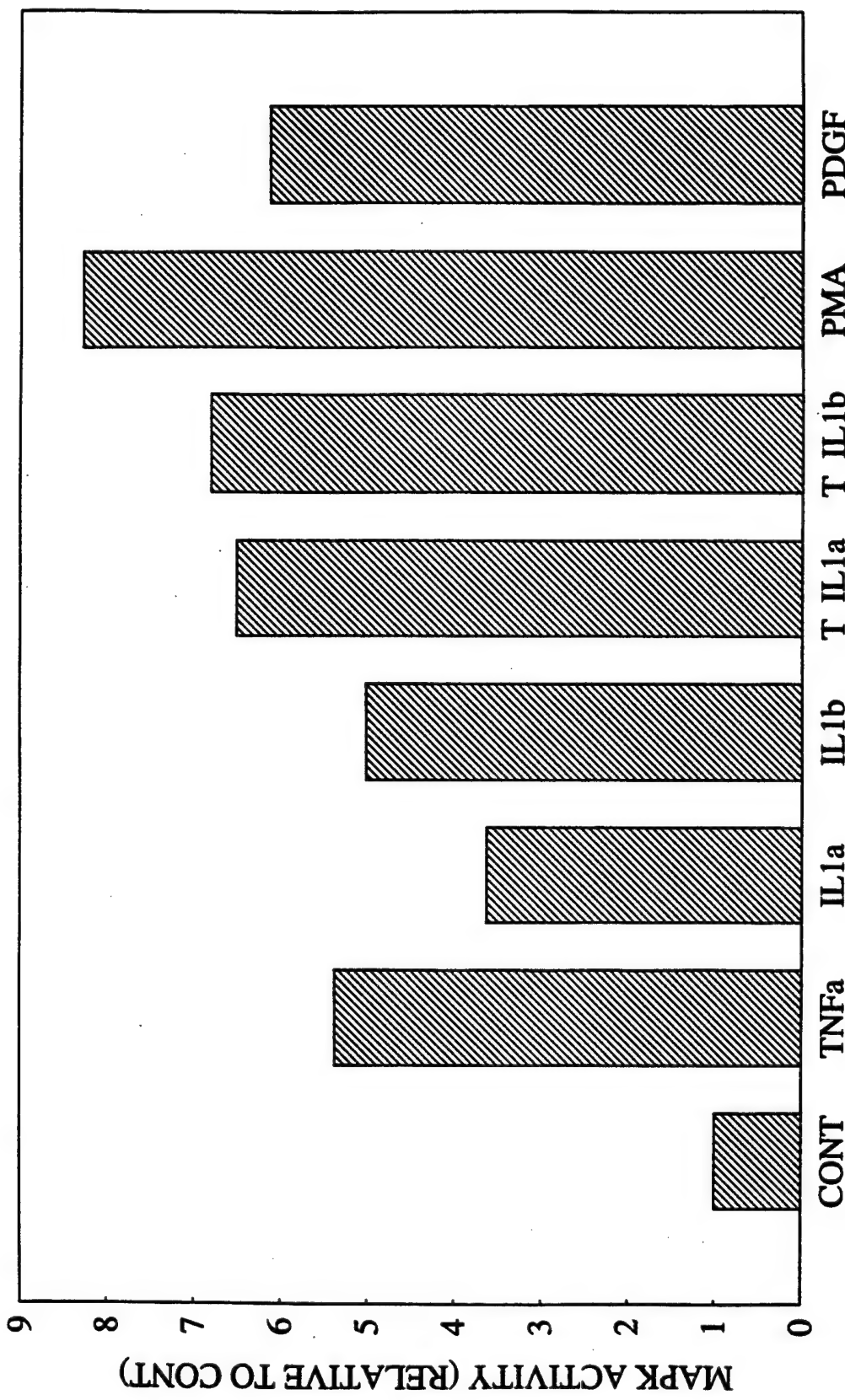
Lu et al
Figure 1 F
TOP ↑



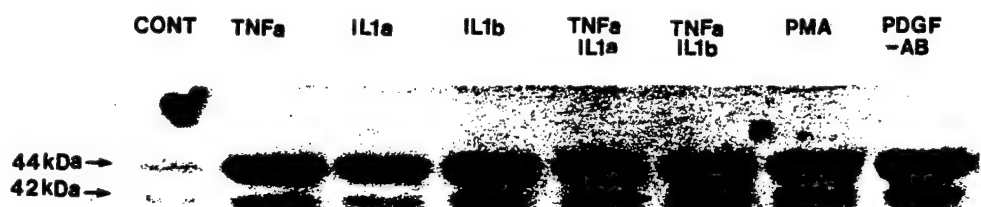
CONT TNF α IL1a IL1b TNF α TNF α PMA PDGF
IL1a IL1b -AB



Lu et al
Figure 3 A
TOP ↑



Lu et al
Figure 3 B
TOP ↑

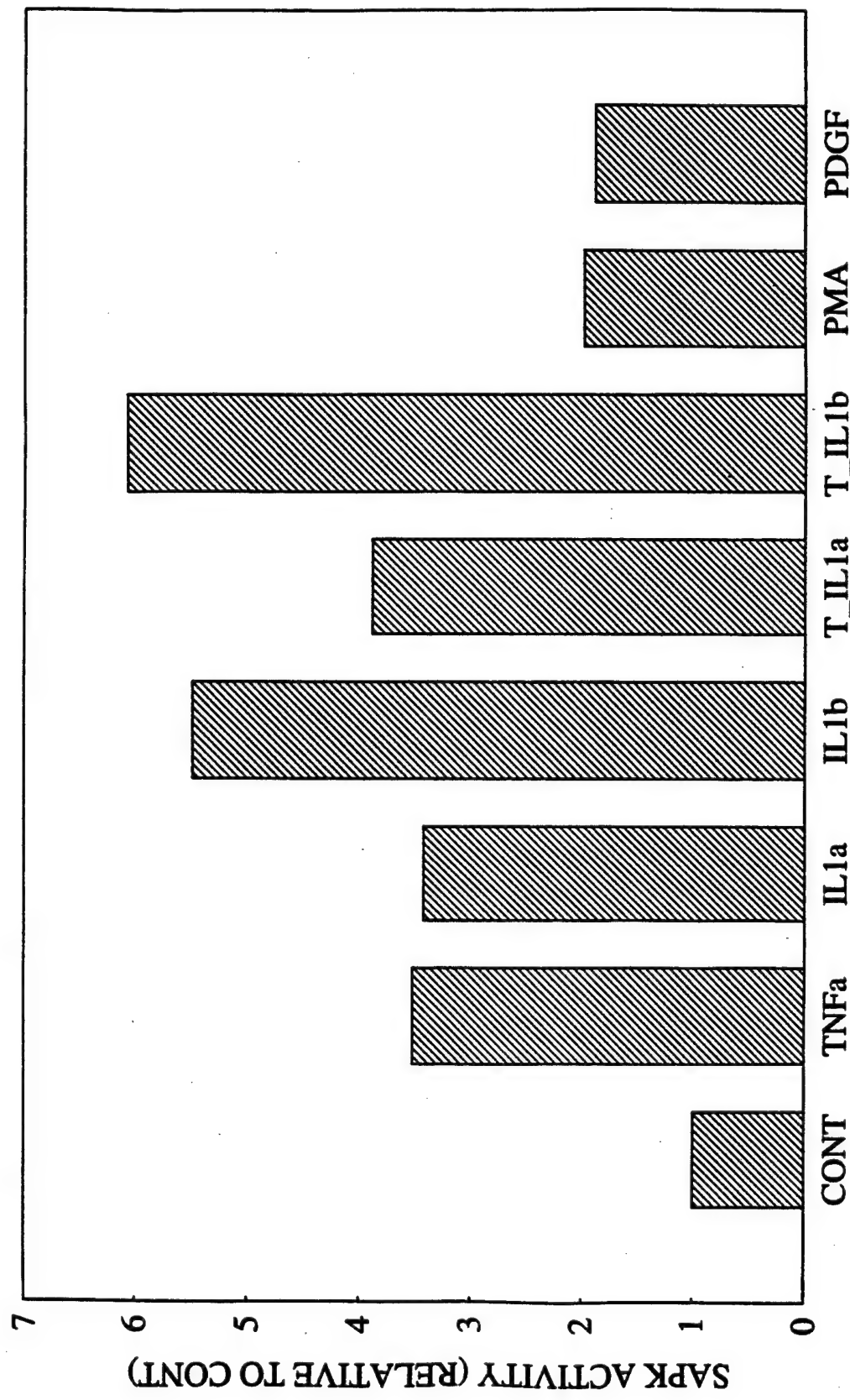


Lu et al
Figure 4
TOP ↑

CONT TNF α IL1a IL1b TNF α IL1a TNF α IL1b PMA PDGF
-AB



Lu et al
Figure 5 A
TOP ↑



Lu et al
Figure 5 B
TOP ↑

NEUROSCIENCE LETTERS

Date submitted: September 25, 1996

Detection Of Substance P In Human Tears

By Laser Desorption Mass Spectrometry And Immunoassay

Ray J. Varnell, Jiong Yan Freeman, Dmitri Maitchouk,

Roger W. Beuerman*, Bryan M. Gebhardt

LSU Eye Center, Louisiana State University Medical Center

School of Medicine, 2020 Gravier St., Ste. B, New Orleans, LA 70112

*Corresponding author. Tel.: 504 568 6700 extension 331; fax: 504 568 4210; e-mail:
roger@neurobio.ophth.lsumc.edu.

Abstract

To determine whether substance P is present in human tears, 1-2 μ l of tears were collected from one eye of each of 12 subjects. Two of the eyes had dry eye syndrome, two wore contact lenses and had dry eye syndrome, and eight were normal. Five of the eight normal eyes were scheduled to undergo excimer laser refractive surgery, and tears were collected from these eyes before and after surgery. Laser desorption mass spectrographs of the 18 tear samples displayed well defined peaks with mass to charge (m/z) ratios ranging from 1343.7 to 1355.9 and/or 1356.9 to 1364.7, corresponding to an average m/z of 1349.8 ± 1.13 for protonated substance P and 1361.2 ± 0.54 for oxidized substance P obtained from 14 spectrographs of standards formulated with substance P concentrations ranging from 10^{-4} M to 10^{-12} M. As confirmation, an enzyme-linked immunoabsorbant assay performed twice on pooled tears from one eye detected substance P in both replicates at a concentration of 125 pg/ml (9.26×10^{-11} M). These results indicate that, as a component of tears, this neuropeptide may play a role in inflammatory cell modulation or corneal wound healing.

Keywords: Dry eye syndrome, human, immunoassay, contact lens, laser desorption mass spectrometry, photorefractive keratectomy, substance P, tears.

Substance P is a neuropeptide that promotes secretion by exocrine glands [12] and may act as a neurotransmitter or modulator in the central and peripheral nervous system [6]. A substance P-like material is present in homogenates of the choroid, retina, optic nerve, optic nerve head, uvea, iris sphincter region, iris dilator and ciliary body, conjunctiva, whole upper eyelid, lacrimal gland, Harderian gland, and extraorbital muscle of the rabbit eye [3,4,15]. In the densely innervated cornea [11], sensory fibers are positive for substance P [3]. Substance P normally is not present or is present only in very low amounts in the aqueous humor of rabbits [15], but a peptide with substance P-like immunoreactivity is released into the aqueous humor when the trigeminal nerve is stimulated [2].

In lacrimal gland sections from rats, guinea pigs, and monkeys, nerve fibers that are immunohistochemically positive for substance P or substance P-like material are located around blood vessels and ducts [7,8]. Based on these findings, Nikkinen et al. [8] and Matsumoto et al. [7] suggested that substance P may be an important modulator of lacrimal gland secretion. In support of this, Williams et al. [14] demonstrated that the number of nerves staining positively for substance P or substance P-like material in rat lacrimal glands declines as the animal ages, and suggested that the decline in substance P-containing nerves corresponds with and may be a contributing factor to reduced tear output in older animals. Another possible role of substance P may be in promoting cellular growth [9,10] and the production of extracellular matrix [9].

Substance P has recently been detected in human nasal lavage fluid [13]. Because lacrimal secretions contribute to nasal fluids via the tear drainage system, it

is reasonable to suspect that substance P also occurs in tears.

In this study, we used matrix-assisted desorption/ionization mass spectrometry (MALDI) and the enzyme-linked immunoabsorbant assay (ELISA) to determine whether substance P can be detected in human tears. MALDI was employed because it is sensitive to the low femtomole range, requires less than a microliter of sample, and is tolerant of salts and other impurities in the complex mixtures typical of body fluids [5]. ELISA was used to confirm the MALDI results.

Unstimulated tears (approximately 1 μ l/min) were collected from the inferior cul-de-sac with fire-polished 10- μ l micropipettes. After collection, tears were either used immediately or stored in capped, 400- μ l, polyethylene microcentrifuge tubes at -20°C. Tears were collected from one eye of each of 12 healthy subjects. Subject age ranged from 26 to 60 years. Six subjects were men and six were women. Eight subjects had normal eyes, i.e., were disease-free and did not wear contact lenses; four subjects, including two who wore contact lenses, had been diagnosed with dry eye syndrome. Five of the eight subjects with normal eyes were excimer laser photorefractive keratectomy (PRK) patients, and their tears were collected before surgery and on the first and/or second day after PRK. Seven postoperative samples were collected, but one preoperative sample was lost. Thus, a total of 18 tear samples were analyzed.

For MALDI, each tear sample was mixed 1:100, v:v, with matrix. The matrix was freshly prepared daily by dissolving an excess of α -cyano-4-hydroxycinnamic acid (Aldrich Chemical Co., Milwaukee, WI) in HPLC-grade acetonitrile containing 0.1% trifluoroacetic acid and diluting the resulting solution 1:1, v:v, with an aqueous

solution of 0.1% trifluoroacetic acid. A 0.5 μ l aliquot of tear-matrix solution was spotted on a stainless steel plate and allowed to air-dry for a few minutes until crystals of matrix and embedded protein formed [1]. The plate was then introduced into a linear MALDI time-of-flight mass spectrometer (Voyager™ Biospectrometry™ Workstation, PerSeptive Biosystems, Framingham, MA) for analysis. The final spectrum generated from the analysis of each sample was averaged over 256 individual single-pulse spectra.

To prepare the standard solutions, substance P was obtained commercially (Cat # S 6883, Sigma Chemical Co, St. Louis, MO) and reconstituted in physiologically balanced, unpreserved sterile saline solution (Alcon Laboratories, Inc., Fort Worth, TX) at concentrations ranging from 10^{-4} to 10^{-12} M (1.35 picograms/ml). Balanced saline solution containing sodium, potassium, calcium, and magnesium salts was used because it is similar to the aqueous phase of tears. Aliquots of the standard substance P solutions were mixed with the α -cyano-4-hydroxycinnamic acid matrix and processed for mass spectrometry in the same manner as the tear samples.

To construct the spectrographs for the tear samples and substance P standards, the ratio of mass to charge (m/z) was plotted on the abscissa and signal intensity in arbitrary units was plotted on the ordinate (Figs. 1 and 2). Figure 1 is a spectrograph of a human tear sample. In Figure 2 (top), a part of the spectrograph from Figure 1 was enlarged to show substance P at m/z = 1351 and oxidized substance P at m/z = 1366; for comparison, spectrographs of a subsample of the tears from Figure 1 with substance P added (Fig. 2, middle) and a substance P

standard (Fig. 2, bottom) were included. All of the 18 tear samples analyzed with MALDI showed a well-defined peak in the m/z range from 1343.7 to 1355.9 or from 1356.9 to 1364.7. These results corresponded to an average m/z of 1349.8 ± 1.13 for protonated substance P $[M+H]^+$ and 1361.2 ± 0.54 for oxidized substance P $[M+O+H]^+$ obtained from the 14 spectrographs of substance P standards with concentrations ranging from 10^{-4} M to 10^{-12} M.

In the spectrograph of the substance P standard (Fig. 2, bottom), the low intensity peak at m/z = 1389 probably was the potassium adduct of substance P, which was contributed by the balanced saline solution. Except for lysozyme (m/z = 14,700) and its doubly protonated ion (m/z = 7360) (Fig. 1), other peaks in Figures 1 and 2 were unidentified.

An Enzyme Immunoassay Kit (Cat # 583751, Cayman Chemical, Ann Arbor, MI) for substance P was used for ELISA analysis of tears. Tears from one eye of one subject (a woman) were collected and frozen at -20°C until $100 \mu\text{l}$ had been obtained and then pooled and divided equally into two wells of the test plate, in accordance with the manufacturer's directions. The analysis was repeated, and substance P was detected in both replicates. The concentration of substance P in the tears from this subject was 125 pg/ml ($9.26 \times 10^{-11} \text{ M}$).

These findings demonstrate that substance P is a component of the tears obtained from normal eyes of men and women ranging in age from 26 to 60 years, from eyes fitted with contact lenses, from eyes with dry eye syndrome, and from eyes 1 and 2 days after excimer laser refractive surgery. However, we have not yet determined whether the concentration of substance P in tears varies with sex, age, or

eye condition, and the source of substance P and its role in tears remain to be discovered.

This study was supported in part by EY04074 (RWB) and EY02377 (CORE grant; LSU Eye Center) from the National Eye Institute, National Institutes of Health, Bethesda, MD; Department of the Army, Cooperative Agreement DAMD17-93-V-3013 (This does not necessarily reflect the position or the policy of the government, and no official endorsement should be inferred.); and Research to Prevent Blindness, Inc., New York, NY.

- [1] Beavis, R.C., Chaudhary, T. and Chait, B.T., α -Cyano-4-hydroxycinnamic acid as a matrix for matrix-assisted laser desorption mass spectrometry. (Letter) Organic Mass Spectrom., 27 (1992) 156-158.
- [2] Bill, A., Stjernschantz, J., Mandahl, A., Brodin, E. and Nilsson, G., Substance P: Release on trigeminal nerve stimulation, effects in the eye. Acta Physiol. Scand., 106 (1979) 371-373.
- [3] Butler, J.M., Powell, D. and Unger, W.G., Substance P levels in normal and sensorially denervated rabbit eyes. Exp. Eye Res., 30 (1980) 311-313.
- [4] Butler, J.M., Ruskell, G.L., Cole, D.F., Unger, W.G., Zhang, S.Q., Blank, M.A., McGregor, G.P. and Bloom, S.R., Effect of VIIth (facial) nerve degeneration on vasoactive intestinal polypeptide and substance P levels in ocular and orbital tissues of the rabbit. Exp. Eye Res., 39 (1984) 523-532.

- [5] Hillenkamp, F., Karas, M., Beavis, R.C. and Chait, B.T., Matrix-assisted laser desorption/ionization mass spectrometry of biopolymers. *Anal. Chem.*, 63 (1991) 1193 A-1203 A.
- [6] Hökfelt, T., Johansson, O., Ljungdahl, Å., Lundberg, J.M. and Schultzberg, M., Peptidergic neurones. *Nature*, 284 (1980) 515-521.
- [7] Matsumoto, Y., Tanabe, T., Ueda, S. and Kawata, M., Immunohistochemical and enzymehistochemical studies of peptidergic, aminergic and cholinergic innervation of the lacrimal gland of the monkey (*Macaca fuscata*). *J. Auton. Nerv. Syst.*, 37 (1992) 207-214.
- [8] Nikkinen, A., Lehtosalo, J.I., Uusitalo, H., Palkama, A. and Panula, P., The lacrimal glands of the rat and the guinea pig are innervated by nerve fibers containing immunoreactivities for substance P and vasoactive intestinal polypeptide. *Histochemistry*, 81 (1984) 23-27.
- [9] Reid, T.W., Murphy, C.J., Iwahashi, C.K., Fontes, B.A. and Mannis, M.J., Stimulation of epithelial cell growth by the neuropeptide substance P. *J. Cell. Biochem.*, 52 (1993) 476-485.
- [10] Reid, T., Nilsson, J., von Euler, A.M. and Dalsgaard, C.-J., Stimulation of connective tissue cell growth by substance P and substance K. *Nature*, 315 (1985) 61-63.
- [11] Rozsa, A. and Beuerman, R.W., Density and organization of free nerve endings of rabbit corneal epithelium. *Pain*, 14 (1982) 105-120.
- [12] Rudich, L. and Butcher, F.R., Effects of substance P and eledoisin on K efflux, amylase release and cyclic nucleotide levels in slices of rat parotid gland.

Biochim. Biophys. Acta, 444 (1976) 704-711.

[13] Schultz, K.-D., Ferkert, J., O'Conner, A., Böttcher, M., Schmidt, M., Baumgarten, C.R. and Kunkel, G., Determination of substance P in human nasal lavage fluid. Neuropeptides, 30 (1996) 117-124.

[14] Williams, R.M., Singh, J. and Sharkey, K.A., Innervation and mast cells of the rat exorbital lacrimal gland: The effects of age. J. Auton. Nerv. Syst., 47 (1994) 95-108.

[15] Unger, W.G., Butler, J.M., Cole, D.F., Bloom, S.R. and McGregor, G.P., Substance P, vasoactive intestinal polypeptide (VIP) and somatostatin levels in ocular tissue of normal and sensorially denervated rabbit eyes. (Letter) Exp. Eye Res., 32 (1981) 797-801.

FIGURE LEGENDS

Fig. 1. A MALDI mass spectrograph of substance P ($m/z = 1360$) naturally occurring in undiluted tears collected from a healthy 28-year-old man who did not wear contact lenses and who was asymptomatic for dry eye syndrome. Lys+H and Lys+2H are lysozyme and its doubly protonated form, respectively [6].

Fig. 2. Top: The mass spectrograph of substance P ($m/z = 1351$) in human tears from Figure 1. Middle: Tears from the same subject with substance P added at a concentration of 10^{-12} M. Bottom: Substance P standard at a concentration of 10^{-10} M in saline solution. In each tracing, the peak at $m/z = 1366$ is oxidized substance P. In the bottom tracing, the peak at $m/z = 1389$ is the potassium adduct of substance P; the potassium is provided by the saline solution.

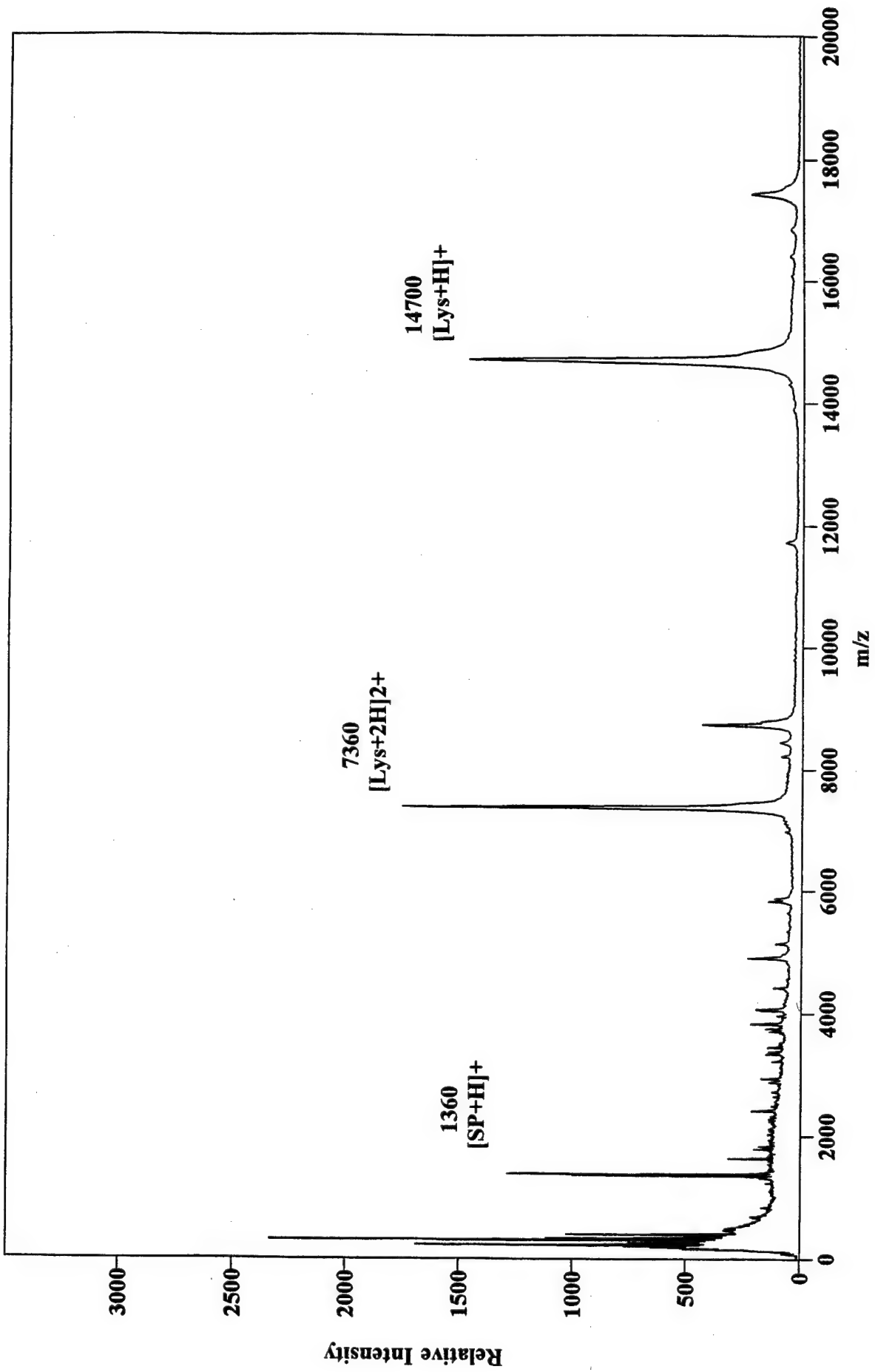


FIGURE 1

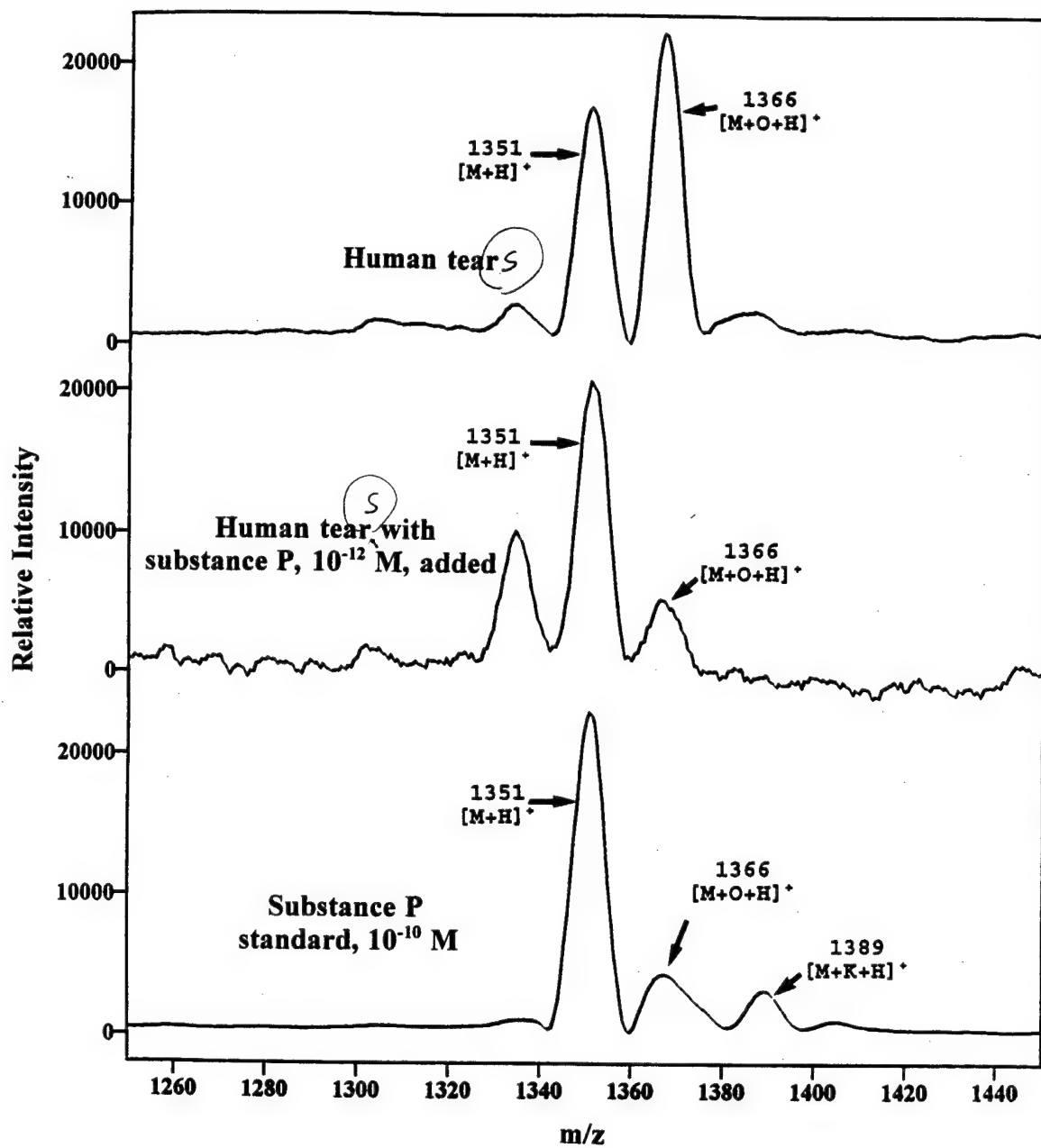


FIGURE 2

Neurotization of Motor Nerves Innervating Lower Extremity By Utilizing Lower Intercostal Nerves

Shurun Zhao,[†] Roger W. Beuerman,[‡] and David G. Kline[†]

[†]Department of Neurosurgery, Louisiana State University Medical School, and

[‡]LSU Lion's Eye Center, New Orleans, Louisiana

Correspondence to: David G. Kline, M.D., Department of Neurosurgery, 1542

Tulane Ave., New Orleans, LA 70112.

Tel. (504) 568-6122. Fax. (504) 568-6127.

Mailing Addresses:

Doctors Shurun Zhao and David G. Kline: Department of Neurosurgery, 1542

Tulane Ave., New Orleans, LA 70112.

Doctor Roger W. Beuerman: LSU Lion's Eye Center, 2020 Gravier Street, Suite B,

New Orleans, LA 70112.

ABSTRACT

An animal model in the rat was developed to study the reinnervation of ventral roots contributing to the lower extremity nerves by use of intercostal nerves. Intercostal nerves and distal cauda equina roots were anastomosed by use of a collagen tube and a microsurgical technique.

Most operated rats could lift their previously paralyzed leg and could walk but with a severe limp by 9 months postoperatively. Recordings of nerve action potentials (NAPs) and muscle action potentials (MAPs) indicated that the intercostal and sciatic nerves had some functional connections. Histologic analysis 12 months after repair demonstrated axonal regeneration extending from intercostal nerves to and down lumbar ventral roots. Most of the regenerated fibers were moderately well myelinated. Some connections between the neurons of anterior horn cells in the lower thoracic spinal cord and the reinnervated sciatic nerve was confirmed by retrograde tracer using fast blue.

Key Words: Intercostal nerves; sciatic nerve; femoral nerve; regeneration; reinnervation; paralysis of lower extremity

INTRODUCTION

Intercostal nerves have been used for a number of years in an attempt to reinnervate the arm in very proximal brachial plexus stretch and avulsive injuries¹⁻¹¹. Although results vary from series to series, some 40 to 50% of patients do regain biceps/brachialis function. It has been difficult however for such a neurotization procedure to provide more than one function. Patients recovering elbow flexion seldom gain shoulder abduction even though intercostal nerves are extended by grafts to axillary and/or suprascapular nerves.

Use of intercostals for origin of axons is one of several forms of neurotization used for the upper extremity. Neurotization techniques for the lower extremity are to date not as feasible as for the upper extremity. This is, at least partly, due to the distance between upper intercostal nerves and femoral and sciatic nerves. In the current study, we designed an animal model of neurotization of the lower extremity nerves by anastomosing ipsilateral or contralateral lower intercostal nerves to the ventral lumbar nerve roots of the cauda equina.

METHODS AND MATERIALS

Surgical technique

Ten healthy adult male Sprague-Dawley rats (weight 270 to 330 grams) were anaesthetized by intraperitoneal injection with pentobarbital (4 mg/100grams). Atropine (0.12 ml) was given intramuscularly to inhibit bronchial secretions. Once anesthesia was satisfactory, rats were intubated with an endotracheal tube which was then connected to a small animal ventilator. Then the rats were placed in a prone position. Under sterile conditions, an incision was made in the midline from thoracic vertebra 8 to lumbar vertebra 3. As the current experiments were designed to use intercostal nerves on either left or right sides, the incision was extended to the left (five rats) and right (five rats) at the thoracic 12 level. This was done at a left or right angle to the midline (Figure 1). In this way, a "L" or "T" type incision was made. The operation was then continued under an operating microscope. The paraspinal muscles were transacted at the thoracic 12 level and were also dissected away from the T8 through L2 lamina. A laminectomy was done between T8 and L2. This was done with both a mini-drill and a small rongeur. Intercostal muscles were then incised along the ribs. Care was taken to maintain the pleura and not to enter the thoracic cavity. The

intercostal nerves of thoracic 9 to 12 on the right side (in 5 rats) or left side (in 5 rats) were carefully separated one by one using micro-tweezers and scissors. The length of the intercostal nerves needed for the anastomosis depended on the distance between the outlets of the intercostal nerves and the ventral roots of the lower extremity nerves. The intercostal nerves at the T9 and T10 levels were sectioned distal to the lateral cutaneous branch and those at T11 and T12 were sectioned proximal to the lateral cutaneous branch. After all four intercostal nerves had been isolated, they were then tunneled under the paraspinal muscles and the soft tissues were closed. The dura at the level of L1 and L2 was opened in the midline. At the upper and lower ends of the opening, dura was cut at a 90° angle, so an incision shaped as “ I ” was made. The sciatic and femoral nerves of the rat receive input from the spinal cord segments of lumbar 3 to 6 via their ventral and some posterior roots¹². Dissections prior to these experiments showed that the nerve roots of L3 to L6 were approachable at an L-1 to L-2 intraspinal level. The exposed spinal cord was gently rotated with a moistened cotton-tipped applicator. The left ventral roots of L3 to L6 were identified and cut with a pair of microscissors below the transition region (TR) of the central and peripheral nervous system¹³. A collagen tube 1.5 mm in diameter and 12 mm in length (product of Colla-Tec, Inc.) was fixed with a 6-0 nylon suture to the ligament of the serratus dorsalis muscle. The position of the tube was between the upper end of L-1 and lower end of L-2 vertebrae. All the previous separated intercostal nerves and

the dissected left L3 to L6 roots were trimmed at their ends and carefully put inside the tube with microtweezers through the openings at both ends of the tube. The intercostal nerves and the ventral roots were adjusted so that their ends were in contact. 9-0 nylon suture was used to fix the intercostal nerves and ventral roots to either side of the tube and to the muscles and ligaments beside the vertebrae (Figure 2). Entubulation of intercostal nerve and distal nerve root prevented effective regeneration of the transected proximal lumbar roots but not of the transected distal roots. Dural defect was then covered with a piece of subcutaneous fat. The superficial back muscles were closed with 4-0 chromic gut and skin with 5-0 mersilene sutures. Each animal was given a 0.5 ml subcutaneous injection of penicillin G and was kept in a warm room for two days, then returned to the routine animal care room in its cage.

Electrophysiological examinations

12 months after the operation the animals were anesthetized with an injection of ketamine (40mg/kg) intraperitoneally. An incision was made at the midthigh level on the left side with the help of an operating microscope. Hamstring muscles were retracted to expose the sciatic complex. For nerve action potential (NAP) recording, the stimulating electrodes were bipolar platinum wire electrodes placed on the sciatic nerve. NAPs were recorded from the T9 to T12 intercostal nerves by using a bipolar platinum wire electrode. The distance between electrodes was 0.5 cm. A ground electrode was placed in the rat's tail. Muscle action potentials

(MAPs) were recorded from the muscles of legs of the rats by stimulation of the T9 to T12 intercostal nerves with bipolar platinum wire electrodes. Recording electrode were two stainless steel needles inserted into more distal leg muscles. The distance between the two sets of the electrodes was 5 cm. A similar electrode was placed subcutaneously in the neck was used as a ground electrode. Either a TECA TD20 electrophysiologic scope or a Gould 400 digital storage oscilloscope was used for recording. Stimulus was a square electric pulse; its duration was 0.05 ms and intensity was 5 to 7 volts. At a bandwidth of 20 to 2000 Hz, NAP and MAP responses were recorded and replicated on the scope's X-Y plotter. While recording, the rectal temperature was maintained at 38 °C by a heating pad.

Neuroanatomical and Histological studies

In the rats for neuroanatomical studies, a fast blue (FB) solution (5 mg in 100 µl distilled water) was applied according to the method by Aschoff and Hollander^{14,15}. The fast blue solution was filled into a small container drawn and thus made from a plastic tube. The sciatic nerve was freshly cut just proximal to its division into the peroneal, posterior tibial and sural nerves, and immediately placed into the fast blue solution. Nerve and container were carefully sealed away from surrounding tissues by bone wax which was softened by mineral oil. Nerve remained immersed in the solution for 90 minutes and was then removed. After FB application, the wounds were closed and the animals allowed to survive 72 to 96 hours. Then the rats were anesthetized with pentobarbital and transcardially perfused for 3 to 5 minutes with

saline (pH 7.2) followed by 8% paraformaldehyde (pH 5.6) for 5 to 10 minutes. Then the thoracic spinal cord extending from T9 to T12 was removed and placed at 4°C in the fixative containing 30% sucrose. The spinal cords were cut 12 hours later in serial transverse sections on a freezing microtome. Sections were mounted on glass slides for study of the spinal neurons under a fluorescent microscope. For the histological studies, the rats were also perfused as above. The T9 to T12 intercostal nerves, L3 to L6 distal ventral roots and sciatic nerve were removed and kept in 2.5 percent glutaraldehyde and 1 percent paraformaldehyde for 24 hours. Postfixation was by 1 percent osmium tetroxide. Tissue samples were then dehydrated with alcohol. Each nerve (or root) was embedded in 100 percent epon and sectioned transversely with an ultramicrotome for light or electron microscopy. Semi-thin sections were stained with toluidine blue and basic fuchsin for light microscopy. The thin sections were stained with uranyl acetate and lead citrate using a 2168 Ultrastainer Carlsberg System (LKB Bromma).

RESULTS

The left lower extremity was completely paralyzed following operation. The rats could move around with their forelegs and right hind leg, but they dragged their left hind leg along. The respiratory function did not show any noticeable changes and urination recovered within a day. The surgery did not obviously affect the growth of the rats, their weight had increased to about 500 grams when they were weighed 12 months later. The muscles on the left hind leg of some rats showed moderate atrophy. Three rats died during the 12 month period of study. Reasons for death were not entirely clear, but were probably pulmonary in origin. About 6 months later, the left lower extremity of some rats could move with respiration, and most rats could lift and walk with their left hind leg although with quite a limp by 9 months after operation.

NAPs were recorded 12 months postoperatively. Most rats showed good responses (figure 3A). MAPs could be recorded from both flexor and extensor muscles of thigh and lower legs. These MAP responses were surprisingly good (figure 3B). Conduction velocities and amplitudes were close to those of normal controls.

Figure 4 presents the histological results from both peripheral nerves and cauda equina roots involved in the regenerative process. Extensive regeneration of nerve fibers can be seen originating from the intercostal nerves attached to the lower

extremity nerves. Electron microscopy indicated that distal to the junction of intercostal nerves and lumbar 3 to 6 ventral roots, many regenerative nerve fibers were present. Myelination was moderately mature (figure 5).

Results with fast blue tracing showed that many neurons in the ventral horns of the thoracic spinal cord extending from T9 to T12 contained the fluorescent materials. It is presumed that these neurons contribute to the reconstructed sciatic nerve. Figure 6 shows a microphotograph taken from the ventral horn of the thoracic spinal cord of a rat at a T10 to T11 level. This provided the evidence that the nerve fibers in the reconstructive sciatic nerve were anatomically connected to these neurons.

DISCUSSION

Studies of the plasticity of the nervous system have been conducted on a wide range of species. The central nervous system has the capacity of adaptation to severe changes in the arrangement of its outputs and inputs through the cross anastomosis of peripheral nerves¹⁶⁻²¹. Intercostal nerves have been used to neurotize patients with otherwise irreparable stretch injuries to the brachial plexus^{1-3,7-11,22-23}, and the bladder²⁴.

The intercostal nerves, especially the upper ones, are distant from the sciatic nerve and femoral nerve in the thigh. The current study showed, however, that it is possible to connect the lower intercostal nerves to sciatic and femoral nerve outflow by anastomosing them to the ventral roots of cauda equina. By one year postoperatively, there had been regeneration of nerve fibers through the anastomosis and into more distal nerves. There was also some reversal of paralysis in the lower extremity of these rats. Such a technique which connects intercostal nerves to ventral lumbar roots seems worth further study.

Mismatching of motor and sensory fibers from donor nerves with their pathways in recipient nerves leads to minimize useful function^{25,26}. For some mixed nerves it has been assumed that only 10% (0.1) of the fibers were motor.

The matching probability for the connection of motor fibers in two such mixed nerves is 0.01 ($P = 0.1 \times 0.1 = 0.01$)²⁶. In the current study, the intercostal nerves contain only 10 to 20 percent of motor nerve fibers²⁶, on the other hand, the ventral roots have 100 percent motor fibers. Thus, the matching possibility for motor nerve fibers was at most 10 to 20 percent. As a result, anastomosis of intercostal nerves to ventral roots gave a higher matching possibility for the motor fibers than connection of intercostal nerves with mixed nerves, such as elements of the brachial plexus.

The motor elements of lower intercostal nerves innervate several thoracic and abdominal muscles, such as the *musculus intercostales externi* and *interni*, *musculus rectus abdominis*, *musculus obliquus internus abdominis*, the *musculus transversus abdominis*, and *musculus obliquus externus abdominis*. These lower intercostal nerves were considered as suitable donors since they can provide at least two different muscle functions²⁶. Narakas pointed out that a few hundred axons seem to be sufficient to reinnervate efficiently a poorly differentiated muscle like the biceps, but thousands are needed to restore the delicate balance of the small intrinsic muscles of the hand and to give them tactile gnosis¹. Muscular activity of the lower extremity is much less delicate than that of the upper extremity. In addition, the technique used in the current study provides a higher matching possibility of the motor fibers. Evidence has showed that the lower

intercostal nerves can provide more motor nerve fibers than the upper intercostal nerves. Ploncard and Samardzic et al indicated that a intercostal nerve of the human contains about 500 to 700 motor nerve fibers^{4,22}, but results by Schalow et al suggest that this number is close to 1000 to 2000²⁶. The differences between the two studies is that the former used upper intercostal nerves in their study, while the latter examined lower intercostal nerves.

Distance needed for intercostal nerves to reach ventral roots either ipsilateral or contralateral is comparable. Thus, some reconnection to lower extremity nerves can be performed using contralateral intercostal nerves. This would be useful when the ipsilateral intercostal nerves are dysfunctional, because of more proximal and unilateral spinal cord or contralateral cerebral injury. Under such circumstances contralateral intercostal nerves can be used to neurotize lower extremity nerves (figure 7). A suitable length of the lower intercostal nerves can be directly attached to the cauda equina roots. This kind of grafting technique might be useful if the intercostal nerves were used to bypass a distal spinal cord injury or cauda equina injury or irreparable injuries to the pelvic plexus.

The current study was conducted on a lower animal, the rat, which is much different than the human. Further studies need to be done on higher animals, such as the primate, before this technique can be applied to the human. Loss of lower intercostal function did not adversely affect abdominal wall function to our

knowledge in the rat. Nonetheless, such may be a more serious complication in higher animals or the human.

Acknowledgment. The authors wish to express their gratitude to Mrs Lia Pedroza for her technical assistance. This study was supported in part by the Department of the Army, Cooperative Agreement DAMD17-93-V-3013 (This does not necessarily reflect the position or the policy of the government, and no official endorsement should be inferred).

REFERENCES

1. Narakas, A.: Surgical treatment of traction injuries of the brachial plexus. Clinical Orthopaedics and Related Research, 1978, 133:71-90.
2. Tomita, Y., Tsai, T., Burns, J., Karaoguz, A. and Ogden, L.: Intercostal nerve transfer in brachial plexus injuries: an experimental study. Microsurgery, 1983, 4:95-104.
3. Dolenc, V.: Intercostal neurotization of the peripheral nerves in avulsing plexus injuries. Clinics in Plastic Surgery, 1984, 11:143-147.
4. Samardzic, M., Antunovic, V., Joksimovic, M. and Bacetic, D.: Donor nerves in the reinnervation of brachial plexus. Neurological Research, 1986, 8:117-122.
5. Sanardzic, M., Grujicic, D., Antunovic, V. and Joksimovic, M.: Reinnervation of avulsed brachial plexus using the spinal accessory nerve. Surg. Neurol., 1990, 33:7-11.
6. Samardzic, M., Grujicic, D. and Antunovic, V.: Nerve transfer in brachial plexus traction injuries. J Neurosurg., 1992, 76:191-197.

7. Nagano, A., Tsuyama, N., Ochiai, N., Hara, T. and Takahashi, M.: Direct nerve crossing with the intercostal nerve to treat avulsion injuries of the brachial plexus. The J. Hand Surg., 1989, 14A:980-985.

8. Friedman A. H., Nunley II, J. A., Goldner, R. D., Oakes, W. J., Goldner, J. L. and Urbaniak, J. R.: Nerve transposition for the restoration of elbow flexion following brachial plexus avulsion injuries. J Neurosurg., 1990, 72:59-64

9. Akasaka, Y., Hara, T. and Takahashi, M.: Free muscle transplantation combined with intercostal nerve crossing for reconstruction of elbow flexion and wrist extension in brachial plexus injuries. Microsurgery, 1991, 12: 346-351.

10. Doi, K., Sakai, K., Kuwata, N., Ihara, K. and Kawai, S.: Reconstruction of finger and elbow function after complete avulsion of the brachial plexus. J Hand Surg., 1991, 5:797-803.

11. Gu, Y. and Ma, M.: Nerve transfer for treatment of root avulsion of the brachial plexus: Experimental studies in a rat model. J. Reconstr. Microsurg. 1991, 7:15-22.

12. Hebel, R. and Stromberg, M. W.: Anatomy of the Laboratory Rat. Waverly Press Inc., 1976, pp.133-135.

13. Berthold, C. H., Carlstedt, T. and Coneliuson, O.: Anatomy of the nerve root at the central-peripheral transitional region. In Dyck, P. J. (ed.), Peripheral Neuropathy, W. B. Saunders Co., Philadelphia, 1984, 156-170.

14. Aschoff, A. and Holländer, H.: Fluorescent compounds as retrograde tracers compared with horseradish peroxidase (HRP). I. A parametric study in the central visual system of the albino rat. *J. Neurosci. Methods*, 6: 179-197, 1982.

15. Illert, M., et al.: Fluorescent compounds as retrograde tracers compared with horseradish peroxidase (HRP). II. A parametric study in the peripheral motor system of the cat. *J. Neurosci. Methods*, 6: 199-218, 1982.

16. Brinkman, C., Porter, R. and Norman, J.: Plasticity of motor behavior in monkeys with crossed forelimb nerves. *Science*, 1983, 220:438-440.

17. Clark, S. A., Allard, T., Jenkins, W. M. and Merzenich, M. M.: Receptive fields in the body-surface map in adult cortex defined by temporally correlated inputs. Nature, 1988, 332:444-445.

18. Vera, C. L., Lewin, M. G., Kase, J. C. and Calderon, M. D.: Central functional changes after facial-spinal-accessory anastomosis in man and facial-hypoglossal anastomosis in the cat. J Neurosurg., 1975, 43:181-190.

19. Seil, F.J.: Tissue culture studies of neural plasticity. Restorative Neurology and Neuroscience, 1989, 1:1-11.

20. Goldberger, M. E.: Different patterns of recovery of motor function associated with different patterns of post-lesion axonal grows. In: Seil, F. J. (ed.), Nerve, Organ and Tissue Regeneration: Research Perspectives. Academic Press, New York, pp. 155-463, 1983.

21. Merill , E. G. and Wall P. D.: Plasticity of connections in the adults nervous system. In: Cotman, C.W.(ed.), Neuronal Plasticity. Raven Press, New York, 1978, 97-111.

22. Ploncard, Ph.: A new approach to the intercostal-brachial anastomosis in the treatment of brachial plexus paralysis due to root avulsion. Late results. Act. Neurochir., 1982, 61:281-290.

23. Kawai, H., Kawabata, H., Masada, K., Ono, K., Yamamoto, K., Tsuyuguchi, Y. and Tada, K.: Nerve repairs for traumatic brachial plexus palsy with root avulsion. Clin. Orthop., 1988, 237:75-86.

24. Carlsson, C. A. and Sundin, T.: Reconstruction of afferent and efferent nervous pathways to the urinary bladder in two paraplegic patients. Spine, 1980, 5:37-41.

25. Sunderland, S.: Discussion of "Functional specificity and somatotopic organization during peripheral nerve regeneration". In: Jewett, D. L. and McCarroll, H.R. (eds.), Nerve Repair and Regeneration. Mosby, St. Louis, 1980, 113.

26. Schalow, G., Aho, A. and Lang, G.: Microanatomy and number of nerve fibers of the lower intercostal nerves with respect to a nerve anastomosis. Donor nerve analysis. I(IV). Electromyogr. Clin. Neurophysiol., 1992, 32:171-185.

LEGENDS

Fig. 1. Schematic illustration depicts the method of connecting intercostal nerves to the distal ventral roots leading to the sciatic and femoral nerves of the rat. A: Left intercostal nerves were connected to the left cauda equina distal ventral roots. B: right intercostal nerves were connected to the left cauda equina distal ventral roots.

Fig. 2. Schematic illustration of anastomosis of intercostal nerves and the distal ventral roots of cauda equina.

Fig. 3. Nerve action potential (NAP) and muscle action potential (MAP) were recorded by stimulating intercostal nerves from a rat 12 months postoperatively. A: NAP recorded from sciatic nerve. Stimulus output is to the left of the tracing. B: MAP recorded from hamstring muscles. C: MAP recorded from flexor muscles of the hip and D: MAP recorded from gastrocnemius muscles.

Fig. 4. A: Photomicrograph of a transverse section of junctional area demonstrating the presence of regenerating nerve fibers in a rat killed 12 months postoperatively. Regenerated nerve fibers are intermixed with the degenerated fibers (magnification X 125). B: Photomicrograph of a transverse section of a distal ventral root showing extensive regeneration of intercostal nerve fibers into the

nerve root (magnification X 125; bar length = 40 μ m). C: Photomicrograph of a transverse section of sciatic nerve. Regenerated fibers are intermixed with intact sensory fibers (magnification X 125).

Fig. 5. A. Electron micrograph of a portion of reinnervated ventral root 12 months postoperatively which illustrates that the regenerated nerve fibers show normal configuration. Arrows: collagens, S: Schwann cell and A: myelination of axons (magnification X 30000).

Fig. 6. Microphotograph of the neurons in the anterior horn between the T10 to T11 level spinal cord marked by fast blue (FB) technique. The dye migrated from proximal sciatic nerve, through the repair site, and then up the intercostal nerve(s) to spinal cord.

Fig. 7. Schematic illustration depicts dysfunction of ipsilateral intercostal nerves because of more proximal spinal cord or contralateral cerebral injury. The Contralateral intercostal nerves might be used to neurotize the lower extremity nerves in such cases.